Time-Optimal Trajectory Generation and Way-Point Sequencing for 5-Axis Laser Drilling

by

Ammar Alzaydi

A thesis

presented to the University of Waterloo

in fulfillment of the

thesis requirement for the degree of

Doctor of Philosophy

in

Mechanical Engineering

Waterloo, Ontario, Canada, 2016

AUTHOR'S DECLARATION

I hereby declare that I am the sole author of this thesis. This is a true copy of the thesis, including any required final revisions, as accepted by my examiners.

I understand that my thesis may be made electronically available to the public.

Ammar Ayad Alzaydi

Abstract

Laser drilling provides a highly productive method for producing arrays of holes on planar and freeform shaped components. Industrial applications include fuel injection nozzles, printed circuit boards (PCB's), inkjet printer heads, pinholes and slits for scientific instrumentation, high-resolution circuitry, sensors, fiber-optic interconnects, medical devices, and gas turbine combustion chamber panels. This thesis deals with time-optimal trajectory planning for two mainstream laser drilling methods: on-the-fly drilling and percussion drilling, which are used in the aerospace industry. The research has been conducted in collaboration with the Canadian aero-engine producer, Pratt & Whitney Canada (P&WC). The algorithms developed have been tested in a target application involving the laser drilling of cooling hole arrays on gas turbine engine combustion chamber panels.

On-the-fly drilling is an operation in which each hole receives one low powered shot at a time while the workpiece is in motion, and the beam focal point is continuously proceeding to the next hole location. The positioning sequence repeats itself until all holes are gradually opened up in small increments. Each hole location has ample time to cool down before the next shot is received. Thus, this process can yield favorable material properties in terms of preserving the desired crystal structure, and also hole quality in terms of dimensional (size) and form (shape) accuracy, due to the reduction of local thermal loading. However, there is no existing trajectory planner, in industry, or in literature, capable of generating time-optimized positioning trajectories for on-the-fly laser drilling. This thesis studies this problem and presents a new algorithm, capable of handling 5 degree-of-freedom (axis) positioning capability. The ability to generate spline-based smooth trajectories is integrated within a Traveling Salesman Problem (TSP) type sequencing algorithm. The sequencing algorithm optimizes both the order of the waypoints (i.e., hole locations) and also the timing levels in between, which affect the temporal (time-dependent) nature of the motions commanded to the laser drilling machine's actuators. Furthermore, the duration between consecutive holes has to be an integer multiple of the laser pulsing period, considering a machine configuration in which the laser is firing at a constant frequency, and unused pulses are diverted away using a quick shutter. It is shown that the proposed algorithm is capable of generating 17-25% reduction in the beam positioning time spent during a manufacturing

cycle, compared to some of the contemporary practices in industry. 17% reduction in the vibrations induced onto the laser optics is also observed, which helps prevent downtime due to the optics hardware gradually losing alignment.

The second type of laser drilling operation for which optimized 5-axis trajectory planning has been developed is percussion drilling. In this process, a series of pulses are sent to each hole while the part is stationary. Once the hole is completely opened up, then positioning to the next hole proceeds. While percussion drilling is less advantageous in terms of local thermal loading and achievable part quality, it is used extensively in industry; due to its simplicity of automation compared to on-the-fly drilling. Thus, a TSP-style trajectory planning algorithm has also been developed for percussion laser drilling. The novelty, in this case, is concurrent planning of 5-axis time-optimal point-to-point movements within the sequencing algorithm, and direct minimization of the total travel time, rather than just distance (in two Cartesian axes); as is the method for which significant portion of TSP solvers and trajectory planners in literature have been developed. Compared to currently applied methods at P&WC, 32-36% reduction in the beam positioning time has been achieved. Also, 39-45% reduction in the peak magnitude of vibration has been realized.

Limited benchmarking with state-of-the-art TSP solvers from combinatorial mathematics, considering only 2-axis Euclidean distance as the objective function, indicate that the proposed sequencing algorithm for percussion drilling is sub-optimal by 9-12%. Thus, it can still use further improvement in future research. Nevertheless, the two trajectory planners that have been developed in this thesis for on-the-fly drilling and percussion drilling have experimentally demonstrated very promising improvements in terms of motion time and smoothness. As more advanced Computer Numerical Control (CNC) systems and laser control electronics with deterministic execution and rapid synchronization capability become available, such algorithms are expected to facilitate significant production gains in laser drilling processes used in different industries.

Acknowledgements

This research has been supported by Pratt and Whitney Canada (P&WC) and the Natural Sciences and Engineering Research Council of Canada (NSERC).

I gratefully acknowledge the assistance of Dr. Amr Elfizy and Dr. Serafettin Engin from P&WC and their feedback in the technical and experimental development of this thesis.

Valuable feedback on the scientific content and presentation of this thesis has been provided by Prof. J. Huissoon, Prof. S. Smith, Prof. M. Collins from the University of Waterloo, and Prof. A. Matsubara from Kyoto University. I would like to thank them for taking the time to read my thesis in its entirety, and especially to Prof. Matsubara for making the journey from Japan to Canada to attend my thesis defense in person.

Some of the benchmarks results, presented in Chapter 5, were conducted using the Concorde and LKH Traveling Salesman Problem solution libraries. I gratefully acknowledge their public domain availability, and their contribution to my research. I also acknowledge the assistance I received from Prof. S. Smith and Mr. Kyongjae (Jay) Woo (MASc student at UW Precision Controls Laboratory) in running these benchmarks.

I sincerely acknowledge the time and commitment that has been provided by my supervisor, Prof. Kaan Erkorkmaz. His devotion to research and the success of his students is seen in everything he does. There are few words that can fully express my gratitude for his guidance and the experience he has provided over these past years. He has been a guide, mentor, teacher, and supporter.

Lastly, I thank my family and my wife for supporting, encouraging, and motivating me during my studies.

Dedication

I lovingly dedicate this thesis to my mother, Lama Hadidi, for her constant, unconditional love and support and for being the greatest influence on my life.

I also dedicate this thesis to my father, Ayad Alzaydi, whose unique challenges through my Ph.D. made me a better person and brought the better me to life.

Last but not least, my lovely wife, Joudi, my love and inspiration. Her support and patience has sustained me throughout my studies.

Table of Contents

List of Figures

List of Tables

Chapter 1

Introduction

1.1 Introduction

Laser drilling provides a highly productive method for producing arrays of holes on planar and freeform shaped components. Industrial applications include fuel injection nozzles, printed circuit boards (PCB's), inkjet printer heads, pinholes and slits for scientific instrumentation, high-resolution circuitry, sensors and detectors, fiber-optic interconnects, medical devices, and gas turbine combustion chamber panels.

There are several methods of laser drilling. One common method is ***percussion drilling***, where a series of laser pulses are sent to each hole while the component being drilled remains stationary. Each pulse causes a certain volume of material removal through ablation, and the laser pulses continue on until the hole is completely opened up. Then, drilling of the next hole proceeds by re-positioning the part with respect to the beam. The percussion drilling method is highly productive, especially when the laser pulses can be delivered at high frequency. However, there is local thermal loading on the part, which may deteriorate the material properties and hole quality. Furthermore, obtaining the optimum sequence of positioning trajectories is an important and open research problem, especially for drilling configurations involving more than three simultaneous translational axes. Optimizing the beam positioning sequence and trajectory subject to the capabilities of a laser drilling machine and process enables minimum cycle time, therefore maximum productivity. *Achieving this optimization for percussion laser drilling in an integrated manner, by jointly considering the sequencing and trajectory optimization problems for beam positioning in 5-axis coordinates, is one of the contributions of this thesis.*

Another laser drilling method, which is advantageous in terms of resulting in better material properties and part accuracy, is ***on-the-fly drilling***. In this method, each hole receives only one low powered shot at a time while the workpiece is in continuous motion with respect to the beam. The positioning sequence repeats itself until all holes are gradually opened up in small increments. In this method, each drilled hole location has

ample time to cool down before the next shot is received. Thus, on-the-fly drilling can result in more favorable material properties in terms of preserving the desired crystal structure around the hole, and better quality in terms of dimensional (size) and form (shape) accuracy. However in the case of on-the-fly drilling, the trajectory planning and sequencing become even more complicated tasks; as there is no industrially available trajectory planner specifically designed for this operation (especially for 5-axis movements). There is only a limited amount of literature which targets mainly two-axis sequencing for percussion type drilling operations (as reviewed in Chapter 2). *Hence, another contribution of this thesis is the development of a novel integrated sequencing and optimized trajectory planning method for 5-axis on-the-fly laser drilling.*

1.2 Problem Description, Thesis Outline, and Summary of Contributions

Figure 1.1 and Figure 1.2 illustrate a sample application for 5-axis laser drilling that is used in the production of gas turbine combustion chamber panels at the Canadian aero-engine producer, Pratt & Whitney Canada. The machine tool shown in Figure 1.1 has five moving axes (with translation in the x-y-z axes, and rotation in the A-C axes). The machine tool is actuated by direct drive motors which provide high velocity and acceleration capability and is used to drill components with hole configurations similar to the one shown in Figure 1.2. Considering the figure, it can be seen that there is a clear need for 5-axis beam positioning capability. The direction and location of the holes are typically optimized to generate a suitable cooling film of air within the combustion chamber of a gas turbine engine.

In both percussion drilling, as well as on-the-fly drilling, the objective is to minimize the total time required to travel from one hole location to the other; i.e. **Objective function:** $T_{\mathbf{tot}} = T_1 + T_2 + \ldots + T_N$. Here, T_i represents the duration spent traveling from hole number (i) to ($i+1$), within the computed drilling sequence.

Defining the joint vector (hole location and orientation in joint coordinates) for the machine's translating and rotating axes as $\boldsymbol{q} = \begin{bmatrix} x & y & z & a & c \end{bmatrix}^T$, the machine constraints considered are that axis velocity ($\dot{\boldsymbol{q}}$), acceleration ($\ddot{\boldsymbol{q}}$), and jerk ($\dddot{\boldsymbol{q}}$) be kept

within their limits. Velocity and acceleration limits ($\mathbf{v}_{max} = [\dot{x}_{max} \quad \cdots \quad \dot{c}_{max}]^T$, $\mathbf{a}_{max} = [\ddot{x}_{max} \quad \cdots \quad \ddot{c}_{max}]^T$) help limit the maximum force or torque demand, which ensures linear operation of the drives without saturation.

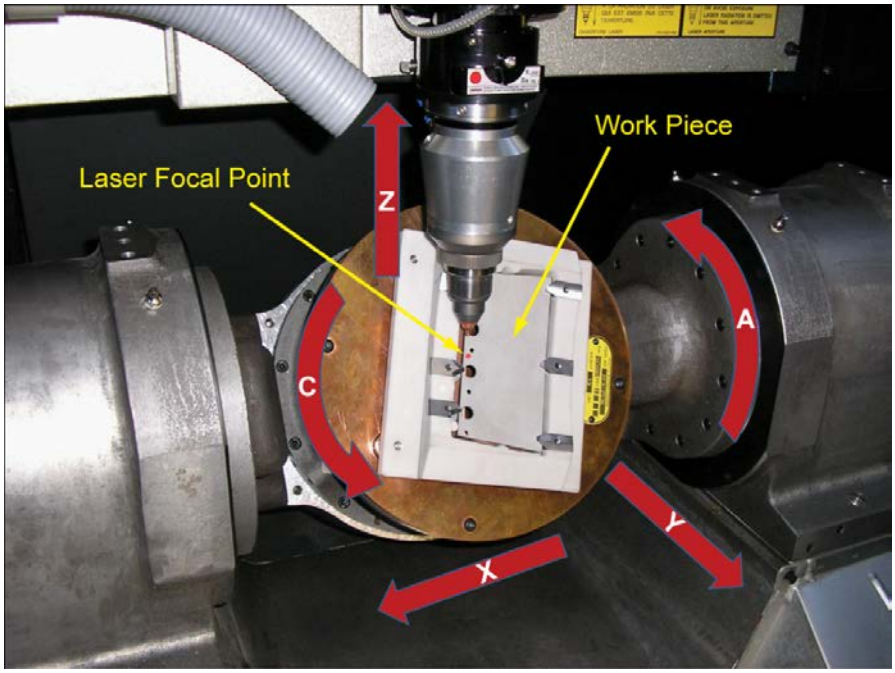

Figure 1.1: Configuration of 5-Axis Laser Drilling Machine Tool.

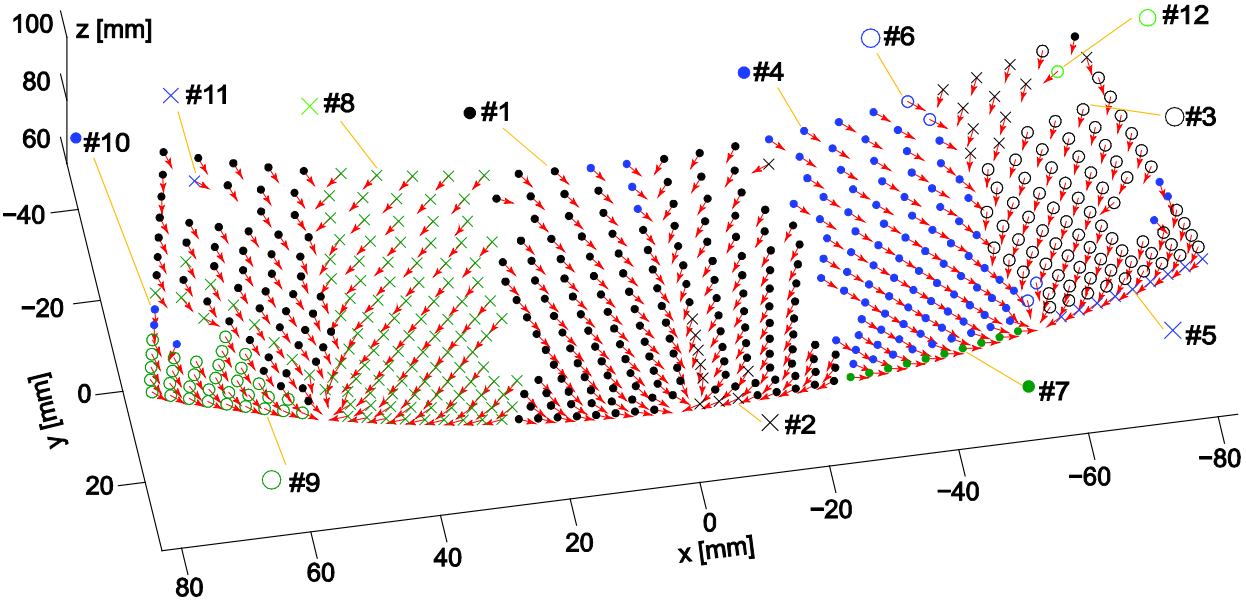

Figure 1.2: Hole locations and orientations for a sample part – Actual part is not shown as it contains company proprietary information.

The jerk limits ($\mathbf{j}_{\max} = \begin{bmatrix} \dddot{x}_{\max} & \cdots & \dddot{c}_{\max} \end{bmatrix}^T$) constrain the high-frequency content in the commanded motion, which indirectly limits the tracking error. This helps retain the beam positioning accuracy at high traverse rates, especially for on-the-fly laser drilling, where the accuracy and repeatability of the beam positioning are crucial. Limiting the jerk commanded to the actuators also reduces the vibrations induced onto the machine structure, and in particular the laser optics. This helps improve the hole quality in percussion drilling. Excessive vibration can cause the laser optics to lose alignment, which requires significant downtime for realignment. Thus, limiting the jerk also has a positive effect on the overall productivity of the laser drilling operation.

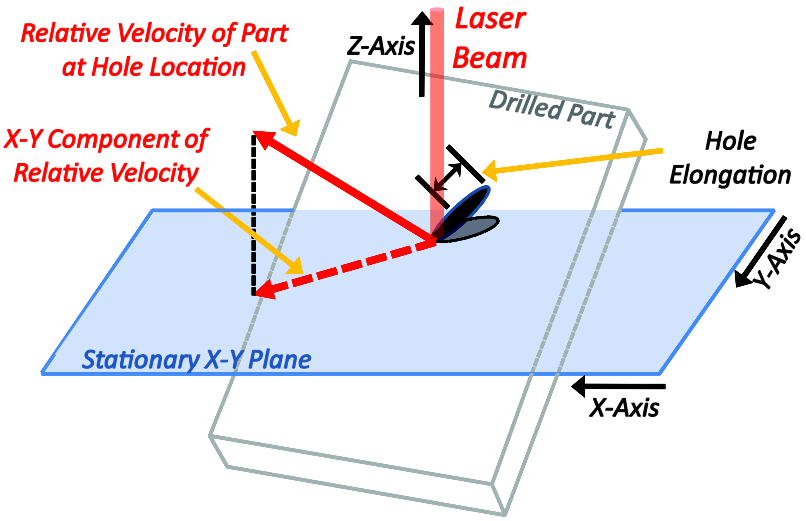

Figure 1.3: Hole elongation due to x-y component of part velocity.

In the case of on-the-fly drilling, there is an extra process constraint that needs to be considered. Since the part is in relative motion with respect to the beam during the drilling operation, there will inevitably be a certain degree of hole elongation as shown in Figure 1.3. Hence, the x-y component of the workpiece velocity at the hole location (v_{xy}) relative to the laser beam needs to be limited. This can be achieved by considering the kinematics of the machine tool and the geometry of the workpiece [90].

While the machine related velocity, acceleration, and jerk constraints need to be respected at all times, both for percussion and on-the-fly drilling, the hole elongation constraint needs to hold only for on-the-fly drilling, and just at the hole locations (thereby

allowing higher x-y plane velocities to be reached in between the holes). Thus, the trajectory generation constraints applicable to both drilling operations can be formally stated in Eq. (1.1) as,

$$\left.\begin{array}{ll} \text{Velocity} & -\boldsymbol{v}_{\max} \le \dot{\boldsymbol{q}} \le \boldsymbol{v}_{\max} \\ \text{Acceleration}: & -\boldsymbol{a}_{\max} \le \ddot{\boldsymbol{q}} \le \boldsymbol{a}_{\max} \\ \text{Jerk}: & -\boldsymbol{j}_{\max} \le \dddot{\boldsymbol{q}} \le \boldsymbol{j}_{\max} \\ \text{Hole Elongation (only for on-the-fly drilling)}: & -v_{xy,\max} \le v_{xy} \le v_{xy,\max} \end{array}\right\} \tag{1.1}$$

While it is possible to use coupled dynamic equations representing the joint torque/force demand for a given trajectory [90], the mainstream industrial practice in the machine tool and manufacturing industry is to represent the actuator capabilities with kinematic (velocity, acceleration, and jerk) constraints. Albeit being slightly more conservative, the constraint set in Eq. (1.1) enables easy transfer of industrial specifications to the trajectory optimization algorithms, such as those developed in this thesis.

Time-optimized trajectory generation has previously received attention in robotics and machine tool literature for contour following applications [3], [10], [41], [72]. There have also been successful works for following way-point data by modulating the time intervals in between the points [67]. Specifically, on-the-fly laser drilling requires the motion duration between consecutive holes to be an integer multiple of the laser firing period, and the entire travel time be minimized. This originates from the hardware configuration that the laser typically pulses at a constant frequency, and unused shots can be diverted away from the workpiece by using a quick-shutter in the optics path. In between the holes, the motion path is not fixed and can be modulated to achieve the maximum possible time reduction. Furthermore, the sequence of the holes can be ordered to achieve the shortest possible travel duration. This presents a new type of trajectory and way-point sequencing optimization problem specific to on-the-fly laser drilling process, which has been studied for the first time in this thesis. Chapter 3 presents the sequencing and integrated trajectory planning method that has been developed for on-the-fly drilling. While the final drilling trajectory consists of a repeating cyclic motion, the connection into and out of this motion

from and to rest (with zero velocity and acceleration boundary conditions) with time-optimal characteristics has also been studied and is presented in Chapter 4.

The problem of finding the optimum sequence for manipulator waypoints can be considered as an extension of the Travelling Salesman Problem (TSP) [51]. In this thesis the problem of percussion laser drilling trajectory optimization has been cast as minimizing the total travel time required to visit each hole location exactly once, such that the positioning trajectory in between the consecutive holes is also time-optimal subject to the first three types of constraints in Eq. (1.1) (i.e., velocity, acceleration, and jerk). Thus, the novel contribution for percussion drilling has been the development of a combined TSP-style sequencing and optimal trajectory planning method for 5-axis laser drilling, and benchmarking this solution both with respect to industrially applied methods (such as the Nearest Neighbor based sequencing, detailed in Chapter 2), and also to a limited context, state-of-the-art TSP solvers from literature; such as the Concorde Cutting Plane and Lin-Kernighan Heuristic (LKH) methods [18]. The proposed sequencing algorithm for 5-axis percussion laser drilling is presented in Chapter 5.

In order to render the main chapters easy to read, the majority of the mathematical details explaining the supporting computations have been placed into the appendices. They consist of: Closed curve fitting using cubic splines (Appendix A), Analytical evaluation of constraints (without requiring full interpolation of the trajectory, Appendix B), Kinematic analysis of the 5-axis laser drilling system (Appendix C), Effect of time scaling on the derivative profiles (Appendix D), Possible adjustments to timing levels for on-the-fly drilling (Appendix E), and Point-to-point minimum-time trajectory planning with zero boundary conditions, subject to displacement, velocity, acceleration, and jerk constraints (Appendix F).

As a result of the contributions in Chapters 3 and 4, 17-25% reduction has been achieved in the beam positioning cycle time for on-the-fly laser drilling over industrially applied sequencing and trajectory planning methods. 17% reduction in the root mean square (RMS) value of vibration has been registered from the laser drilling optics, indicating that the quality of the motion smoothness has also been improved.

Using the proposed sequencing and optimal trajectory planning method in Chapter 5 for percussion laser drilling, a 32-36% reduction has been achieved in the beam

positioning cycle time compared to currently applied methods in industry for sequencing and actuator positioning. Furthermore, the peak value of resultant vibration induced onto the laser optics has been reduced by 39-45%. 2-axis Euclidean distance based benchmarks performed with respect to some of the most powerful TSP algorithms [18] indicate that 9-12% further cycle time improvement should be achievable in future research, upon integrating the 5-axis machine kinematics and time-optimal trajectory planning algorithms with more advanced TSP solvers, like the Concorde Cutting Plane and LKH methods.

1.3 Conclusion

This chapter has presented an overview of the trajectory planning problem for two mainstream kinds of laser drilling operations, percussion and on-the-fly. Also, an outline of the contents and contributions of this thesis has been presented.

Chapter 2

Literature Review

2.1 Overview

Manufacturers of turbine engines for aircraft propulsion and power generation have benefited from the productivity of lasers for drilling small (0.3–1 mm diameter) cylindrical holes at 10-90º to the surface in cast, sheet metal, and machined components. The ability to drill holes at shallow angles at high rates per second has enabled new designs incorporating film-cooling holes for improved fuel efficiency, reduced noise, and lower Nitric Acid (NO), Nitrogen Dioxide (NO_2) and CO emissions [4].

Common techniques used in laser drilling are percussion hole drilling, on-the-fly drilling, and trepanning. Percussion drilling is a process where multiple pulses are applied per hole, while the part is stationary, to disperse sufficient material in order to open up the hole cavity. The on-the-fly drilling process is where the holes are drilled with a single shot at a time, while the part is in relative motion with respect to the laser beam, and the shots are repeated as required in order to open up the holes. Trepanning is a process where certain contours are cut by drilling closely spaced holes. Each of these laser drilling techniques will be explained further in this chapter. Compared to percussion drilling, on-the-fly laser drilling offers important advantages, which are:

- Better material properties and feature quality; due to reduced thermal loading on the part;
- Smoother axis motion (as opposed to stop-and-go movements, as required in percussion drilling), which reduces vibrations induced onto the laser optics;
- Less downtime for optics realignment (which would be caused by vibrations);
- Higher productivity, since motion ‘smoothness’ can be translated into higher processing speed.

However, the feasibility of using percussion drilling might surpass that of on-the-fly drilling techniques in certain scenarios, especially when the laser pulsing period is much shorter than the servo drives’ positioning time. It must be predetermined whether on-the-fly drilling is feasible for a particular application. Therefore, there is a need to study trajectory and hole sequence optimization methods for both percussion and on-the-fly laser drilling.

Incremental improvements in laser process and control technologies have led to substantial increases in the number of cooling holes used in turbine engines. Fundamental to these improvements and increased use of laser drilled holes is an understanding of the relationship between process parameters, hole quality, and drilling speed.

Laser drilling is a successful manufacturing solution for many industries due to its advantages over conventional drilling techniques. Advantages include non-contact processing, low heat input into the material, flexibility to drill a wide range of materials, accuracy and consistency. Other benefits include drilling sub-micron holes, small holes with large aspect ratios and drilling at angles.

Lasers can also be focused to spot sizes as small as 10 – 20 microns. Coupling the high peak power with short pulse widths, a laser beam offers very good drilling capabilities in thin sheets. The optics configuration is designed to achieve the right spot size required for drilling various hole diameters. High power lasers are also used for rock drilling applications, drilling of flow filters and strainers, sub-micron drilling in flexography ceramic rolls, high-speed drilling of guide vanes, hole drilling of silicon, drilling diamonds for removing imperfections, and on-the-fly drilling of cooling holes.

Laser systems are also used to manufacture micro-holes in fuel injection components, vertical probe cards, metered dose inhaler products, pinholes and slits for scientific instrumentation, inkjet printer nozzles, sensors and detectors, high-resolution circuitry, fuel cells, fiber-optic interconnects, and medical devices. UV and visible laser have been used in drilling small holes in ceramics, diamond, silicon and other semiconductors, polymers, glass, and sapphire. Other shapes of holes are also possible, such as rectangular and other complex geometries [84].

This thesis focuses on trajectory planning for laser drilling of cylindrical holes in turbine engine components. This process occurs through melting and vaporization (also referred to as ‘ablation’) of the workpiece material through absorption of energy from a focused laser beam.

Manufacturers are applying results of process modeling and experimental methods to better understand and control the laser drilling process. The result is higher quality and more productive processes, that in turn lead to better end products such as more fuel-efficient and cleaner burning aircraft and power generating turbine engines. To take full advantage of the

improvements achieved in the process, there is also an urgent need to design suitable motion control trajectories; as targeted in this thesis.

The remainder of this chapter presents a review of literature and industrial practice in the areas of laser drilling, optimal trajectory planning, and sequencing. Prior work conducted in these areas constitutes the background knowledge for the research presented in this thesis.

In Computer Numerical Control (CNC) of machine tools, the toolpath geometry and feedrate (i.e., time-dependent progression along the toolpath) are typically planned as separate tasks. Computationally intensive tasks, such as toolpath parameterization, can be either handled in the Computer Aided Manufacturing (CAM) system or in the pre-processing by the CNC executive kernel. Feedrate generation and feed optimization are coupled tasks within the trajectory generation module of the CNC controller. Reducing machining cycle time along curved toolpaths relies on the ability of the feed optimization algorithm to command the feed motion along a toolpath, so as to drive the machine tool and process within the physical limits, while maximizing productivity.

Compared to traditional machining operations, where the toolpath has to follow a continuous contour, on-the-fly laser drilling poses significantly different technological requirements. This process requires the travel duration between consecutive hole locations, which corresponds to the laser firing period, to be kept constant (or as an integer multiple of the laser pulsing period), and minimized throughout the part program. Motion paths between the holes, however, are not restricted in shape and can be modulated to allow maximum possible reduction in the laser firing period. Since the drilling is realized while the part is in relative motion with respect to the beam, hole elongation also needs to be considered and capped in order to avoid violating the part tolerances. Furthermore, the sequence in which the holes are drilled needs to be optimized to ensure motion efficiency and a shorter drilling cycle time. A machine tool's 5-axis kinematic structure [90], [71] and velocity, acceleration, and jerk limits also need to be taken into account. Some of these issues have been considered and incorporated in the candidate's previous work; namely in generating time-optimized trajectories for given hole sequences and seamless, as well as jerk- and time-optimal, connections between optimized cluster (group of holes) trajectories.

In the process of sequencing for percussion drilling, all machine constraints must also be maintained except for hole elongation, which can be omitted due to the stationary nature of the part during the drilling operation.

The main contributions in this Ph.D. thesis focus primarily on improving the hole drilling sequence and positioning trajectories for both percussion and on-the-fly laser drilling. In the proceeding sections, background literature related to the research points under focus is reviewed.

2.2 Literature on Laser Drilling

Laser drilling provides a highly productive method for producing holes on freeform surfaced parts, especially sheet metal. There have been detailed studies that characterize the process of laser drilling [89], [42] and evaluate various machine configurations [27]. This section provides a brief review of laser drilling methods, as well as advantages and disadvantages.

In laser drilling, a short laser pulse with high power density feeds energy into the work-piece extremely quickly, causing the material to melt and vaporize. Figure 2.1 shows the basics of a laser pulse hitting the surface of a work-piece. The greater the pulse energy, the more material is melted and vaporized. Vaporization causes the material volume in the drilled hole to increase suddenly, creating high pressure. The pressure expels the molten material from the hole. Over the years, several drilling processes have developed from this basic method.

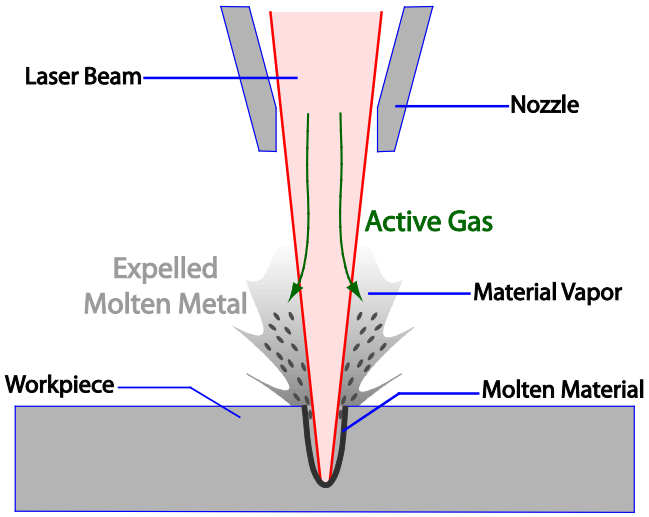

Figure 2.1: How laser drilling works: The laser melts and vaporizes the material. The vapor pressure expels the molten material from the hole.

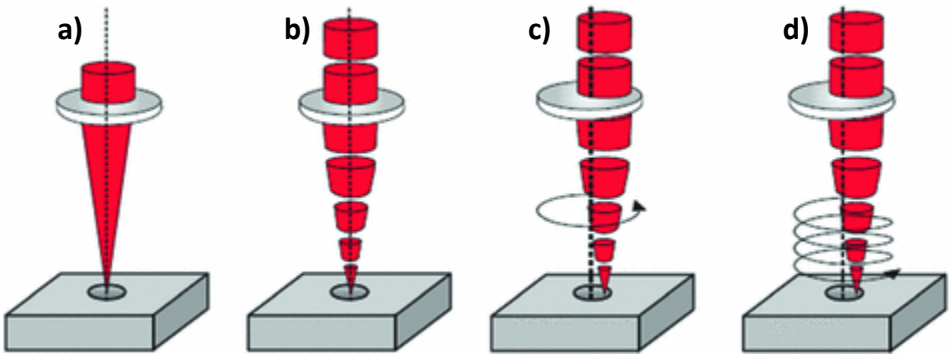

Figure 2.2: Laser drilling techniques: Single pulse drilling, percussion drilling, trepanning, helical drilling (from left to right) [64].

Single-shot and Percussion Drilling: In the simplest case, a single laser pulse with comparatively high pulse energy can be used to produce a hole. This method enables a large number of holes to be created in an extremely short amount of time, compared to mechanical drilling methods. In percussion drilling, the hole is produced using multiple short-duration, low-energy pulses. This technique produces deeper, more precise holes than single-shot drilling, and also enables smaller hole diameters. Figure 2.2a and Figure 2.2b show the difference between single shot versus percussion drilling. On-the-fly laser drilling uses the single-shot laser drilling method while the machine axes are in continuous motion, by reducing the power of the shot and repeating the passes. This way, thermal energy build-up

on the part can be greatly reduced. Thus, deep and narrow holes with excellent dimensional and material quality can be produced by applying on-the-fly drilling with repeated passes. However, the dynamic accuracy of the machine tool's motion is crucial for the successful application of on-the-fly drilling.

Trepanning: Trepanning uses multiple laser pulses to produce the hole. In this process, a pilot hole is first created using percussion drilling. Then the laser enlarges the pilot hole, moving over the work-piece in a series of increasingly larger circles. Most of the molten material is expelled downwards through the hole. Figure 2.2c illustrates this laser drilling method.

Helical Drilling: Unlike trepanning, helical drilling does not involve the creation of a pilot hole. Right from the start, the laser begins moving in circles over the material as the pulses are delivered, with a large amount of material shooting upwards in the process. The laser continues to work its way through the hole in a downward spiral. The beam focus point, meanwhile, can be adjusted so that it is always at the base of the hole. Once the laser has pierced through the material, it can complete a few more revolutions to enlarge the base of the hole and smooth out the edges. Helical drilling makes it possible to produce very large and deep high-quality holes. However, there is persistent thermal loading at the hole bottom, which can have undesirable effects in terms of material properties. This operation is shown in Figure 2.2d.

The two main drilling techniques this thesis focuses on, for trajectory planning, are percussion and on-the-fly laser drilling. These two methods are widely used in the aerospace industry in gas turbine engine production.

General Advantages and Disadvantages of Laser Drilling:

Lasers can be used to drill holes in a variety of materials, ranging from wood and plastics to metals and ceramics. Typical examples of laser drilled holes in practical applications are cooling holes in aero-engine components, holes in fuel injection nozzles, ink-jet printer heads, and micro-via's in PCBs [79][84].

Some of the main advantages of using lasers for drilling are [79]:

- Non-contact technique: The drilling medium is a beam of light, therefore there is no physical contact between (moving) parts and the work-piece. This prevents contamination of the work-piece and (gradual) wear of the drilling part.
- High aspect ratios. With lasers, holes with aspect ratios (depth to width) of, for an example, 30:1 are easily produced.
- Holes at shallow angles: Laser drilling is particularly suited for drilling holes at an angle with the surface of the work-piece, for example, cooling holes in aero-engines. With laser drilling, holes at an angle as small as 10° with the surface can be produced.
- Drilling of difficult to process materials: Lasers can be used to drill a wide range of materials, from rubber and wood, to very hard materials such as diamond and ceramics.
- High speed and accuracy: Laser drilling is fast, accurate and readily automated.
- Availability of photolytic drilling with photolytic processes: (i.e. those involving the breaking of chemical bonds for material removal, rather than melting and evaporation); virtually no recast layer and haze are formed, due to the fact that there is hardly any heat generation in some applications.

Disadvantages of the use of lasers for drilling may be [79]:

- High capital investment: The capital investment needed to purchase or custom develop a laser machine tool can be considerable.
- Thermal effects: Due to heating, a haze (surface thermal reaction and/or collection of expelled molten material – generally resulting in a cloudy and rough surface) may be present around the hole, particularly with pyrolytic processes (i.e. those involving heat generation). Furthermore, thermal shock may lead to micro-cracks in some materials.
- Hole edge and surface quality: With pyrolytic processes, due to the melting and evaporation of material, a recast layer and dross build up at the entrance and exit of the hole may be present. These reduce the repeatability and quality (for example fluid flow characteristics) of the holes.

- Taper in deep holes: Particularly in holes with a large aspect (depth to width) ratio, a considerable taper may be present which may be unacceptable.

2.3 Optimized Trajectory Generation Methods

2.3.1 General Trajectory Optimization

There has been a lot of research in literature in generating optimized trajectories that pass through (or near) given way-points. While some of the research has focused on generating the toolpath (geometry) and feedrate (progression speed) separately, other works have attempted to solve the commanded actuator trajectories directly as a function of time.

In trajectory generation, it is essential to have continuous acceleration profiles, and bounded jerk, in order to avoid generating unwanted high-frequency content in the motion commands. Hence, different jerk bounded [16], [32], [33], [43] and jerk continuous [34], [56], [57], [69], [78], [81] motion planning techniques have been proposed in literature. In addition, when the manufacturing process allows, optimizing the feed profile to minimize the cycle time can result in significant cost savings and productivity increase. Some of the feed optimization work has been pioneered in the robotics and machine tool literature with [10], [13], [58], [82], which at initial stages resulted in acceleration discontinuous trajectories that were fast, but detrimental to production machinery. Later, as jerk and torque rate limits and the cutting process model were considered, various feed and trajectory optimization methods have emerged, which have been shown to be more effective [3], [17], [20], [23], [34], [41], [53], [55], [67], [72], [73], [80], [83], [87]. Some of these methods make some kind of optimality trade-off in favor of faster computational speed, which is often in the form of constraining the feed profile to well-known shapes for an easy mathematical solution, or adopting conservative feed limits based on the worst-case assessment. Elaborate techniques like the one in [3], which utilize full-blown sequential quadratic programming [62], typically yields the shortest cycle times. However, such complicated methods are not always practical for reliable industrial implementation.

There have also been studies to generate quick and smooth actuator trajectories by minimizing the integral square of jerk [48], [49], [68], [76], [77], which has its roots in

characterizing the movement of humans and primates [35]. This idea was first proposed for robotics, and also applied in machine tool feed optimization for generating a parametric feed profile [3].

2.3.2 Candidate's Earlier Research on Trajectory Optimization for 5-axis On-the-fly Laser Drilling

During on-the-fly laser drilling, since the toolpath is not fixed between the hole locations, maintaining a certain feed profile is less of an issue; but coming up with an appropriate trajectory shape that will allow the shortest (quantized) travel durations between consecutive holes, while keeping the relevant kinematic profiles within the machine and process limits, is crucial. Due to the specialized nature of the operation, current Computer Numerical Control (CNC) systems and Computer Aided Design and Manufacturing (CAD/CAM) software do not offer support for on-the-fly laser drilling trajectory generation. Instead, customized solutions are co-developed by end user companies and machine builders, based on the application.

Earlier research conducted by the candidate [4], [29], had focused on developing time-optimized trajectory generation algorithms for traveling through given sequences of waypoints (i.e., hole locations). These sequences were determined using a customized algorithm, similar to the Nearest Neighbor approach explained in Section 2.4. The sequencing algorithm has been developed at P&WC, and its principal details are given in Section 3.3 in order to provide context for the comparative simulation results presented in Chapter 3. Essentially, every next point is determined based on closest proximity using a weighted Euclidean 2-norm in 5-axis coordinates, and each time the distance to the closest next point exceeds a given threshold a new cluster (group of holes) of waypoints is initiated.

Based on these pre-sequenced clusters, the following solution was developed by the candidate in earlier research (which is exemplarily illustrated in Figure 2.3):

Step 1: Trajectory 'shape' optimization: For each cluster of waypoints, the 'shape' of the displacement profile is optimized as a function of time. This is done by modifying the first and second time derivatives at the hole locations so that maximum time compression can be achieved for the displacement profile while holding all kinematic

(velocity, acceleration, jerk, and hole elongation) constraints. This method makes use of the fact that when the timing of the displacement profile is scaled by factor (α), the resulting velocity, acceleration, and jerk profiles are scaled inversely proportionally to the first, second, and third powers of α. During the shape optimization, it is assumed that every laser pulse would be used for drilling a hole within the cluster. Thus, the travel duration between the consecutive hole pairs is kept constant and equal throughout the sequence.

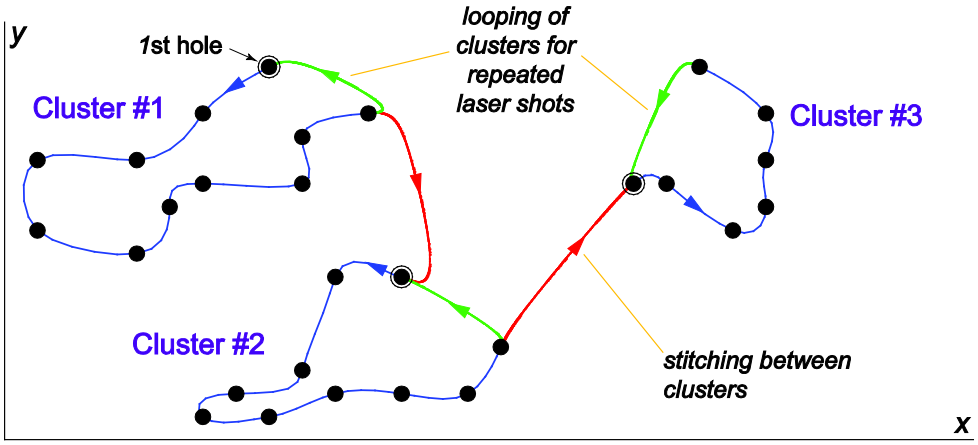

Figure 2.3: Earlier developed strategy by candidate for on-the-fly drilling trajectory generation [4][29], comprising of: 1) Optimizing each hole cluster separately, 2) Looping and stitching of individual clusters using time-optimal connections.

Step 2: Time-optimized looping and stitching of cluster trajectories: As on-the-fly drilled holes require repeated shots, the pre-optimized clusters are connected back onto themselves as required, or time-optimal connections are made to consecutive clusters (when the necessary repeats are complete). The connection trajectories are planned to be integer multiples of the laser pulsing period in terms of duration, anticipating the use of the quick shutter in the optics path to divert unused pulses away during the positioning motion. These trajectories are designed to connect given boundary conditions of position, velocity, and acceleration, while obeying velocity, acceleration, and jerk limits throughout the motion.

In the candidate's earlier work, following the idea of minimum-jerk splines, a 'minimum-snap' quintic spline was used as the initial guess for fitting a spline through the given waypoints. This was followed by profile 'shape optimization' in order to achieve the smallest time scaling factor, hence fastest trajectory for each cluster. This method was successfully applied in the trial production of several gas turbine components. The experimental results had demonstrated 13-46% reduction in the vibrations induced onto the laser optics, and also ~10% improvement in the laser pulsing frequency (i.e., beam positioning time), compared to using the Computer Numerical Control system's existing trajectory planning function. The latter consists of blending linear toolpath segments using smooth corners at the waypoints. However, several issues were also identified with the earlier developed algorithm, as listed in the following. Attempting the resolution of these issues has motivated and guided the majority of the research presented in this thesis.

- For each cluster, a minimum possible laser pulsing period is determined as a result of the displacement profile shape optimization. Upon the optimization of all clusters, the largest overall laser period is adopted for the whole trajectory. This is because time-wise, it is very costly to alter the laser pulsing period on the fly. The power electronics in the current machine tool require a minimum of 40 seconds to discharge and re-charge the capacitors, in order to mount a new laser 'recipe'. Thus, the most critical portion of a single sequence, which dictates a large laser period, ends up slowing down the process for the whole cluster, and thus the whole trajectory. Furthermore, when the sequencing of points is not done optimally, such critical regions emerge more often, which causes major bottlenecks in the productivity of the process. Hence, a profound need was identified to:
    i) Improve the optimality of the sequencing algorithm in a way which considers the temporal nature of the commanded actuator trajectories.
    ii) Enable travel durations between consecutive hole locations to be integer multiples of a laser pulsing period, rather than exactly one pulse, in order to enable further flexibility for slowing down during critical portions of a drilling trajectory, and also being able to go fast when the geometry allows.

- The second issue was that the 'time-optimized' looping and stitching algorithm developed in the earlier work [4], [29], was based on an ad-hoc approach without any optimality proof, or even proof of feasibility. In later benchmarks conducted, this method was seen to sometimes fail. In the sequencing and trajectory planning methods developed in this thesis (Chapter 3), the need to use looping and stitching trajectories has been eliminated altogether, by removing the construction of clusters. However, there is still a need to perform time-optimal connections into and out of the repeating drilling trajectory, from and to rest (stopping) boundary conditions. In this thesis, these connections have been established with optimality proof and also feasibility analysis in Chapter 4, thus addressing the shortcomings of the earlier work.

The combination of the new sequencing algorithm and time-optimal connection methods developed in Chapters 3 and 4 of this thesis have resulted in 55-76% improvement in the motion cycle time over the earlier solution in [4], [29], while staying within the same kinematic limits. The new trajectory planning approach has been published in [30], and is being tested in further production trials at P&WC.

The next section, relevantly, reviews the current state of literature and technology in sequence optimization algorithms.

2.4 Sequencing Algorithms

Different methods have been implemented to produce trajectories through a set of points [14], [27], [86]. The trajectory generation technique developed in earlier work [4], [29] assumes that the holes are already sequenced by the Computer Aided Design/Manufacturing (CAD/CAM) software, and solves the time-optimal solution for traversing these holes on-the-fly.

Hole sequencing techniques can also be related to the *Vehicle Routing Problem*, which was introduced more than 50 years ago in "The Truck Dispatching Problem" by Dantzig and Ramser [19], [50].

In Chakraborty et al. [14], the sequence optimization problem is applied to robotics, with full stop trajectory planning at given waypoints. In this case, the distance minimization of the path planning problem is effectively equivalent to the time minimization problem with

appropriately chosen velocity profiles, since the robot velocities in independent axes are decoupled.

[86] solves a general time-optimal trajectory problem in the presence of obstacles, but does not take into account the process constraints, as such would be found in laser drilling like fixed laser pulsing frequency, or hole elongation limit. It deals with the problem of determining the optimum route for an end effector that visits a number of task points in a similar, but not identical fashion to the well-known traveling salesman problem (TSP) [6]. The authors suggest that the measure to be optimized is time instead of distance, and that the travel time between two points is significantly affected by the manipulator configuration. Therefore, solutions to the inverse kinematics problem need to be taken into consideration. [17] provides process models and trajectory planning techniques for preserving sharp cornered geometries during laser cutting.

As previously determined, the problem of finding the optimum sequence of a manipulator's task points can be considered as an extension of the well-known traveling salesman problem (TSP) [51]. The TSP is one of the most widely studied and discussed problems in combinatorial optimization [36], [65]. The salesman has to visit exactly once each one of a finite number of cities and return to the starting city. Given the distances between the cities, the objective of the optimization is to find the optimum total tour the salesman should follow.

Solving a TSP can also consider a manipulator's or machine tool's kinematic constraints [44]. Adapting TSP to 5-axis laser drilling, the measure to be minimized is time instead of distance. In other words, the challenge is to determine the path which ensures that the laser focal point passes through the hole locations, with the correct orientation, with the minimum possible cycle time. The machine axis velocity, X-Y plane hole elongation limit, acceleration and jerk limits need to be considered to prevent any constraint violation in the case of on-the-fly drilling. For percussion drilling, only the axes' velocity, acceleration and jerk limits need to be considered while moving between consecutive holes. Also, the duration between consecutive hole pairs can be variable, but has to be an integer multiple of the laser pulsing period[1].

[1] In between the holes, the laser can be diverted away from the workpiece using a quick-activated shutter.

Several optimization techniques have been proposed to determine the minimum cycle time of a manipulator visiting a number of task points. The most prominent of these techniques are presented and discussed in the following.

Little's algorithm [54] is a "branch and bound" method presented to solve the traveling salesman problem. The set of all tours (feasible solutions) is broken up into increasingly small subsets by a procedure called branching. For each subset, a lower bound on the length of the tours therein is calculated. Eventually, a subset is found which contains a single tour whose length is less than or equal to some lower bound for every tour. Dubowsky and Blubaugh [24] used Little's algorithm to determine the minimum time to accomplish a manipulator task. The authors solved the TSP by distinguishing three cases. They solved the TSP where the task points may be visited in any order and tested their algorithm using a PUMA 260 manipulator, which had to 'visit' six points. In the second case, they solved the TSP, where some points may be visited in any sequence, and whereas some others must be visited in an exact sequence. Lastly, they investigated tasks which are not in the usual TSP form, including those where the manipulator has to change its tools during an operation. In all these TSP-type problems, the computation time required was quite reasonable for the current application. However, there was no reference to the multiple solutions of the inverse kinematics problem. Also, if the group of points to be visited was to be increased (such as in the laser drilling problem studied in this thesis), the processing time grows roughly exponentially [91]. Therefore, larger problems appear to be less suitable for Little's algorithm.

Abdel-Malek and Li [2] developed a method for finding the optimum sequencing of robotic task performance. They introduced the application of inverse kinematics in determining the sequence that minimizes the cycle time in a robot cell. In their work, an extension of the Travelling Salesman Algorithm as solved by [37], [40], which uses a more efficient branch and bound based method, was found to be suitable for obtaining optimized sequences and cycle times. The kinematic structure of the robot affects the time spent traveling between any two particular points. The travel time between any two points replaces the distance between the nodes that is then entered in a table providing the necessary input for the Travelling Salesman Algorithm. This algorithm addresses problems only when the robot starts and stops at given way-points. Hence, in the context of this thesis could be

suitable for percussion laser drilling. It does not, however, consider motions with non-zero velocity and acceleration connections at the waypoints; and thus cannot be used for on-the-fly laser drilling.

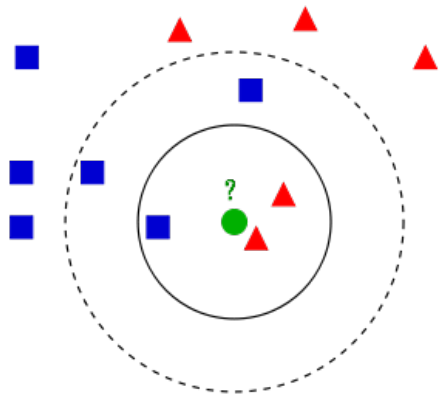

Figure 2.4: Nearest neighbor (NN) search method.

In pattern recognition, the Nearest Neighbor algorithm (NN) is a non-parametric method for classifying objects based on closest training examples in the feature space. This reduces the computational time and converges well, even for a large number of points. The selection method of the NN algorithm is displayed in Figure 2.4. NN was one of the first algorithms used to determine a solution to the TSP. In it, the salesman starts at a random city and repeatedly visits the nearest city until all cities have been visited. The algorithm is easy to implement and executes quickly, but due to its "greedy" nature [7], [9], [38] it can sometimes miss shorter routes which are easily noticed with human insight. Edan et al. [26] applied the NN algorithm for fruit-harvesting robots in order to find the near-optimum-time path between fruit locations. The work focused mainly on assessing the influence of the robot's kinematic and dynamic parameters and spatial distribution of fruit on the motion sequence. Thus, the goal was not primarily time-optimized motion, but rather selection of the most efficient robot design for a robot having to perform a sequence of tasks at given known locations.

Shin and Mckay [75] have shown that the total time t_c to pass along the path between two points is proportional to the geodesic distance (A travel distance along a curved surface or a sphere) S. So, the cost function was defined as the distance along the geodesic in the

inertia space, since calculating the geodesic distance in this space is equivalent to calculating time. Furthermore, the suggested algorithm takes into account the kinematic and dynamic properties of the robot when determining the path through the task points, ***and shows, in some instances, that minimum time is not in general equivalent to the minimum distance.***

Simulated annealing (SA) is a random-search method for finding the global minimum of a cost function that may possess several local minima. A random perturbation with decreasing amplitude is applied to heuristically taken logical decisions. SA was developed to deal with highly nonlinear problems and approaches the global minimization (or maximization) problem similarly to using a bouncing ball that can bounce over mountains from valley to valley [12]. Dissanayake and Gal [22] used SA for determining a near-optimum sequence of travel for redundant manipulators. Because of the non-linearity of the optimization problem, the method of sequential quadratic programming is used to find the robot's optimum configurations and the optimum location in the work cell for a given sequence of tasks. Overall, SA is a robust technique that performs well in solving complex problems and does not need much computational time when the number of the task points is less than 10. However, this is much less than the number of waypoints points dealt with in this thesis, which is typically in the order of hundreds to thousands for laser drilling of jet engine components.

The Elastic Net Method (ENM) of Durbin and Willshaw [25] is another successful approach to solving the TSP. The elastic net can be thought of as a number of beads connected by elastic bands to form a ring. The essence of the method is to iteratively elongate the closed path in a non-uniform way until it eventually passes sufficiently near all the ‘cities’ that define a tour. Each point on the path moves under the influence of two types of force:

1. The first type of force moves a point towards the cities to which it is nearest.
2. The second type of force pulls the point towards its neighbors on the path, acting to minimize the total path length.

By this process, each city becomes associated with a particular section on the path. The tightness of the association is determined by how the force contributed from a city depends on its distance, and the nature of this dependence changes as the algorithm progresses. Initially, all cities have roughly equal influence on each point of the path. Subsequently, a

larger distance becomes less favored and each city gradually gets more influential on the points on the path closest to it. Figure 2.5 illustrates the progression of the elastic net method as applied to the traveling salesman problem for 100 cities.

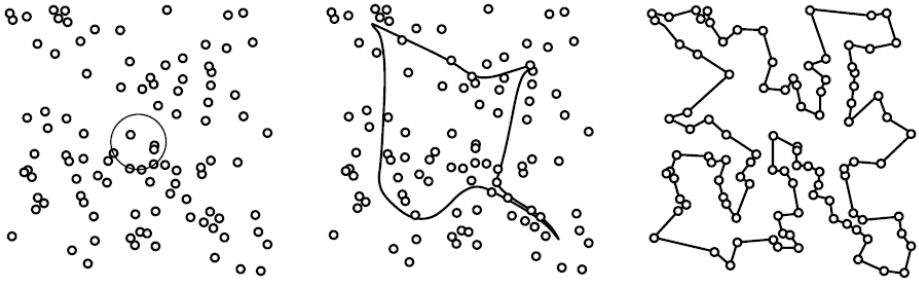

Figure 2.5: ENM progression in the TSP with 100 points [25], [38].

Petiot et al. [66] used the elastic net method to minimize the cycle time of robotic tasks. The method is well adapted to the problem of finding the optimum sequence of a manipulator's end effector movements from point to point. This is achieved by minimizing an energy function E using a modified gradient method. However, the algorithm may not converge due to the wrong choice of the parameters, and this is reported in [66] for 5% of the tests. Furthermore, benchmarking this method with another approach, such as Dubowski's method applying Little's algorithm, comparable results were obtained. Attempts to reduce the computation time of the ENM for TSP have been made by Junyan et al. [45], but still this application lacks the direct minimization of total cycle time due to the lack of direct translation between distance and actual cycle time for the general case of robotic manipulators.

In literature, the algorithms mentioned in the previous paragraphs have been tested for 2- and 3-DOF manipulators with the observation that the cost cannot be easily generalized as distance, due to the complicated and time consuming evaluations of kinematic models as machines increase in degree of freedom and in complexity. While these algorithms do not require too much time to find the optimum solution for a number of points up to 10; the computational time significantly increases for more than 10 points, and in some cases, convergence may become an issue [86], [91].

The gold standard in TSP has emerged as a collection of some of the most powerful algorithms developed so far, which have been implemented and clustered inside a software library named the 'Concorde TSP Solver' under the direction of Prof. W. Cook [18]. As new TSP algorithms are developed, they are typically benchmarked with respect to this package and several solution methods have been implemented and integrated systematically. These include: the TSP Cutting Planes Method, which has its roots in formulating the TSP as a Linear Programming relaxation problem, the Lin-Kernighan Heuristic [74], which is based on implementing optimized 2-, 3-, and higher numbers of segment swaps to the travel path in search of incremental improvements to the overall path, branch-and-bound based methods, which pre-establish lower bounds on the fitness values of possible solutions that proceed a current decision step, and various other heuristics as well. The Concorde library includes over 700 functions, permitting users to create specialized codes for TSP-like problems, and currently is available as an executable function with a Graphical User Interface (GUI). The GUI enables benchmarks to be conducted for x-y plane datasets, based on minimizing the travel distance.

Within the context of this thesis, the Concorde library has been used in Chapter 5 to conduct benchmarks with the proposed sequencing method that was developed for percussion laser drilling. However, benchmarks were conducted only for x-y plane data and considering the minimization of travel distance rather than time. In future research, the intention is to adapt the Concorde solver to work directly with travel duration data, which is pre-computed by generating time-optimal trajectories between every possible way-point pair, based on the 5-axis kinematics and velocity, acceleration, and jerk limits of the laser drilling machine tool, as explained in Chapter 4.

As for on-the-fly laser drilling, since the sequence and timing between the waypoints (i.e., hole locations) profoundly impacts the temporal (time-dependent) nature of the commanded actuator trajectory, including the velocity, acceleration, and jerk characteristics, it seems more difficult to directly adapt the Concorde library to this process. Sequencing for on-the-fly drilling cannot be implemented based on distance alone. Thus, in future research, as the Concorde routines are better learned and understood, it should be possible to integrate polynomial trajectory planning within the objective function calculation following the methodology explained in Chapter 3.

2.5 Conclusion

This chapter has provided a review of literature covering the topics of laser drilling, optimal trajectory planning, and sequencing. The main and novel accomplishment in this thesis is the development of integrated optimal trajectory planning and sequencing algorithms, which also consider knowledge of the machine kinematics and process constraints, in order to improve the productivity and part quality in 5-axis laser drilling operations. Aerospace component manufacturing is chosen as an application example, however as outlined at the beginning of this chapter, the resulting algorithms can also be extended to a vast array of other laser drilling applications as well.

Chapter 3

Time-Optimized Hole Sequence and Joint Trajectory Planning for 5-Axis On-the-Fly Laser Drilling

3.1 Overview

On-the-fly laser drilling requires the use of acceleration continuous trajectories, which are typically planned using time parameterized spline functions, such as the ones used in [4] and [29]. In this operation, the choice of hole drilling sequence and positioning timings in between the holes play a critical role in determining the achievable cycle time. This chapter presents a new algorithm for sequencing 5-axis on-the-fly laser drilling hole locations and timings. The algorithm considers machine tool and process constraints, as well as the temporal nature of the final commanded spline trajectory. The achievable productivity and motion smoothness improvement are demonstrated in the production of gas turbine combustion chamber panels. Simulation results comparing the proposed approach with the earlier solution of the modified Nearest Neighbour (NN) based sequencing [28] and trajectory shape optimization [29] are presented for on-the-fly laser drilling of three combustion chamber panel examples. This is followed by experimental results, comparing the proposed approach with two trajectory generation methods that are currently in use in industry.

The hole sequencing task resembles the Traveling Salesman Problem (TSP) known from combinatorial mathematics [6], where a minimum-cost, e.g. travel distance, connection needs to be found that passes through all given waypoints only once. However, there are aspects of on-the-fly laser drilling that make the problem different and possibly more challenging than the classical TSP:

1. Since the final trajectory will be a spline that smoothly connects the sequenced waypoints, the travel durations in between the holes (which strongly influence the spline parameterization) have to be carefully selected. *Hence the sequencing algorithm has to solve for both the order of the waypoints and also the timings in between.* If there are multiple laser pulses between two consecutive holes, the extra

pulses in between the positioning are directed away from the workpiece using a controlled quick shutter in the optics path.

2. The objective is to minimize the drilling cycle time while adhering to the machine tool and process constraints. *Therefore, the temporal nature of the final spline trajectory needs to be considered, along with the machine kinematic configuration, as well as the machine's feed drive limits and the process related limits.*

For a part with only M (=10) holes and k (=5) possible timing levels, there can be $M!\times k^M$ ($\sim 3.54\times 10^{13}$) trajectory sequences. In gas turbine combustion chamber panels, the number of holes may vary between hundreds to thousands. Hence, the need for an efficient and effective sequencing method has been the motivation behind the heuristic algorithm presented henceforth in this chapter.

3.2 Proposed Sequencing Algorithm

The inputs to the proposed sequencing algorithm are the hole locations $\boldsymbol{q}_k \left(k = 1 \ldots M\right)$ defined in joint (actuator) coordinates $\boldsymbol{q} = \left[x \;\; y \;\; z \;\; a \;\; c\right]^T$; the feed drives' velocity, acceleration, and jerk limits; and the hole elongation velocity limit. For a clear presentation of the algorithm, the candidate evaluation is explained first in Section 3.2.1. This is followed by the steps of the proposed sequencing algorithm in Section 3.2.2. Throughout the chapter, the implementation is described in sufficient detail to enable thorough replication of the proposed idea. Lengthy equations, however, are avoided for the sake of brevity. Instead, they are provided in the related appendices at the end of this thesis.

3.2.1 Candidate Sequence Evaluation

Considering Figure 3.1, for a candidate sequence with N elements, the optimization variables are the order of the waypoints ($\boldsymbol{S}$) and the timings in between ($\boldsymbol{P}$) (measured in number of laser pulses). Since on-the-fly drilling needs the positioning trajectory to repeat itself, preferably without coming to a full stop, the closed cubic spline has been the natural choice for the trajectory curve. It is acceleration continuous (i.e., jerk limited) and a very

efficient solve. The implemented closed cubic spline formulation has been presented in Appendix A.

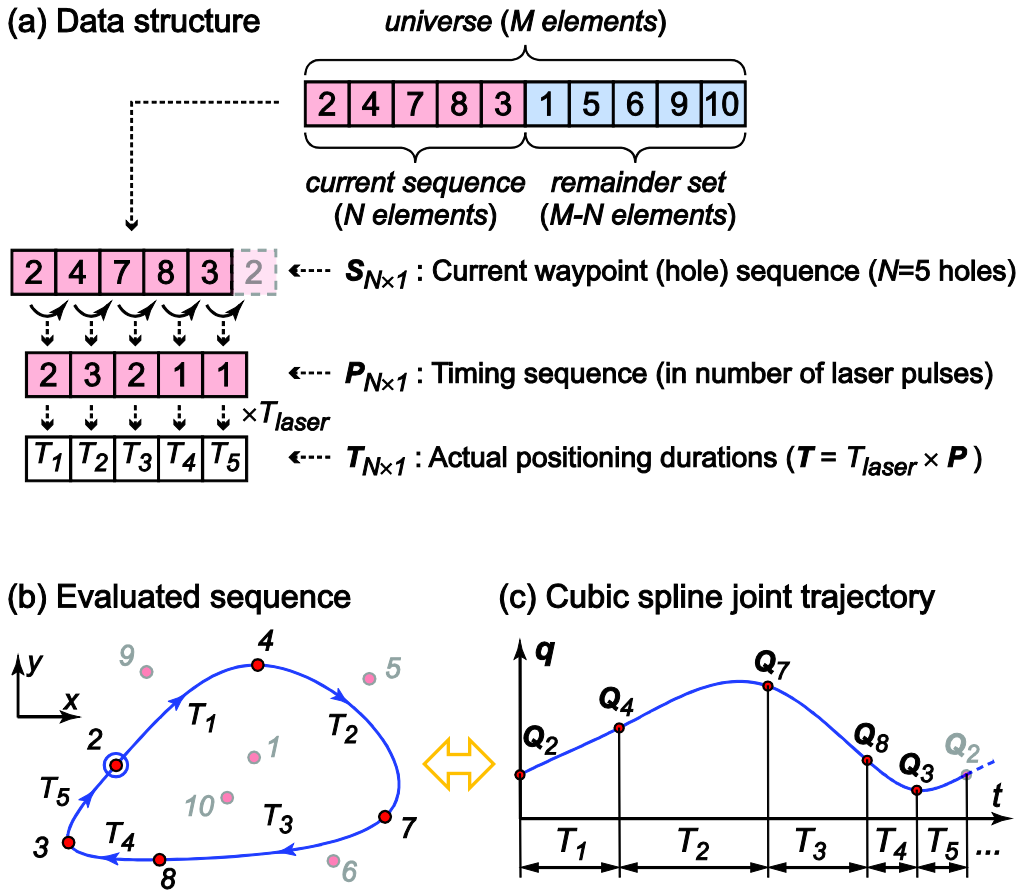

Figure 3.1: Data structure and candidate sequence evaluation.

The closed cubic trajectory is computed by setting up a system of N linear equations, in which the unknowns are actuator velocities ($\boldsymbol{V}_j$) at hole locations (i.e., $\boldsymbol{L}(T)\cdot\boldsymbol{V}_j = \boldsymbol{\xi}_j$, $j = x, y, z, a, c$). Since, $\boldsymbol{L}(\boldsymbol{T})$ is block diagonal and common to all axes, the calculations are accelerated by re-using its inverse to solve the command profiles for all of the axes. The cubic has piecewise constant jerk, linear acceleration, and parabolic velocity in each segment, thus allowing the peak jerk, acceleration, and velocity values to be evaluated analytically without requiring interpolation, as shown in Appendix B. The velocity component v_{xy} at the drilling location (Figure 1.3), which influences hole elongation, is also calculated from the spline coefficients and by considering the machine tool kinematics. The 5-axis laser drilling

machine tool kinematics, and the calculation of the relative velocity component v_{xy}, are presented in Appendix C.

During each sequence evaluation, the cubic spline is first constructed assuming a unit laser pulsing period (T_{laser} = 1 s) in computing the initial segment durations ($\boldsymbol{T} = T_{laser} \times \boldsymbol{P}$). Afterwards, time scaling is applied to the whole trajectory by updating the laser pulsing period to T'_{laser}, such that:

1. All of the profiles for actuator velocity, acceleration, and jerk are within their designated limits. Also, v_{xy} is limited at the drilling instances. The smallest possible time scaling factor $\alpha_{\min}$, which ensures that all of the kinematic profiles are within their bounds, and that at least one of them reaches its limit, is determined by considering that time scaling by α leads to velocity, acceleration, and jerk scaling by α^{-1}, α^{-2} and α^{-3}, respectively. The effect of time scaling on the derivatives of the trajectory profile is explained in Appendix D. After computing $\alpha_{\min}$, T'_{laser} is chosen as $T'_{laser} \geq \alpha_{\min}$.
2. T'_{laser} has to be above a certain minimum duration $T_{\min}$ (≅ 27 ms) required for the quick shutter in the optics path to engage and disengage. The quick shutter serves to divert the laser away from the workpiece when the positioning duration is longer than a single laser pulsing period.
3. $1/T'_{laser}$ has to be an integer frequency in Hertz. This is a programming requirement for the laser control power electronics.

After these adjustments are implemented, the final segment durations are computed as ($\boldsymbol{T} = T'_{laser} \times \boldsymbol{P}$). Time scaling is applied to the earlier fit spline, by multiplying the third, second, and first degree coefficients by $(1/T'_{laser})^3$, $(1/T'_{laser})^2$, and $(1/T'_{laser})$, respectively. This avoids the need to re-fit the cubic trajectory.

The objective function in evaluating a candidate sequence is defined as the time required to complete one full pass of the on-the-fly drilling trajectory while adhering to all of the constraints given in Eq. (1.1);

$$\textit{Objective Function :} \quad T_{tot} = T_1 + T_2 + \ldots + T_N \tag{3.1}$$

Minimizing this duration enables the minimization of the part cycle time.

Here, as the machine constraints, actuator velocity, acceleration, and jerk limits are considered, as they can be conveniently determined from the machine's Computer Numerical Control (CNC) system. If a dynamic model of the drive system is available, then torque/force limits can also be included into the update of T'_{laser}, following an approach similar to [3] [10] [17].

3.2.2 Proposed Sequencing Algorithm

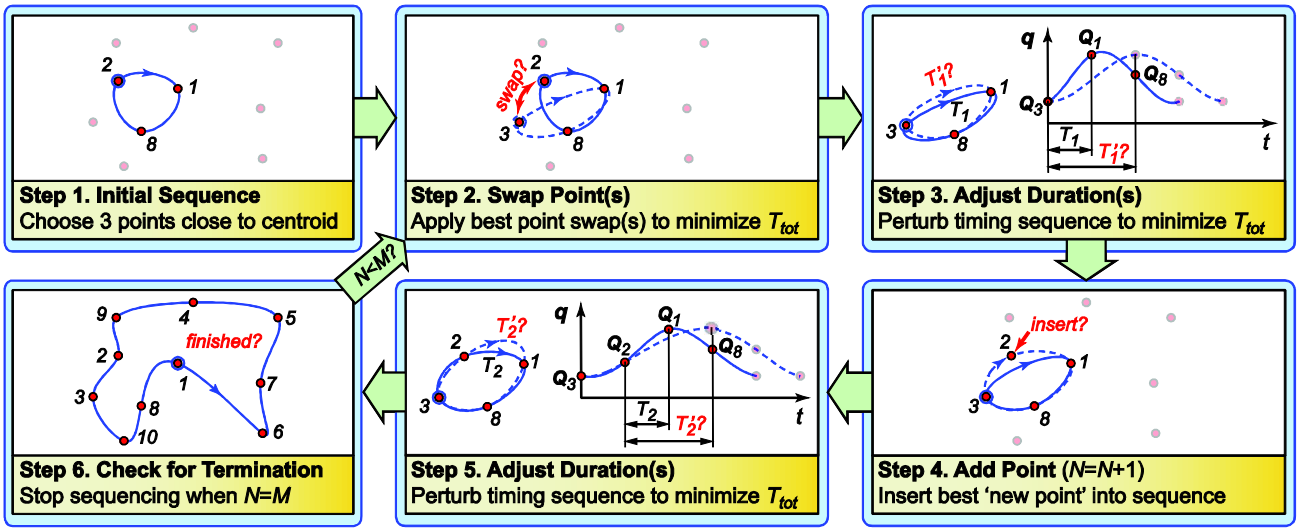

Figure 3.2: Proposed waypoint and duration sequencing algorithm.

An overview of the proposed waypoint and duration sequencing algorithm in shown in Figure 3.2. The details of each step of the algorithm are explained in the following.

Step 1 - Initial Sequence

The initial sequence $\boldsymbol{S}$ is chosen to include one hole that is closest to the centroid of the given set of M holes, and two additional holes that are closest to this hole. Distances in 5-axis joint space are computed by normalizing the axis coordinates with respect to a 'characteristic distance' specific to each axis, and then applying the Euclidean norm, as shown in Eq. (3.2). The 'characteristic distance' is defined as the displacement required to accelerate an axis from rest to maximum velocity, while utilizing the maximum acceleration

and jerk capabilities of that axis, as illustrated in Figure. 3.3. Its computation can be established following a procedure similar to that in Appendix F.

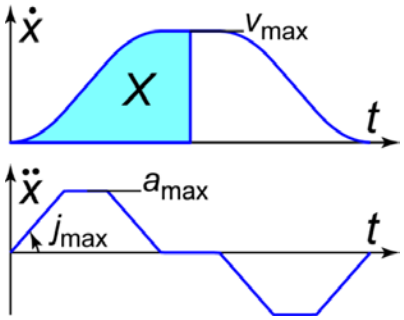

Figure 3.3: Computation of the characteristic distance for an axis 'x'.

Naming the characteristic distances in the joint space as X, Y, Z, A, and C, the normalized coordinates ($\boldsymbol{q}^n$), and normalized distances (d_{ij}^n) between points i and j, are obtained as:

$$\mathbf{q}^n = [x/X \quad y/Y \quad z/Z \quad a/A \quad c/C]^T \quad , \quad d_{ij}^n = \left\| \mathbf{q}_i^n - \mathbf{q}_j^n \right\|_2 \tag{3.2}$$

This normalization allows for feed drives with different velocity, acceleration, and jerk capabilities to be considered in a somewhat balanced manner when evaluating approximate travel durations.

During the initialization of the algorithm, a table of normalized Euclidean distances between every possible hole pair is constructed. Considering the distance between the closest two holes (Δ), when setting up the initial duration sequence $\boldsymbol{P}$, it is assumed that this distance would be traveled in one laser period and other normalized distances between adjacent points in the sequence would require proportionally longer durations. These durations are then rounded to the nearest integer values, representing durations in terms of number of laser pulses. Also, for each hole location in the given universe set, a list of the remaining $M-1$ holes, ordered according to increasing normalized distance, is constructed. Once initial $\boldsymbol{S}$ and $\boldsymbol{P}$ are determined, the candidate sequence is evaluated as described in Section 3.2.1.

Step 2 - Swap Point(s)

For each point in the sequence, swaps with the neighborhood of closest V points (within or outside the sequence) are evaluated. In the implementation, V was chosen as 20. If any of these swaps reduce T_{tot}, then the swap that yields the lowest cycle time is implemented. Testing of another round of swaps continues on until no further improvement can be obtained. During a swap, the travel durations that already exist between adjacent points are preserved. Durations for new point connections (i.e., 'edges') (p'_{ij}), which did not exist before, are assigned by considering the ratio of their respective normalized distances to the average normalized speed ($\bar{v}^n$) for the 'pre-swap' sequence. Hence, $\bar{v}^n$ and p'_{ij} are defined as:

$$\bar{v}^n = \frac{\{\text{sum of normalized distances between sequenced points}\}}{\{\text{sum of segment durations in number of laser pulsing periods}\}} \quad , \quad p'_{ij} = d^n_{ij} / \bar{v}^n \qquad (3.3)$$

The outcome durations for the newly inserted edges are then rounded to the nearest integers, as done in Step 1. Hence, $p_{ij} = \text{round}(p'_{ij})$.

Step 3 - Adjust Duration(s)

Further cycle time improvement is sought by perturbing the integer travel durations in $\boldsymbol{P}$. Similar to the swapping step, the perturbation that yields the smallest T_{tot} is implemented, and the testing of duration perturbations continues on until no further improvement can be obtained. It is important to note that the duration adjustment is not just a matter of reducing the number of laser pulses per segment. Sometimes, increasing the travel duration for an edge, in relation to the other edges, can help smoothen the shape of the kinematic (i.e. acceleration and jerk) profiles, thus allowing the overall trajectory to be traveled at an accelerated rate (i.e. smaller laser period).

A 1-element perturbation mask with a maximum magnitude of 1 laser period can have 2 possibilities; {+1} or {-1}. These can be applied at any of the N durations (for the connecting edges) within the sequence. If a negative perturbation yields a zero segment duration, this is bumped back up to one laser period. Similarly, the set of 2-element masks (excluding those that can be constructed with the 1-element mask) are: {-1,-1}, {-1,+1}, {+1,-1}, {+1,+1}. These, together with the 1-element case, lead to $(2+4)N$ possible

perturbations. Generalizing on this idea, scanning up to an *r*-element mask, limited only to one pulse sized perturbations, requires $[2+4\sum_{k=2\ldots r}3^{k-2}]N$ possibilities to be checked (as demonstrated in Appendix E).

While developing the sequencing algorithm, the capability to test perturbations up to 6-elements was implemented. This results in 486*N* possibilities for each round of testing. However, it was observed that over-structuring the timing perturbation led the sequence to lock in early on to a sub-optimal shape. This prevented useful future point swaps from being found and implemented. Through trial and error, it was determined that a 1-element mask led to the most suitable performance in terms of enabling the algorithm to continue on making useful improvements as the sequence size increased. The possibility of implementing complex perturbations with elements larger than one laser period was also not tried out, due to this early observation. However, this is an idea that is worth investigating further in future research.

Details on the timing perturbation masks that were implemented and tested, and calculation of the number of possible cases are presented in Appendix E.

Step 4 - Add Point

The 'best point' out of those not already in the sequence is inserted into the 'best location' in the sequence. For each edge connecting adjacent points $\boldsymbol{S}(k)$ and $\boldsymbol{S}(k+1)$, insertion of the nearest external V (=20) points is evaluated. Existing travel durations are inherited from the 'pre-add' state, and new durations to and from the inserted point are constructed using the procedure for new edge insertion, as explained in Step 2. The point insertion that yields the lowest T_{tot} among those tested is actually implemented.

Step 5 - Adjust Duration(s)

The procedure in this step is identical to the one in Step 3, which enables the timings to be improved as much as possible before moving on to point swaps once again.

Step 6 - Check for Termination

After Step 5, when $N = M$, this means that all waypoints and timings have been sequenced. While a global optimum is very difficult to guarantee, the search procedure ensures that the intermediate solutions are always improvements from and towards local optima.

Practical Implementation Considerations

In the implementation of the algorithm, logic was incorporated into Steps 2, 3, and 5 to ensure that identical candidate sequences would not be re-evaluated; in order to save computational time. Also, time optimal connections into and out of the final cyclic trajectory were generated, to ensure that the overall NC code would start and terminate with all of the axes being at rest, as illustrated in Figure 3.4. The computation of these trajectories has been detailed in Chapter 4.

Upon finalization of the sequence and connection trajectories, the resulting time-parameterized cubic spline trajectory is interpolated at a frequency of 160 Hz, which can be executed on the machine tool's existing CNC system, e.g., a Fanuc 30i, using 'inverse-time' feed programming mode. In inverse-time feed mode, the destination points and travel durations are provided within the part program. In experimental implementation, it was observed that if the duration between the destination points was kept small enough (e.g., 6.25 ms), the CNC does not try to plan a new feed (tangential velocity) profile along each segment in the toolpath, but rather seems to transfer the temporal data points directly to the feed drive controllers. At this level, the planned trajectory is typically re-sampled at the servo loop closure frequency using time parameterized cubic B-spline interpolation; which is a common approach followed in CNC architectures. This retains the originally planned velocity, acceleration, and jerk profiles in the motion commands, which are re-interpolated at a higher frequency.

While Fanuc controller documentation does not specifically disclose the operational details of the CNC and drives, the experimental observations confirmed that the planned trajectories were being executed with the expected cycle times, while performing the programmed motions without any unexpected jerkiness, thus validating these hypotheses. Of

course, further validation using motion capture equipment (like accelerometers) would be helpful in future research, to further confirm these assumptions and observations.

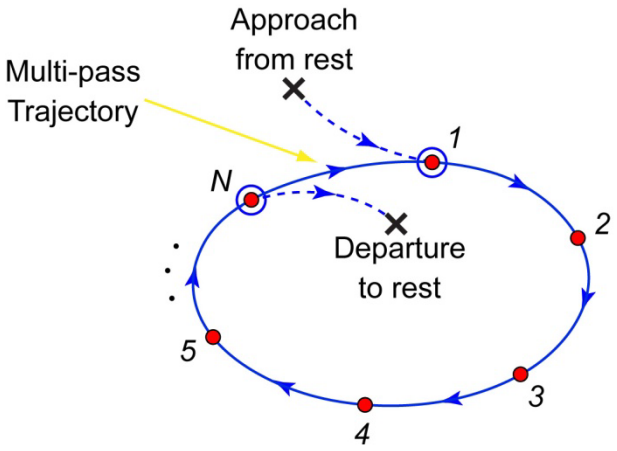

Figure 3.4: Approach to and departure from sequenced closed cubic spline drilling trajectory.

3.3 Simulation Results

The proposed sequencing and joint trajectory planning algorithm has been benchmarked in simulations to the method of applying a modified Nearest Neighbor (NN) [28] sequencing algorithm, followed by an optimal trajectory planning method [29] which was developed by the author in earlier Master's thesis research.

NN sequencing is currently the method used at the sponsoring company (P&WC) for planning on-the-fly and percussion laser drilling operations. The steps of the NN sequencing method in use are as follows:

i. The starting point (i.e., first hole to be drilled) is chosen by the process planner.

ii. Distances to neighboring points are calculated in joint coordinates using a weighted approach Euclidean norm,

($R = \sqrt{\alpha(\Delta x)^2 + \alpha(\Delta y)^2 + \alpha(\Delta z)^2 + \beta(\Delta a)^2 + \beta(\Delta c)^2}$) the weights α and β are used to combine the translational and rotational degrees of freedom in one single measure of distance.

iii. The 'new point' in the sequence is chosen as the hole location with the smallest 'R' value with respect to the current one.

iv. If the weighted distance to the nearest un-sequenced point exceeds a certain threshold ($R_{\max}$), a new cluster is initiated.

The values of α , β , and $R_{\max}$ are set by P&WC process planners, and have not been disclosed by the company. However, the drilling sequences produced with this algorithm have been made available and used in this thesis for benchmarking purposes.

In earlier work, sequences produced with the above NN procedure were used as input waypoints for the trajectory optimization approach in [29]. This method would fit quintic splines which pass through the given waypoints in a manner that the first and second derivative boundary conditions at the hole locations are optimized, in order to allow these trajectories to be traversed in minimum time.

Since there are no existing machine tool or robotic trajectory planners specifically developed for 5-axis on-the-fly laser drilling (Chapter 2), the combination of [28] and [29] can be regarded as the state-of-art prior to the research reported in this thesis; in terms of providing the best accuracy and smoothness in the commanded trajectory. Another approach used at P&WC for on-the-fly drilling is to apply NN sequencing followed by interpolating the hole location commands as blended linear motion segments. This approach, unfortunately, suffers from distortion of the toolpath away from the target drilling points due to the corner rounding, and also leads to unnecessary acceleration and jerk content in the commanded profiles. Thus, its evaluation has been kept outside of the simulation studies, but has been included into the experimental benchmarks for practical validation purposes.

The simulation benchmarking has been carried out based on three different gas turbine combustion chamber panel components, with 567, 284 and 474 hole locations respectively. The hole configurations for the three sample parts are shown in Figure 3.5. Hole clusters which were sequenced by the NN algorithm, as implemented at P&WC, and sample sequences for a single cluster are also shown in the same figure. The machine and process limits which have been used in the simulation studies have been summarized in Table 3.1. While the actual velocity, acceleration, and jerk limits for the laser drilling machine tool and process are different than those in this table, and not disclosed by P&WC, the limits considered in the table can be regarded as being reasonably representative of the capabilities of current 5-axis machine tools applying a typical laser drilling scenario.

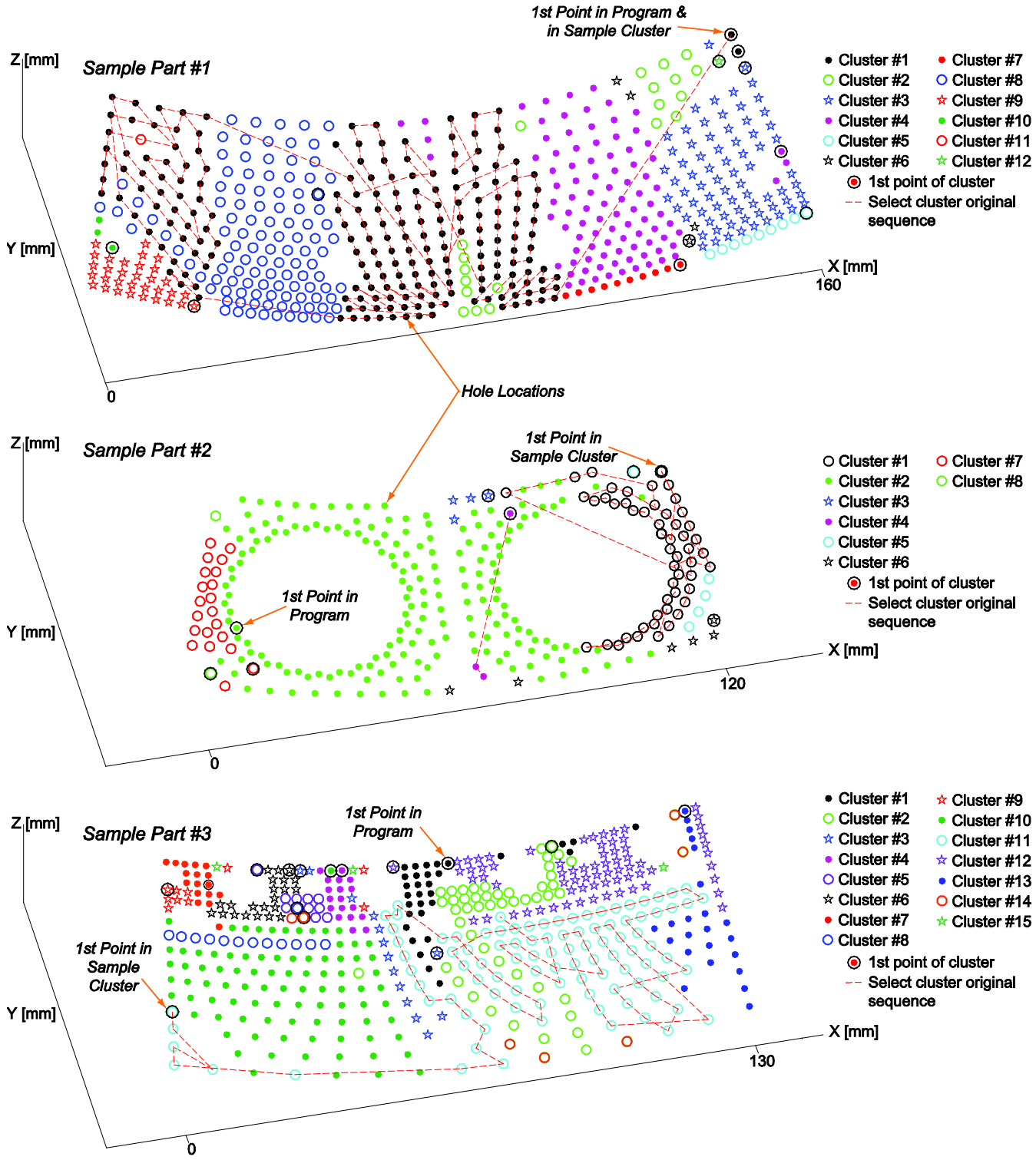

Figure 3.5: Hole configurations for three different gas turbine engine combustion chamber panels, shown in part (Cartesian) coordinates. Clusters and sample hole sequencing are also shown.

Table 3.1: Machine and process kinematic limits considered in simulation studies.

	X-Axis	**Y-Axis**	**Z-Axis**	**A-Axis**	**C-Axis**
Velocity	0.5 m/s	0.5 m/s	0.5 m/s	400 deg/s	600 deg/s
Acceleration	10 m/s^2	10 m/s^2	10 m/s^2	10000 deg/s^2	12000 deg/s^2
Jerk	400 m/s^3	400 m/s^3	400 m/s^3	400000 deg/s^3	600000 deg/s^3
Hole elongation (v_{xy}) velocity limit				0.2 m/s	

The sequencing algorithm was implemented as compiled Matlab code and executed on an Intel Core i5 2410M computer with 8 GB RAM, running Windows 7. Completion of the sequencing for the three parts took:

- For sample part #1 (567 Points): 12.22 hr.
- For sample part #2 (284 Points): 4.68 hr.
- For sample part #3 (474 Points): 20.19 hr.

For off-line process planning for gas turbine components which are to be manufactured in large quantities, this kind of computational time can be acceptable. Many of the operations in the sequence optimization algorithm, such as candidate sequence evaluation, can also be implemented in parallel. Thus, if needed it would be possible to significantly reduce the computational time by distributing these calculations over a parallel processing architecture.

The progression of the algorithm in terms of swap and time perturbation operations is shown for the three sample parts in Figure 3.6. As can be seen, useful swaps (> 1) and time perturbations (> 2) regularly take place throughout the convergence, thereby preventing the final trajectory from being ‘stuck’ in a sub-optimal shape. It is interesting to note that while sample part #3 possesses a lower number of holes than sample part #1, its computation has taken longer. One reason for this may be the larger number of duration perturbation steps which have been tested in the sequence optimization for this part, as seen in Figure 3.6.

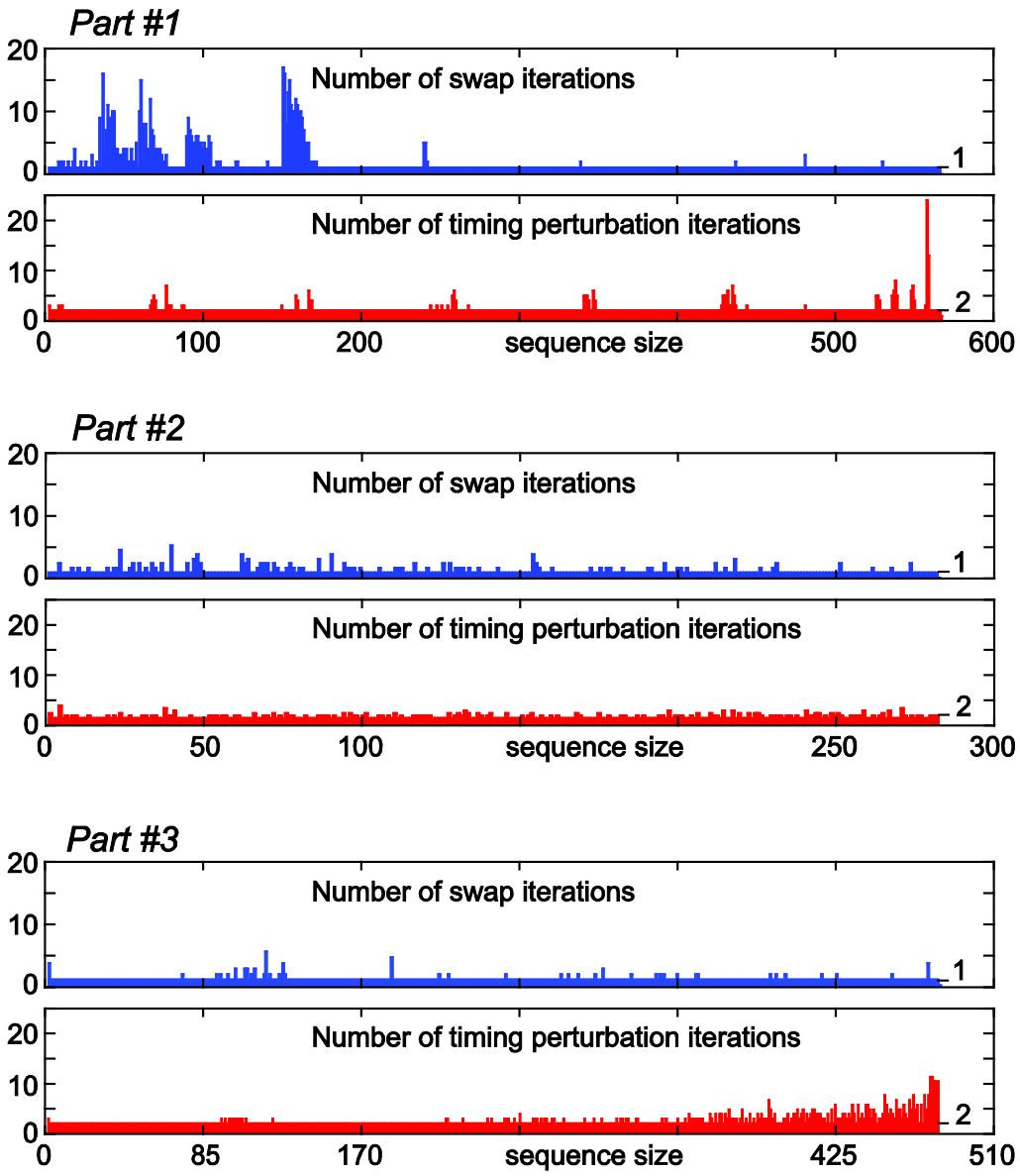

Figure 3.6: Swap and duration perturbation iterations for sample parts #1, #2, and #3.

Sample Part #1

After conducting the sequence optimization for this part, the result was benchmarked to the earlier published result in [29] for a scenario in which each hole receives two laser shots. The results are shown in Figure 3.7.

The earlier method, produced through the combination of [28] and [29], repeats each cluster once and then moves on to the next one using stitching trajectories as detailed in [4]. The proposed new method processes all of the sequenced holes one after another as a single

cluster, without any intermediate loops or repeats. After each of the holes receives one laser shot, the pattern repeats itself as illustrated in Figure 3.4.

With the earlier approach, for the given actuator and process limits, a laser pulsing period of 0.125 [s] (corresponding to a frequency of 8 [Hz]) could be achieved. This is the duration for traversing between two consecutive points within each cluster. With the new sequencing and joint trajectory planning technique, the laser pulsing period could be reduced to 0.05 s, which corresponds to increasing the laser frequency to 20 [Hz]. Total duration comparison between the two approaches shows that in the drilling of this part with two laser shots per hole, 55% cycle time reduction could be obtained over the earlier research results.

Sample Parts #2 and #3

In the evaluation of sample parts #2 and #3, it is assumed that each hole receives only a single laser shot and no repeating shots take place. This is in order to produce results that are directly comparable to those presented in the candidate's earlier work [4], which had also examined this scenario. In the case of sample part #2, the earlier method (combination of [28] and [29]) had enabled a laser pulsing frequency of 7 [Hz]. With the new approach, due to the fact that the sequencing directly considers the resulting joint trajectories, and that the positioning duration between two consecutive holes can now be more than one laser period, the laser pulsing frequency could be increased up to 20 [Hz]. Comparison of the results is shown in Figure 3.8. For this part, the achievable cycle time reduction for a single pass is 73%.

Similarly, sample part #3 which could be laser drilled at 8 [Hz] with the earlier technique can now also be drilled at 20 [Hz], as shown in Figure 3.9. This allows a cycle time reduction of 76% for a single pass over the earlier developed technique, without violating the given feed drive and process related kinematic limits.

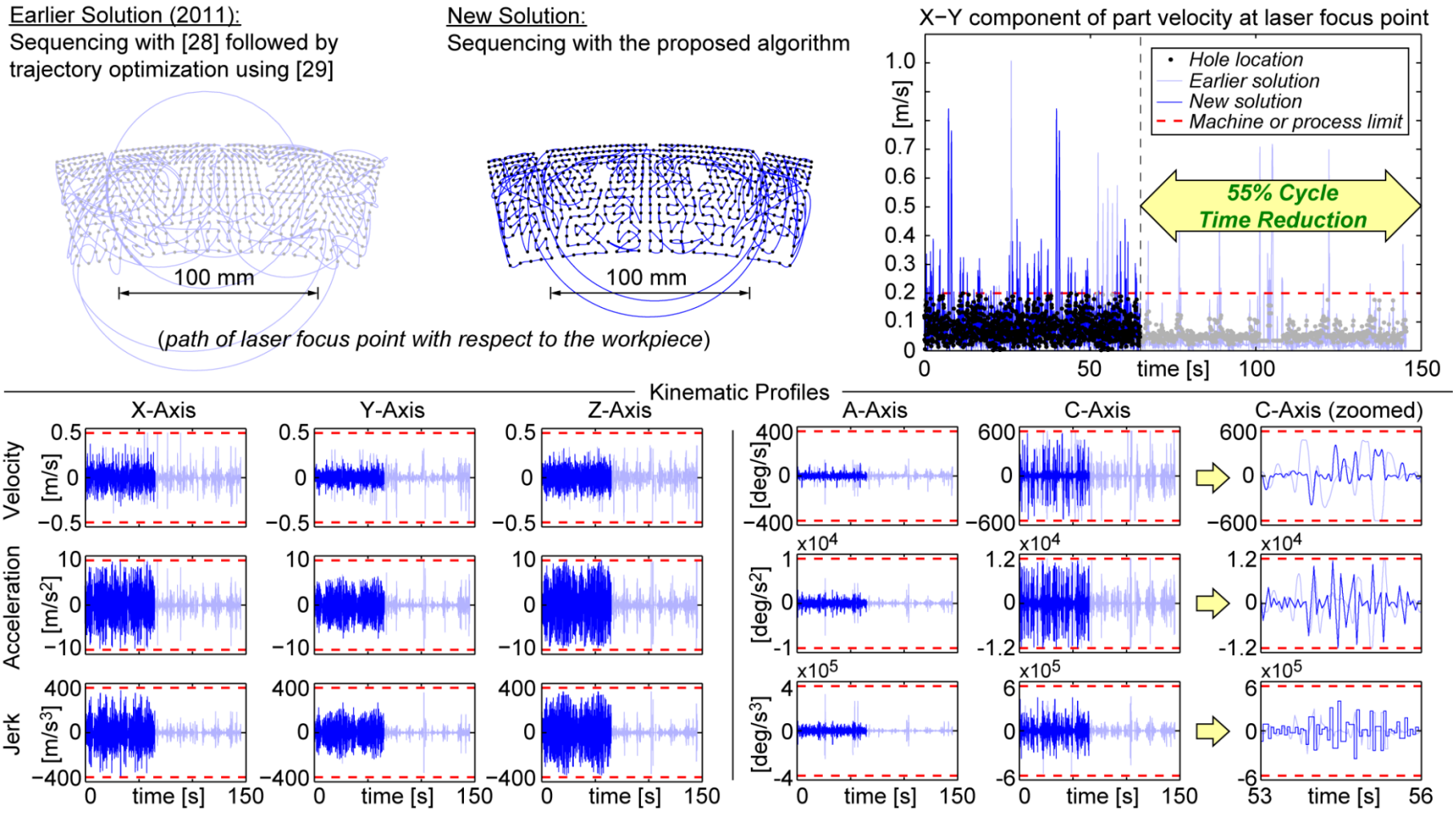

Figure 3.7: Cycle time improvement obtained with the proposed sequencing algorithm for a two pass on-the-fly drilling trajectory [Part #1 with 567 holes].

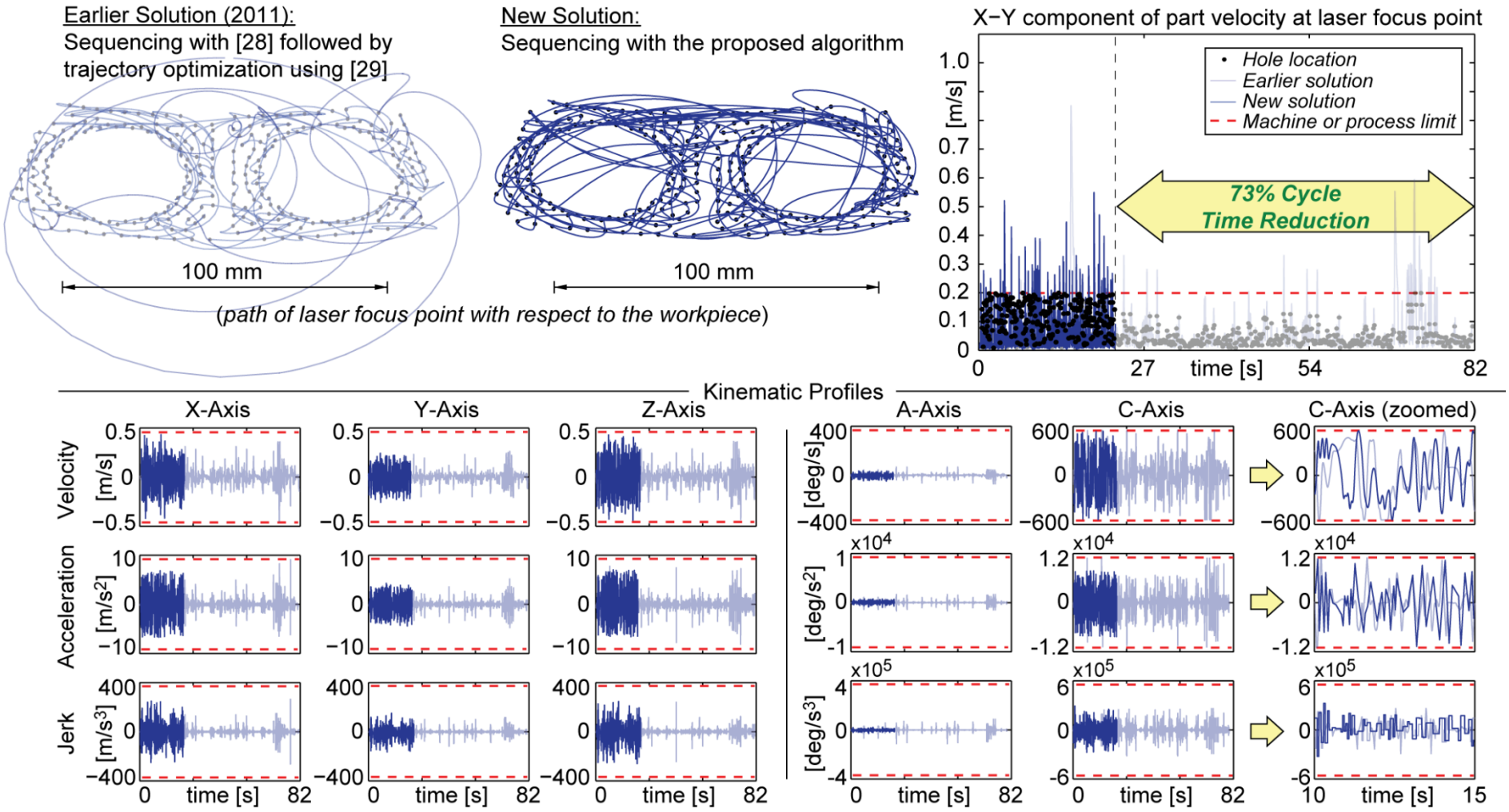

Figure 3.8: Cycle time improvement obtained with the proposed sequencing algorithm for a single pass on-the-fly drilling trajectory [Part #2 with 284 holes].

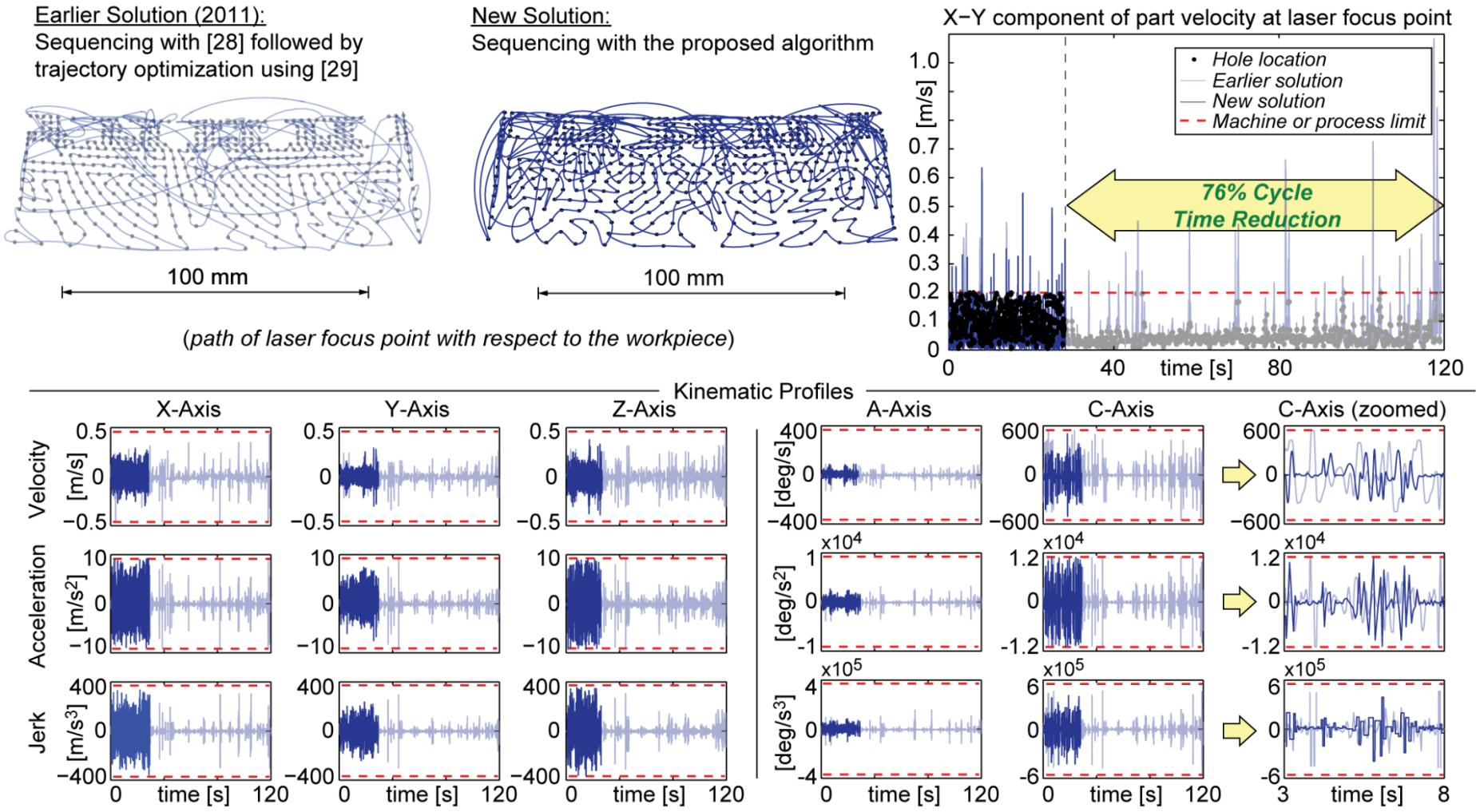

Figure 3.9: Cycle time improvement obtained with the proposed sequencing algorithm for a single pass on-the-fly drilling trajectory [Part #3 with 474 holes].

3.4 Experimental Evaluation

Following the simulation studies, the effectiveness of the proposed sequencing and trajectory planning technique for on-the-fly laser drilling was evaluated experimentally. In this case, the benchmarking was conducted against two trajectory generation approaches which are currently being used in industry. Hence, the following three scenarios have been evaluated:

1. On-the-fly drilling with the proposed sequencing algorithm and off-line cubic spline trajectory interpolation, re-played on the Fanuc 30i using 'inverse-time' feed mode.
2. On-the-fly drilling using NN sequencing [28], and positioning with linear interpolation segments that are blended at the hole locations, executed by Fanuc 30i CNC.
3. Percussion drilling using NN sequencing [28], and positioning with linear interpolation using full stops at the hole locations, executed by Fanuc 30i CNC.

The workpiece considered was Sample Part #1 (with 567 holes), which was also used in Section 3.3. However, the trajectory was planned so that each hole receives 8 laser shots. Implementation of the earlier developed method (i.e., combined use of [28] and [29]) was excluded from the experiments, as the simulation results in Section 3.3 already validated significantly shorter cycle times with the newer technique. Instead, the objective of these experiments was to benchmark the proposed technique with current best practices used in industry. Furthermore, comparison of the developed solution (scenario #1) with scenarios #2 and #3, which rely on the CNC system for trajectory interpolation is interesting; because due to the lack of documentation provided by the CNC builder (Fanuc), it is very difficult to predict deterministically and simulate exactly how the CNC interprets and executes the commanded joint motions. Hence, the experimental results provide a useful industrial benchmark, which would otherwise be very difficult to achieve, with simulation studies alone.

Scenario #2 is the current methodology used at P&WC for on-the-fly laser drilling. Since the CNC system, which was originally designed for metal cutting applications like milling and turning, does not have a trajectory generation function specific to on-the-fly laser drilling, the current practice at P&WC is to program the commanded hole locations and orientations as 5-axis linear toolpath interpolation destinations in joint coordinates. In order to avoid increasing the cycle time by stopping at the corner (end) points, the linear interpolation segments are played back in a mode known as 'G64' (or 'continuous-feed mode'

in NC programming), which rounds off the corners without coming to a full stop at the hole locations, as shown in Figure 3.10. In the implementation tested at P&WC, the corner rounding tolerance had been specified as <10 um.

While there have been several corner rounding strategies proposed in literature such as quintic spline fitting and clothoid curves [31], [59], [60], [61], [88], unfortunately, no description could be found within the documentation of the Fanuc CNC. It is sometimes customary for CNC vendors to prevent their algorithms from being reverse engineered, by limiting the disclosed information. Also, any feedrate modulation which takes places at the corners is not documented or disclosed.

In principle, the corner rounding strategy has two major drawbacks:

i) The laser never actually strikes the desired hole location, but in close vicinity. Hence, there is an accuracy problem associated with this type of toolpath planning.

ii) Unnecessary accelerations and jerks are generated from trying to force the approach and departure segments around the desired hole location. These segments are of linear nature in 5-axis Euclidian space. Furthermore, they are abruptly blended into each other using curves which are constrained within very small geometric dimensions (i.e., < 10 microns). Providing longer distances for gradual curvature modulation, as done in the proposed cubic spline trajectory planning scheme, allows higher actuator velocities and shorter cycle times to be achieved.

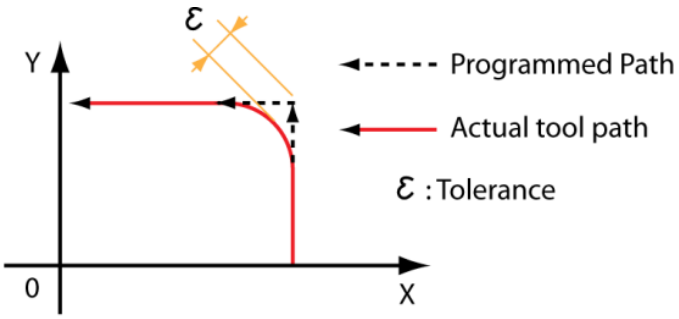

Figure 3.10: Example of programmed vs. actual tool paths between two blocks executed using corner round (i.e., G64) mode.

Scenario #3 (i.e., percussion drilling) is the alternative laser drilling approach. While this technique has some detrimental effects, especially related to local thermal loading on the part being drilled, its comparison has been included into the experimental results in order to gauge the relative productivity increase or decrease, and motion smoothness, that can be achieved with the proposed on-the-fly trajectory planning scheme.

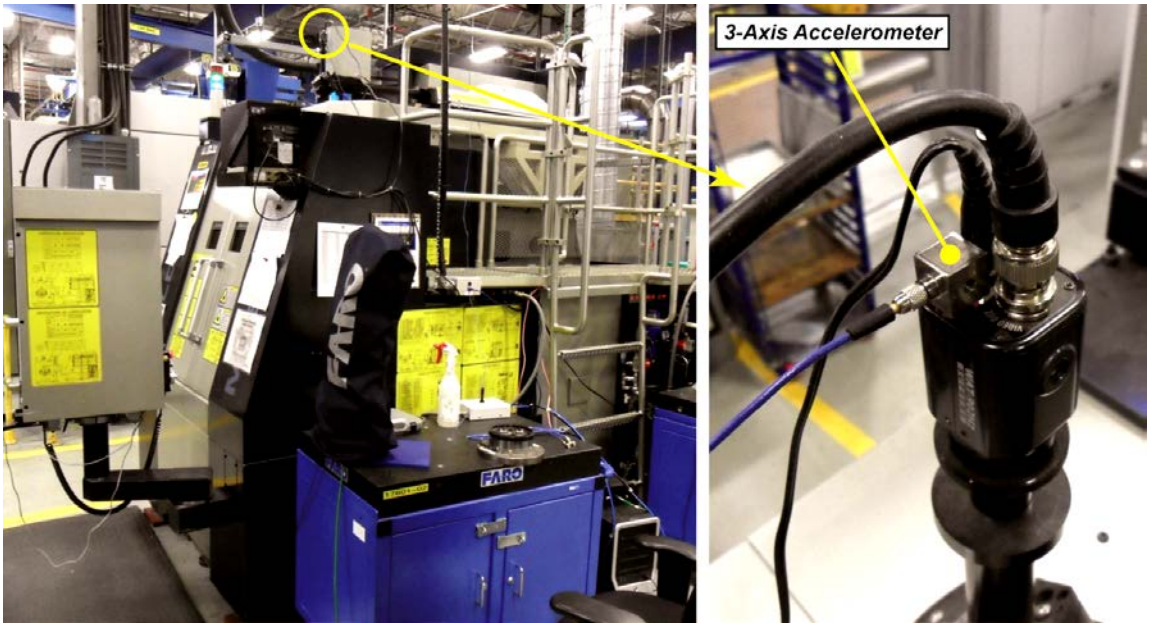

Figure 3.11: Experimental setup and laser optics vibration measurement.

The experimental setup is shown in Figure 3.11. The 5-axis configuration of this machine tool was earlier shown in Figure 1.1. It is important to note that the actual kinematic limits of the machine tool and the laser drilling process are different than those used in the simulation studies in Section 3.5. The real limits, due to confidentiality, are not disclosed in this thesis. Nevertheless, the relative cycle time comparison presented henceforth provides a useful indication of the productivity increase which can be achieved through industrial implementation of the proposed sequencing and trajectory planning approach for on-the-fly laser drilling.

Machine vibrations, especially those affecting the optical components in the laser delivery path (which can gradually cause loss of alignment and focus), are highly detrimental to the process productivity. Hence, during the experiments a three-axis accelerometer was

placed on the process monitoring camera (as a convenient spot for measuring vibrations) and three-axis acceleration data was collected while testing each scenario. Also, each test was conducted at least three times, to ensure the repeatability of the cycle time and vibration measurements.

A relative comparison of the experimentally measured cycle times between the three scenarios is shown in Figure 3.12, where it can be seen that the proposed sequencing algorithm and trajectory generation technique reduce the cycle time by 25% over Scenario #2, which is the current industrially used solution for 5-axis on-the-fly laser drilling. There is also 19% time reduction over Scenario #3. It is noteworthy to mention that the difference in cycle time reduction, over the earlier simulation results in Section 3.3, is attributed to the compared trajectory generation techniques and actual machine tool limits being different. Nevertheless, there is a noticeable productivity increase over the current on-the-fly drilling trajectory generation method.

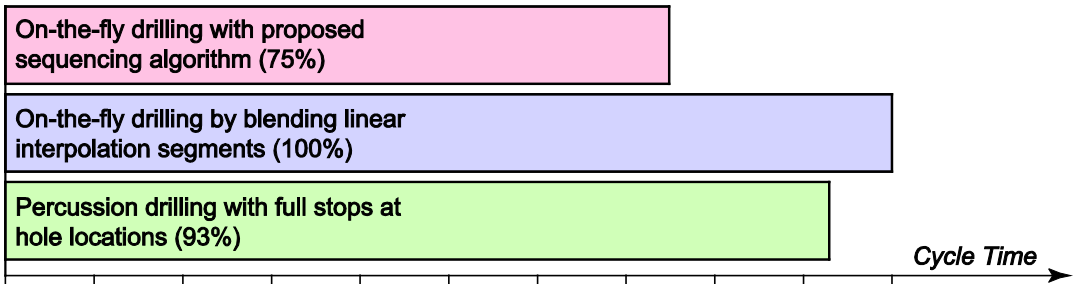

Figure 3.12: Comparison of experimental cycle times for 8-shot trajectory.

The vibration signals collected during a single full pass in each scenario are shown in Figure 3.13. In the data, it was verified that the 169 Hz harmonic is caused by the fans and chiller of the laser drilling machine tool, and there is nothing that can be done through trajectory generation to suppress this component. However, apart from this, it can be seen that the vibrations induced during the proposed on-the-fly drilling trajectory are actually less than those measured in Scenarios #2 and #3, in spite of the achieved cycle time reduction. In particular, there is 17% decrease in the RMS value of resultant vibration over the other two scenarios, which are the current industrial solutions in use. Hence, while achieving an

increase in productivity, the smoothness and quality of the commanded motion has also been increased, and the likelihood of downtime due to optics re-alignment has been decreased.

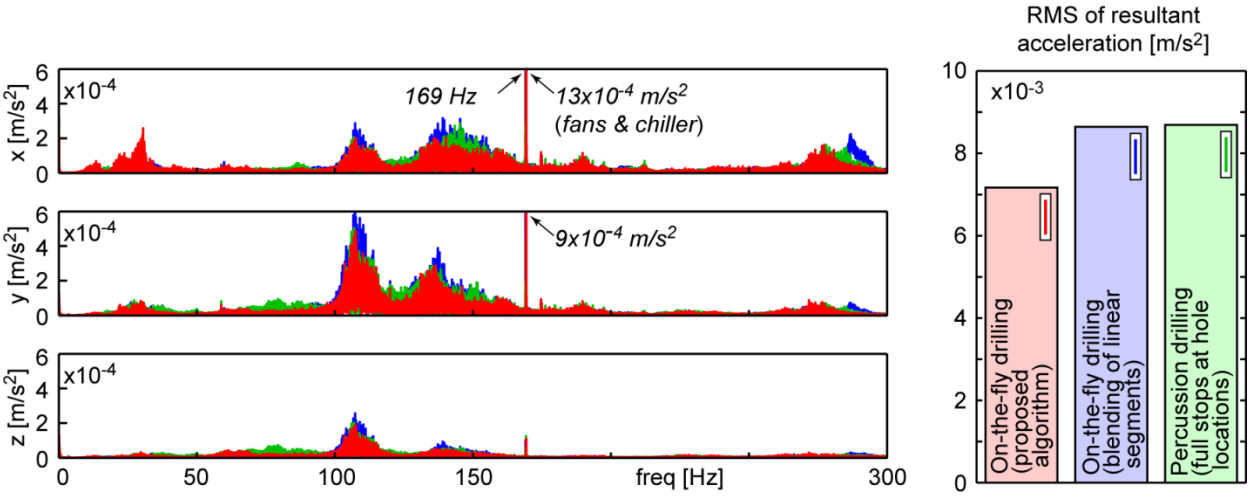

Figure 3.13: Vibration measurements collected from laser optics.

3.5 Conclusion

This chapter has presented a new waypoint and timing sequencing algorithm for 5-axis on-the-fly laser drilling. The algorithm considers the temporal nature of the final spline trajectory and is capable of improving both cycle time and motion smoothness while satisfying the specified machine tool and process kinematic constraints. This algorithm is currently being tested further in production trials at Pratt & Whitney Canada.

Chapter 4

Time-Optimal Connection Between On-the-fly Drilling Trajectories and Rest Boundary Conditions

4.1 Introduction

This chapter details the generation of connection trajectories into and out of the closed cubic spline trajectory, which is used for repeating on-the-fly laser drilling passes. These connection trajectories have to either start from a rest state (i.e., zero velocity and acceleration condition) and blend into the closed cubic curve with the correct position, velocity, and acceleration boundary conditions; or they have to leave the closed cubic spline with the aforementioned boundary conditions and proceed to a rest state. The position assumed at the 'rest' condition is not constrained, and is assumed to be within the travel stroke of the machine tool's feed drives (which can be checked once such a trajectory is generated).

The connection trajectories from and to rest are generated to yield the shortest motion duration, subject to the velocity, acceleration, and jerk limits defined for each axis. Hence, they are of 'bang-bang' character in the jerk profile. Since path following along a specified contour is not required, and only actuator velocity, acceleration, and jerk limits are considered, the trajectories for the individual axes can be planned independently of one another. Even if the individual actuator movement durations turn out to be different, the execution of these trajectories can be coordinated in a manner that all axis movements blend into, or out of, the closed cubic spline correctly; by passing through the designated boundary conditions at the same time.

Since the solution method for all axes is the same, henceforth the connection trajectory planning for only a single axis is described. For simplicity of notation, the velocity, acceleration, and jerk profiles for the axis of consideration will be denoted as v, a, and j; with their respective magnitude limits being denoted as $V > 0$, $A > 0$, and $J > 0$.

First, the connection to (and from) a nonzero velocity state with zero acceleration boundary conditions will be demonstrated in Section 4.2. It is known from optimal trajectory

planning literature [70] that such trajectories are time-optimal (i.e., satisfying minimum time requirement, subject to velocity, acceleration, and jerk bounds).

Afterwards, this method will be generalized in Sections 4.4 and 4.5 into connecting from (and to) nonzero velocity and non-zero acceleration boundary conditions. By applying the principle of optimality [47] (summarized in Section 4.3), it will be shown that the trajectories starting (or ending) with such nonzero acceleration boundary conditions are also time-optimal.

4.2 Connection Between Rest and Zero Acceleration and Nonzero Velocity Boundary Conditions (b.c.)

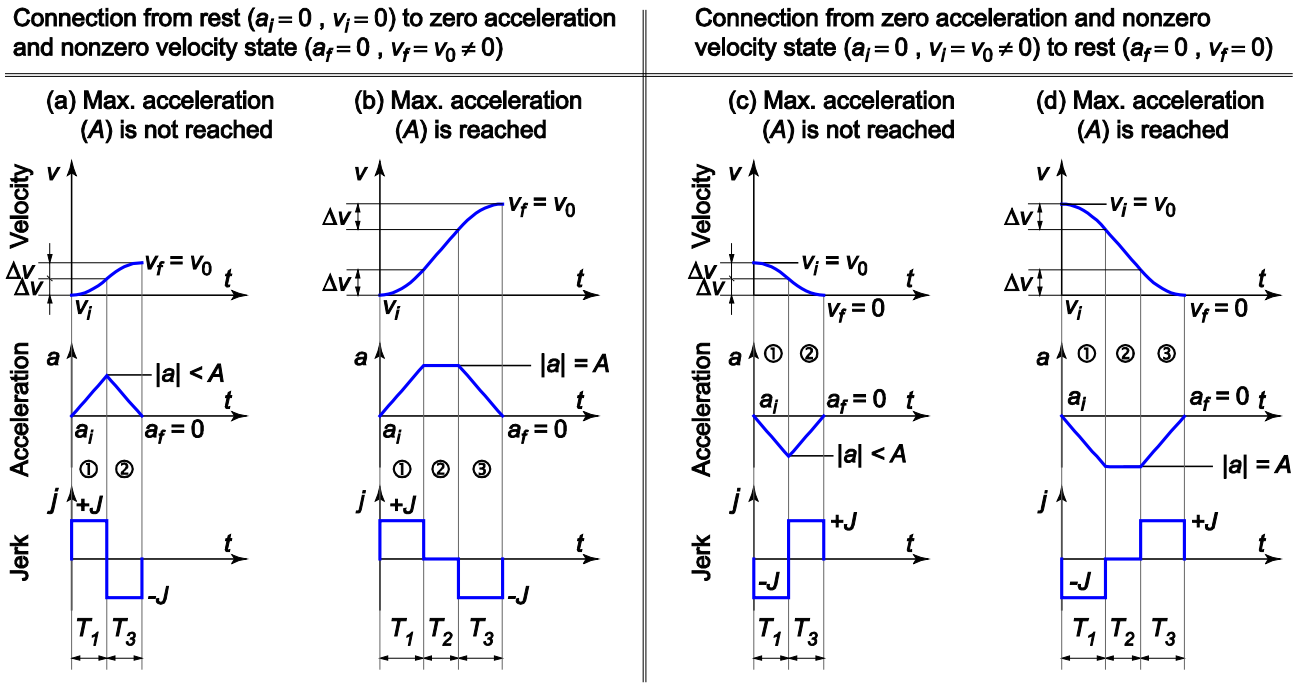

Figure 4.1: Connections between rest and b.c. with nonzero velocity and zero acceleration.

4.2.1 From rest to given nonzero velocity and zero acceleration b.c.

Considering Figure 4.1(a) and (b), in which the initial state is ($v_i = 0$, $a_i = 0$; subscript i denotes 'initial') a final velocity of $v_f = v_0$ can be achieved by applying a jerk sequence

of $j = \text{sgn}(v_f - v_i)\cdot\{+J, 0, -J\} = \text{sgn}(v_0)\cdot\{+J, 0, -J\}$ throughout time intervals of $\{T_1, T_2, T_3\}$, and integrating the jerk profile with respect to time to obtain the designated acceleration and velocity profiles. Here, the end velocity v_0 can be either positive or negative.

Based on the value of v_0, A, and J, the acceleration profile assumes either a triangular or trapezoidal shape:

i) When $|v_0| \leq A^2 / J$ ⇨ Triangular Acceleration Profile (Figure 4.1a)

The phase durations are calculated as:

$$T_1 = T_3 = \sqrt{|v_0| / J}\ ,\ T_2 = 0$$

In this case, the maximum acceleration magnitude may not reach its designated limit:

$$\max(|a|) = \sqrt{J\,|v_0|} \leq A$$

The velocity inflection point happens in the middle of the range from v_i (=0) to $v_f\ (= v_0)$ with

$$\Delta v = |v_f - v_i|/2 = |v_0|/2$$

ii) When $|v_0| > A^2 / J$ ⇨ Trapezoidal Acceleration Profile (Figure 4.1b)

The phase durations are calculated as:

$$T_1 = T_3 = A/J \quad ,\quad T_2 = |v_0|/A - A/J$$

The acceleration profile reaches, and is capped by, its maximum allowed magnitude:

$$\max(|a|) = A$$

The velocity inflections happen at offsets of Δv from initial and final velocities, where

$$\Delta v = A^2 / (2J)$$

Proof:

Since initial and final acceleration values are zero, the acceleration profile will be symmetrical (along the time axis) and $T_1 = T_3$ will always hold. Also, the velocity

differences (Δv) to the inflection points in Phases ① and ③ will be identical, as these represent the area underneath the acceleration profile in Phases ① and ③.

When the acceleration profile has a triangular shape, as shown in Figure 4.1(a), this implies that $T_2 = 0$. By inspecting the figure, the highest acceleration magnitude at the end of Phase ① can be obtained to be: $\max(|a|) = J T_1$. On the other hand, the area underneath the acceleration curve in Phases ① and ③ represents the velocity difference:

$$|v_f - v_i| = |v_0 - 0| = \frac{1}{2}\max(|a|)\cdot(T_1 + T_3) = \max(|a|)\cdot T_1 = J \cdot T_1^2$$

The duration T_1 $(= T_3)$ and resulting maximum acceleration magnitude required to reach the final velocity value of v_0 can be obtained as:

$$T = \sqrt{|v_0|/J} \quad , \quad \max(|a|) = \sqrt{J|v_0|}$$

It can be verified that when $|v_0| \le A^2/J$, the acceleration magnitude will not exceed its given limit ($|a| = \sqrt{J|v_0|} \le A$). Thus, a triangular acceleration profile can be successfully used to achieve the desired velocity change from $v_i\,(=0)$ to $v_f\,(=v_0)$, by making use of the given jerk limit J, and staying within the acceleration limit A.

On the other hand, when $|v_0| > A^2/J$ this implies that the acceleration magnitude would exceed its limit of A if a triangular acceleration profile was used. To prevent this situation, the acceleration profile needs to be capped by its limit A, and extended in duration (along the middle portion as necessary), so that its area underneath achieves the desired velocity difference $\left|v_f - v_i\right| = \left|v_o\right|$. This leads to a trapezoidal shape with $T_2 > 0$ as shown in Figure 4.1(b).

In this case, $\max(|a|) = A$, and $T_1 = T_3 = \max(|a|)/J = A/J$. Considering that the area underneath the acceleration profile has to cover for the velocity change in Phases ①, ②, and ③,

$$\frac{1}{2}A(T_1 + T_3) + AT_2 = |v_f - v_0| \;\Rightarrow\; T_2 = \frac{|v_0|}{A} - T_1 = \frac{|v_0|}{A} - \frac{A}{J}$$

Furthermore, the velocity differences leading to the inflection points can be found as:

$$\Delta v = \frac{1}{2}J T_1^2 = \frac{1}{2}J\frac{A^2}{J^2} = \frac{A^2}{2J}$$

4.2.2 From given nonzero velocity and zero acceleration b.c. to rest

The kinematic compatibility conditions for connecting from a nonzero velocity and zero acceleration b.c. to rest (as shown in Figure 4.1(c) and (d)) can be derived in an identical manner to those already explained in Section 4.2.1. for the cases shown in Figure 4.1(a) and (b). The phase durations T_1, T_2, and T_3 would be computed by checking the value of $|v_i| = |v_0|$ with respect to A^2 / J, and the appropriate jerk sequence $j = \text{sgn}(v_f - v_i) \cdot \{+J, 0, -J\} = \text{sgn}(-v_0) \cdot \{+J, 0, -J\}$ would be integrated with respect to time, to produce the acceleration, velocity, and position profiles. For brevity, these intermediate steps, very similar to those in Section 4.2.1, are not repeated in the presentation.

4.3 The Principle of Optimality

The demonstrated connections between rest and the given boundary conditions (with zero acceleration), shown in Figure 4.1(a)-(d), all have the property of being minimum-time, as reported in [70]. By applying the principle of optimality [47], summarized below, it will be shown that the trajectories starting (or ending) with nonzero acceleration conditions, as covered in Sections 4.4 and 4.5, are also time-optimal.

The following is a subsection taken out of [47], summarizing the principle of optimality:

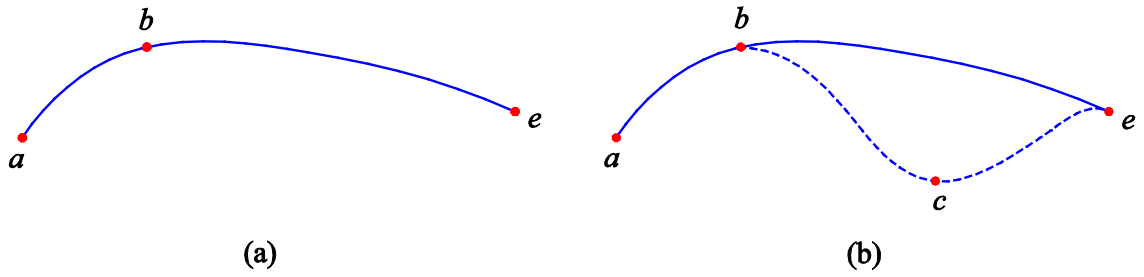

Figure 4.2: (a) Optimal path from states *a* to *e*. (b) Two candidate optimal paths from states *b* to *e*.

The *optimal* path for a multistage decision process is shown in Figure 4.2 (a). Suppose that the first decision (made at state *a*) results in segment *a*-*b* with cost C_{ab} and that the

remaining decisions yield segment *b*-*e* has to be a cost of C_{be}. The *minimum* cost C_{ae}^{*} from *a* to *e* is therefore,

$$C_{ae}^{*} = C_{ab} + C_{be}.$$

If *a*-*b*-*e* is the optimal path from *a* to *e*, then *b*-*e* is the optimal path from *b* to *e*. This can be proven by contradiction: Suppose *b*-*c*-*e* in Figure 4.2 (b) is the optimal path from *b* to *e*; then

$$C_{bce} < C_{be}$$

and

$$C_{ab} + C_{bce} < C_{ab} + C_{be} = C_{ae}^{*} \tag{4.1}$$

However, Eq. (4.1) can only be satisfied by violating the condition that *a*-*b*-*e* is the optimal path from *a* to *e*.

Bellman [8] has called the above property of an optimal policy the principal of optimality: *"An optimal policy has the property that whatever the initial state and initial decision are, the remaining decisions must constitute an optimal policy with regard to the state resulting from the first decision"* [47].

4.4 Connection from nonzero velocity and acceleration boundary conditions to rest

The connection from initial conditions of nonzero velocity and acceleration to rest are achieved by extending (or cropping) Phase ① of the trajectory which connects zero initial acceleration and nonzero initial velocity b.c. to rest. There are four possible cases:

i) **Case #1:** From ($v_i \geq 0$, $a_i > 0$) to rest ($v_f = 0$, $a_f = 0$)

ii) **Case #2:** From ($v_i \geq 0$, $a_i < 0$) to rest ($v_f = 0$, $a_f = 0$)

iii) **Case #3:** From ($v_i < 0$, $a_i < 0$) to rest ($v_f = 0$, $a_f = 0$)

iv) **Case #4:** From ($v_i < 0$, $a_i > 0$) to rest ($v_f = 0$, $a_f = 0$)

Case #1: Connecting from ($v_i \geq 0$, $A \geq a_i > 0$) to rest ($v_f = 0$, $a_f = 0$)

Considering Figure 4.3, the basic idea is to bridge a connection from the given nonzero acceleration boundary condition to the quickest reachable state with zero acceleration, as

shown in the red highlighted portion of Figure 4.2. This is achieved by projecting the trajectory forwards from the initial state by considering a jerk input of $-J$ (with maximum magnitude). The velocity reached at the zero acceleration state is denoted as v_{0f}. The subscript '0' indicates 'zero-acceleration state', and the subscript '*f*' indicates projection in the '*forwards*' direction in time. From this point onwards, a zero initial acceleration trajectory is planned, as explained in Section 4.2.2, based on one of the two templates in Figure 4.1 (c) or (d). The 'zero initial acceleration to rest' portion of the trajectory has to be planned starting at the initial velocity of v_{0f}. Afterwards, the complete trajectory can be accomplished by extending the duration of the first phase as $T_1' = T_1 + T_a$.

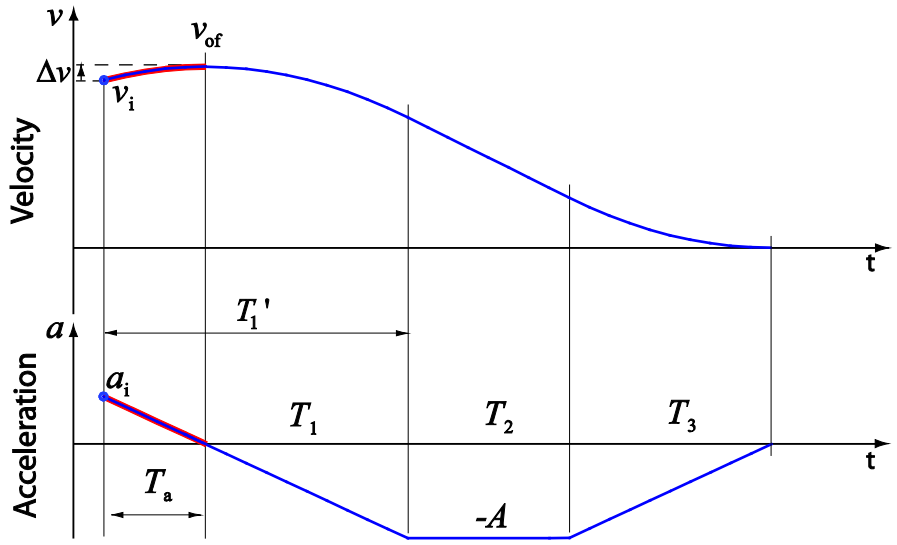

Figure 4.3: Case #1: Connection from ($v_i \geq 0$, $A \geq a_i > 0$) to rest.

v_{0f} and T_a can be calculated as follows (noting that because $a_i > 0 \rightarrow |a_i| = a_i$):

$$J = |a_i| / T_a \rightarrow T_a = |a_i| / J$$

$$\Delta v = a_i T_a - \frac{1}{2} J T_a^2 = \frac{a_i |a_i|}{J} - \frac{J |a_i|^2}{2J^2} = \frac{|a_i|^2}{2J} = \frac{a_i |a_i|}{2J} > 0$$

$$v_{0f} = v_i + \Delta v$$

The overall connection trajectory is obtained by integrating the jerk sequence of [$-J$, 0, J], for the durations of [T_1' , T_2 , T_3], starting with the initial conditions ($v_i \geq 0$, $a_i > 0$).

From the Principle of Optimality summarized in Section 4.3, since the connection from the initial state (v_i , a_i) to the intermediate state (v_{0f} , $a = 0$) is a minimum-time trajectory, along with the connection from (v_{0f} , $a = 0$) to rest ($v_f = 0$, $a_f = 0$), it follows that the complete trajectory from ($v_i \geq 0$, $a_i > 0$) to rest is also time-optimal.

As an important note, considering that in the extreme case $a_i = A$ can hold, in order for the velocity profile to remain within the limit of $v_{0f} \leq V$, v_i has to be less than $v_i \leq V - A^2/(2J)$. This requirement ($|v_{0f}| \leq V$) has to be taken into account when selecting the entry and exit points into the cyclical on-the-fly drilling trajectory, to ensure that the connection profiles do not violate the velocity limits of the drives.

Case #2: Connecting from ($v_i \geq 0$, $-A \leq a_i < 0$) to rest ($v_f = 0$, $a_f = 0$)

In this case, zero acceleration states are projected both in the forwards and backwards directions (in time) from the given initial condition of ($v_i \geq 0$, $a_i < 0$), as shown in Figure 4.4. Here, v_{0b} indicates the velocity reached by projecting '*backwards*' and v_{0f} by projecting '*forwards*' (as explained in Case #1). The travel time T_a to zero acceleration state (which is identical in both directions), and the respective values of v_{0b} and v_{0f} can be found as follows:

$$T_a = \frac{|a_i|}{J},\ \Delta v = \frac{a_i |a_i|}{2J} < 0,\ v_{0f} = v_i + \Delta v, \text{ and } v_{0b} = v_i - \Delta v$$

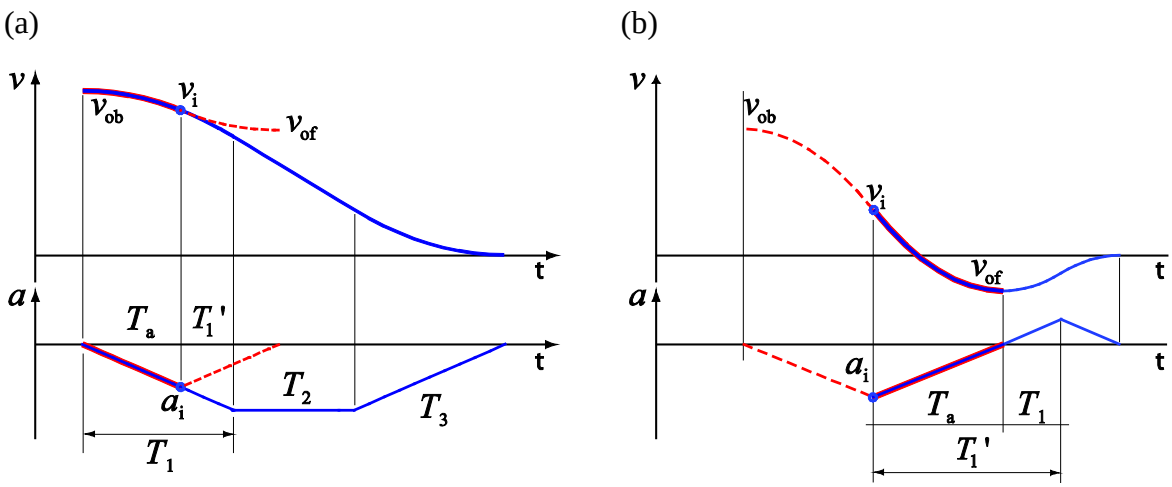

Figure 4.4: Connection from ($v_i \geq 0$, $a_i < 0$) to rest: (a) when $v_{0f} \geq 0$, (b) when $v_{0f} < 0$.

Based on the value of v_{0f}, two possibilities emerge:

i) If $v_{0f} \geq 0$, as shown in Figure 4.4(a), then the trajectory is planned as a connection from zero initial acceleration (with positive initial velocity) to rest, as explained in Section 4.2.2, starting with the initial velocity of v_{0b}. Afterwards, the duration of T_a is cropped out of T_1 (i.e., $T_1' = T_1 - T_a$) and the final motion profile is generated by integrating the jerk sequence of $[-J,\ 0,\ J]$, which is applied for the durations of $[T_1',\ T_2,\ T_3]$, starting with the initial conditions ($v_i \geq 0$, $a_i < 0$). Since $|a_i| \leq A$, it can be guaranteed that $T_a \leq T_1$. Since the parent trajectory from (v_{0b}, $a = 0$) to rest is already minimum time, and the given initial conditions ($v_i \geq 0$, $a_i < 0$) are on this trajectory, then from the Principle of Optimality the cropped trajectory from (v_i, a_i) to rest will also be minimum time.

ii) If $v_{0f} < 0$, as shown in Figure 4.4(b), then the trajectory is planned as a connection from zero initial acceleration (with negative initial velocity) to rest (as

explained in Section 4.2.2), starting with an initial velocity of v_{0f}. Afterwards, the duration of T_1 is extended backwards (i.e. T_a is added to T_1; $T_1' = T_1 + T_a$). The final motion profile is generated by integrating the jerk sequence [$+J$, 0, $-J$], which is applied for the durations of [T_1', T_2, T_3], starting with the initial conditions ($v_i \geq 0$, $a_i < 0$). Since the trajectory from the initial conditions ($v_i \geq 0$, $a_i < 0$) to the intermediate state ($v_{0f} < 0, a = 0$) is time optimal (i.e., achieved with largest possible jerk magnitude), and the latter part (from (v_{0f}, $a = 0$) to rest) is also time-optimal, then from the Principle of Optimality, it follows that their connected sequence will also be time-optimal.

Case #3: Connecting from ($v_i < 0$, $-A \leq a_i < 0$) to rest ($v_f = 0$, $a_f = 0$)

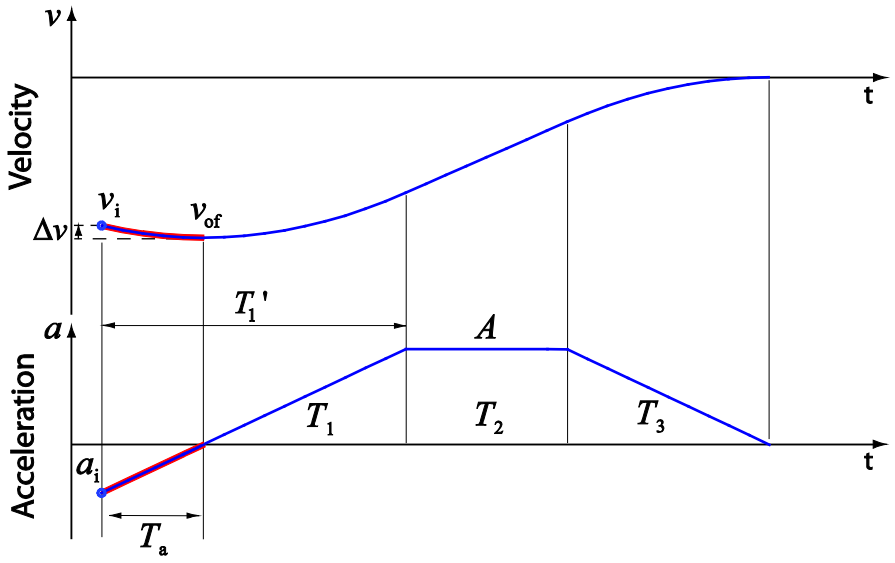

Figure 4.5: Case #3: Connection from ($v_i < 0$, $-A \leq a_i < 0$) to rest.

Considering Figure 4.5, this case can be considered as the mirror image of Case #1 with respect to the time axis. The strategy is the same; to project forwards in time towards a zero acceleration state with the velocity denoted as v_{0f}, and then to plan a zero initial acceleration trajectory to rest starting with this velocity. Afterwards, the duration of Phase ①

of the latter trajectory is extended backwards by the acceleration duration T_a ($T_1' = T_1 + T_a$) and a jerk sequence of [$+J$, 0, $-J$] is executed for the duration array [T_1', T_2, T_3], starting with the initial conditions of ($v_i < 0$, $a_i < 0$). As proven for Case #1, this trajectory is also time-optimal.

As explained for Case #1, to guarantee that the magnitude of the velocity profile does not exceed its limit (i.e., to keep $-v \le V$), in the extreme case that $a_i = -A$, v_i then has to satisfy $v_i \ge -V + A^2/(2J)$. Similarly, the connection point has to be chosen such that $|v_{0f}| \le V$.

Case #4: Connecting from ($v_i < 0, a_i > 0$) to rest ($v_f = 0$, $a_f = 0$)

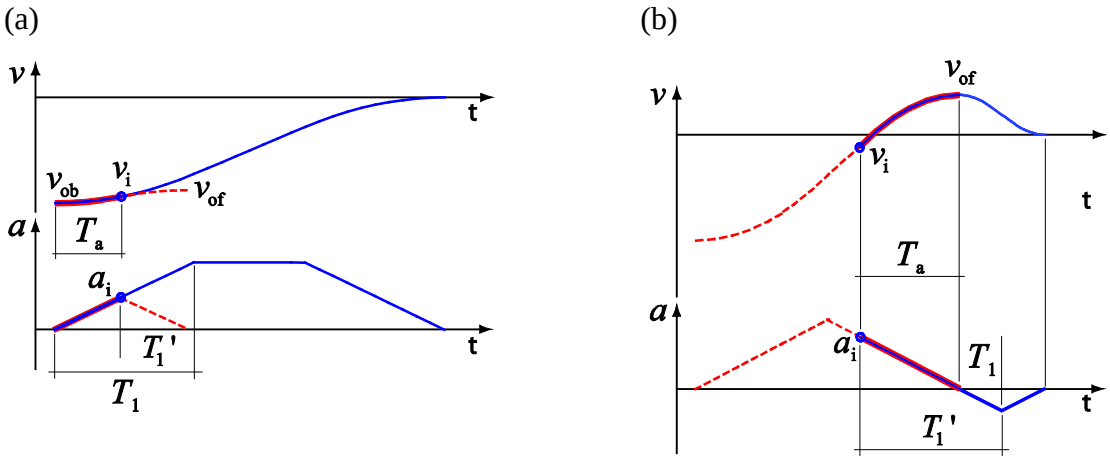

Figure 4.6: Connection from ($v_i < 0, a_i > 0$) to rest: (a) when $v_{0f} < 0$, (b) when $v_{0f} \ge 0$.

Considering Figure 4.6, it can be seen that the treatment of this case is similar to that of Case #2. The velocity v_{0f} corresponding to the forward projected zero acceleration state is determined. Then, two possibilities arise:

i) If v_{0f} is negative, then the trajectory is planned from the backward projected zero acceleration state velocity, v_{0b}, as shown in Figure 4.6(a). The beginning of

Phase ① is cropped ($T_1' = T_1 - T_a$). Then, the jerk sequence of [$+J$, 0, $-J$] is applied with a duration array of [T_1' , T_2 , T_3], starting with the initial conditions ($v_i < 0$, $a_i > 0$). Since the parent trajectory from (v_{0b} , $a = 0$) to rest is time-optimal, and the initial conditions ($v_i < 0$, $a_i > 0$) are on this trajectory, then from the Principle of Optimality the cropped trajectory from (v_i , a_i) to rest will also be time-optimal.

ii) If v_{0f} is positive, then the trajectory is planned from v_{0f} onwards to rest, as shown in Figure 4.6(b). T_1 is extended backwards as $T_1' = T_1 + T_a$. The jerk sequence of [$-J$, 0, J] is executed with the duration array of [T_1' , T_2 , T_3], starting with initial conditions ($v_i < 0$, $a_i > 0$). Since the trajectory from the initial conditions ($v_i < 0$, $a_i > 0$) to the intermediate state ($v_{0f} \geq 0$, $a = 0$) is time optimal (i.e., achieved with largest possible jerk magnitude), and the latter part (from (v_{0f} , $a = 0$) to rest) is also time-optimal, then from the Principle of Optimality it follows that their connecting sequence will also be time-optimal.

4.5 Connection from rest to nonzero velocity and acceleration boundary conditions

The handling of these conditions can be achieved in a similar manner to the four cases in Section 4.4. To avoid repeating similar explanations, the handling of these conditions is summarized graphically in Figures 4.7-4.10 with only brief comments. Proof of time-optimality for these solutions can be achieved using the Principle of Optimality, as was done for the four cases described in Section 4.4.

Case #1: Connecting from rest ($v_i = 0$, $a_i = 0$) to ($v_f \geq 0$, $a_f < 0$)

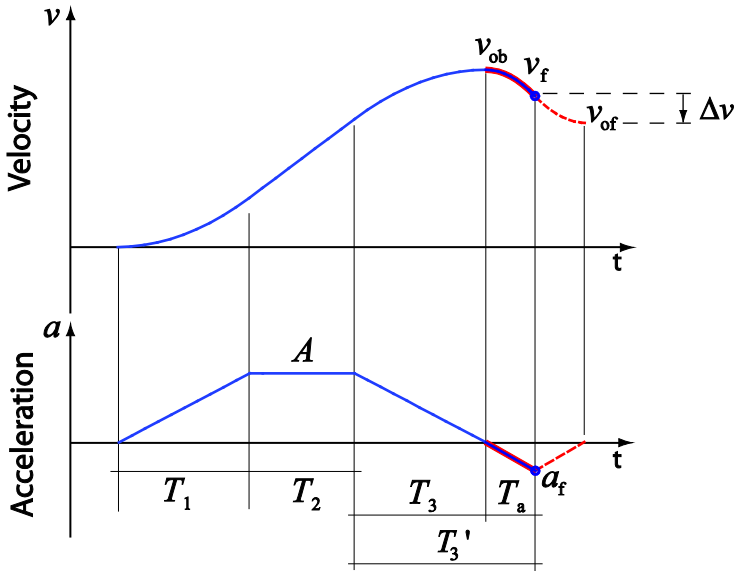

Figure 4.7: Connection from rest ($v_i = 0$, $a_i = 0$) to ($v_f \geq 0$, $a_f < 0$).

This case, shown in Figure 4.7, can be regarded as a mirror image of Case #1 in Section 4.4. A trajectory from rest to zero acceleration boundary condition is planned until v_{0b}. Here, $v_{0b} = v_f - \Delta v$, where: $\Delta v = a_f |a_f| / (2J) < 0$. The connection from v_{0b} to the final state ($v_f \geq 0$, $a_f < 0$) is achieved by extending T_3 by T_a (i.e., $T_3' = T_3 + T_a$, where $T_a = |a_f| / J$). Executing the jerk sequence [$+J$, 0, $-J$] for the duration array of [T_1, T_2, T_3'] from the initial conditions of ($v_i = 0$, $a_i = 0$) leads to the desired final state (v_f, a_f). For the trajectory to be feasible, it is also important that $v_{0b} \leq V$ holds. Otherwise, a different connection point needs to be selected in the repeating sequence, for which the connection trajectory does not violate the actuator velocity limits.

Case #2: Connecting from rest ($v_i = 0$, $a_i = 0$) to ($v_f \geq 0$, $a_f > 0$)

(a) (b)

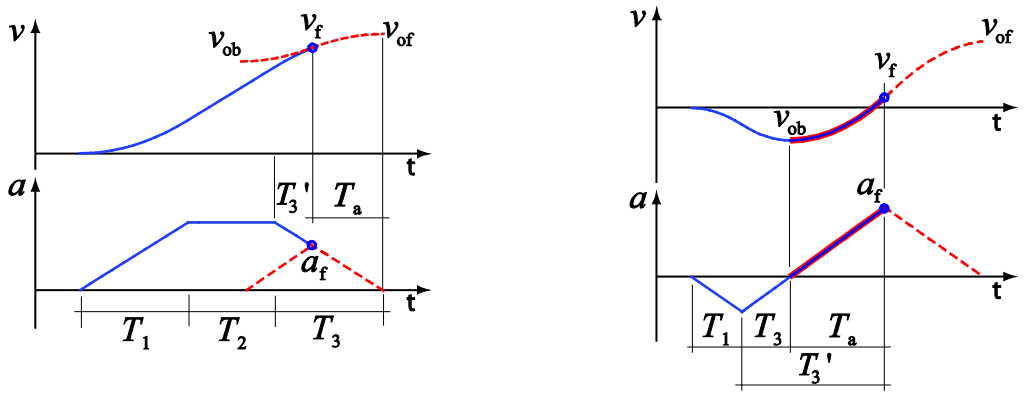

Figure 4.8: Connection from rest to ($v_f \geq 0$, $a_f > 0$): (a) when $v_{0b} \geq 0$, (b) when $v_{0b} < 0$.

This case, shown in Figure 4.8, can be regarded as the mirror image of Case #2 in Section 4.4. In this case, a zero acceleration state is projected backwards from the given final condition. Naming the velocity at this state as v_{0b}, two possibilities emerge and are handled as shown in Figure 4.8(a) and (b), depending on the sign of v_{0b}.

i) If $v_{0b} \geq 0$, a trajectory from rest to v_{0f} is planned, and the end of Phase ③ is cropped by T_a ($T_3' = T_3 - T_a$). Starting with zero initial conditions, executing the jerk sequence of $[+J, 0, -J]$ with timing values of $[T_1, T_2, T_3']$ leads to the desired final conditions.

ii) If $v_{0b} < 0$, a trajectory from rest up to v_{0b} is planned and this time the duration of the *3*rd phase is extended by T_a ($T_3' = T_3 + T_a$). Starting with zero initial conditions, the desired final conditions can be reached by executing the jerk sequence of $[-J, 0, J]$ with the durations of $[T_1, T_2, T_3']$.

Case #3: Connecting from rest ($v_i = 0$, $a_i = 0$) to ($v_f < 0$, $a_f > 0$)

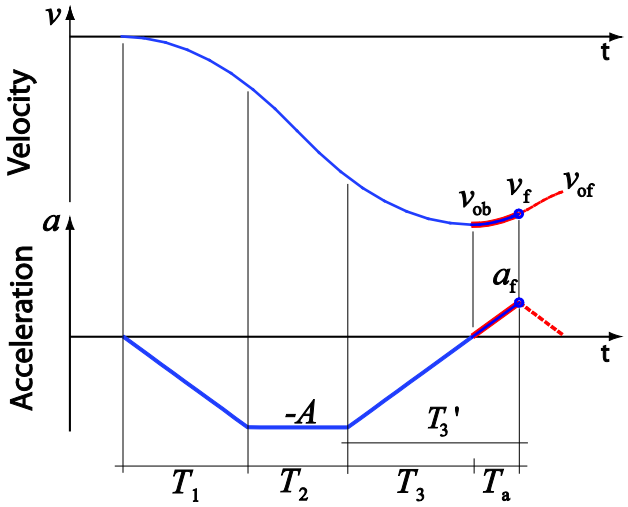

Figure 4.9: Connection from rest to ($v_f < 0$, $a_f > 0$).

This case, shown in Figure 4.9, can be regarded as the mirror image of Case #3 in Section 4.4. In this case, the base trajectory is planned from rest to (v_{0b}, $a = 0$), and afterwards T_3 is extended as $T_3' = T_3 + T_a$. Starting at rest, execution of the jerk sequence of $[-J, 0, J]$ with the durations $[T_1, T_2, T_3']$ yields the desired final conditions (v_f, a_f).

Case #4: Connecting from rest ($v_i = 0$, $a_i = 0$) to ($v_f < 0$, $a_f < 0$)

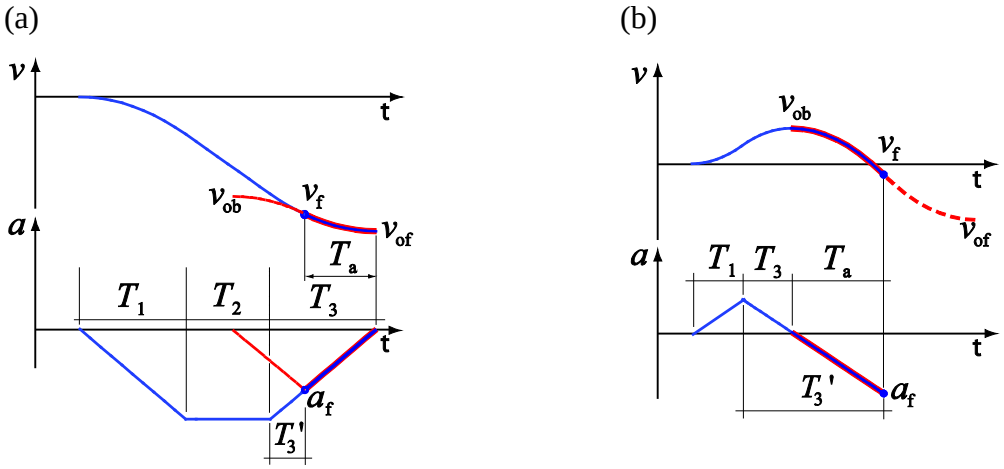

Figure 4.10: Connection from rest to ($v_f < 0$, $a_f < 0$): (a) when $v_{0b} < 0$, (b) when $v_{0b} \geq 0$.

This case, shown in Figure 4.10, can be regarded as the mirror image of Case #4 in Section 4.4. In this case, a zero acceleration state is projected backwards from the given final condition. Naming the velocity at this state as v_{0b}, two possibilities emerge and are handled as shown in Figure 4.10 (a) and (b) depending on the sign of v_{0b}.

i) If $v_{0b} < 0$, a trajectory from rest to v_{0f} is planned and the end of Phase ③ is cropped by T_a ($T_3' = T_3 - T_a$). Starting with zero initial conditions, executing the jerk sequence of [$-J$, 0, J] with timing values of [T_1, T_2, T_3'] leads to the desired final conditions.

ii) If $v_{0b} \geq 0$, a trajectory from rest up to v_{0b} is planned, and this time the duration of the 3rd phase is extended by T_a ($T_3' = T_3 + T_a$). Starting with zero initial conditions, the desired final conditions can be reached by executing the jerk sequence of [$+J$, 0, $-J$] with the durations of [T_1, T_2, T_3'].

4.6 Validation of connection trajectories for a single actuator

The possible connections analyzed in Sections 4.2, 4.4, and 4.5 have been tested numerically for a single axis for different positive and negative initial and final velocity and acceleration boundary conditions.

In performing the validation, the velocity, acceleration, and jerk magnitude limits considered were V = 2500 [mm/s], A = 10000 [mm/s^2], and J = 200000 [mm/s^3]. The tested initial/final velocity and acceleration values were v_i / v_f = 2250, 1800, 1350, 900, 450, 0, -450, … , -2250 [mm/s], and a_i / a_f = -10000, -8000, -6000, -4000, -2000, 0, +2000, … , +10000 [mm/s^2].

The resulting connection trajectories are shown in Figure 4.11. As can be seen, they always remain within the defined velocity and acceleration limits, and there is always a successful connection between the given initial / final boundary condition and the resting state ($a = 0$, $v = 0$). These simulations validate the correctness of the developed time-optimal connection method for a single actuator.

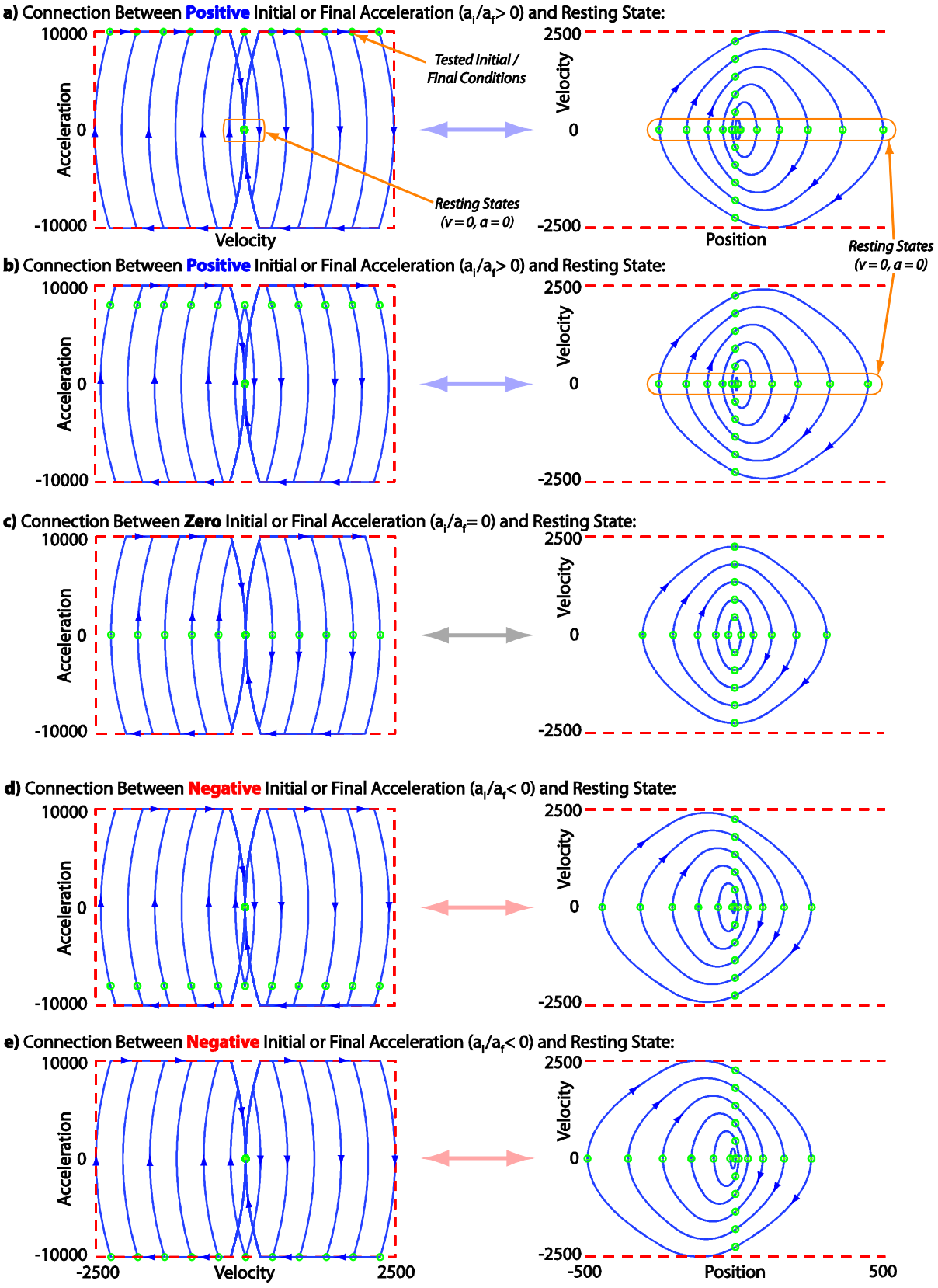

Figure 4.11: Validation of connection trajectories from and to rest for a single axis.

4.7 Validation of connection trajectories for the 5-axis case

Following validation of the single axis case, the generation of 5-axis connection trajectories for blending into and out of the cyclic on-the-fly drilling trajectory (developed in Chapter 3) was implemented and tested. A sample result is shown in Figure 4.12, which details the entry and exit portions of an actual trajectory which was used to produce the gas turbine engine combustion chamber panel designated as Part #1 in Chapter 3.

In the figure, the connection from rest is shown in the top section and the departure to a full stop on the bottom. As can be seen, the joining boundary conditions of velocity and acceleration are successfully satisfied at correct instances, into and out of the drilling trajectory. Since the different actuators for x-, y-, z-, a-, and c-axes have different velocity, acceleration, and jerk limits, and the connection boundary conditions are different, the transition motion durations are also different. Hence, while the global trajectory starts and ends asynchronously among the different actuators, the connection segments link up with the repetitive cyclic trajectory at the correct moments. It is also verified that the actuator jerk, acceleration, and velocity limits are always respected.

4.8 Conclusion

This chapter has presented a method for generating connection trajectories between a given initial or final state, comprised of position, velocity, and acceleration boundary conditions, and a resting state, in which the velocity and acceleration are required to be zero. The position at the resting state is not constrained and is assumed to be within the reach of the actuator(s). Based on these requirements, the resulting time-optimal trajectories which emerge in all possible cases have been analyzed and solved. Their global optimality has been demonstrated using the Principle of Optimality.

The proposed connection trajectories have been implemented in 5-axis positioning for the on-the-fly laser drilling application, in which they are used to connect into and out of the cyclic drilling trajectory with minimum productivity loss, while guaranteeing that vibration and dynamic positioning error on the actual machine stays within acceptable bounds (by limiting the trajectories' velocity, acceleration, and jerk profiles).

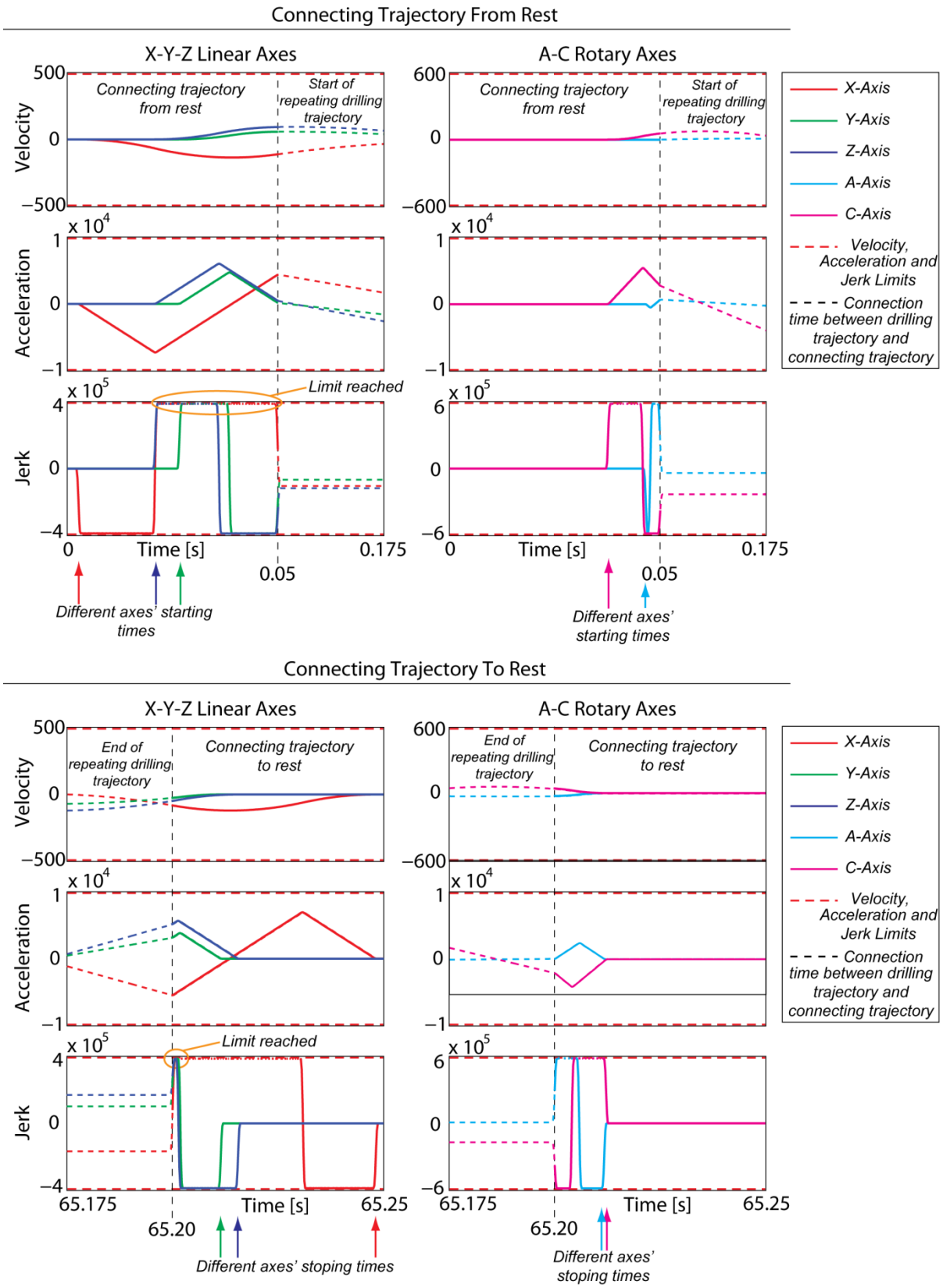

Figure 4.12: Validation of connection trajectories from and to rest for 5 axes.

The correctness of the formulation and the overall technique has been validated in 1- and 5-axis simulation studies. The resulting connection trajectories were also the ones used in the experimental results reported in Chapter 3.

Chapter 5

Way-Point Sequencing for 5-Axis Percussion Laser Drilling

5.1 Introduction

On-the-fly drilling is a suitable technology for producing better material properties and form accuracy in laser-drilled components, like combustion chamber panels. However, there are still some practical obstacles that need to be overcome, so that this technology can be adopted at full potential. For example, the following issues were observed while conducting the experiments reported in Chapter 3:

i) Jitter (i.e., period variation) in the laser pulsing period: Even a small percentage of period variation can result in significant timing and hole positioning error when drilling a large number of holes, as is the case in combustion chamber panels. This is because the laser period is used as the basic timing unit for the trajectory planning. The laser drilling machine tool utilized in the experiments was a prototype developed by combining a commercial laser with the Fanuc 30i controller. In the experimental results, the laser delivery system displayed 2-4% jitter, which can clearly present a problem in terms of causing tolerance violations in the hole locations. The jitter problem can be solved by adopting more advanced control and synchronization functions between the CNC and laser control electronics, in proceeding machines.

ii) Time synchronization errors between the CNC and laser electronics: Between executing the motion commands and turning the laser on and off, there are certain delays in the control system caused by auxiliary functions and checks. It was observed that these delays (ranging as 140-160 ms per hole location) unfortunately displayed poor repeatability, thus making their pre-compensation very difficult. However, in future machines system, it is expected that this problem would be solved again through better integration of the CNC and laser control electronics.

iii) Dynamic positioning errors in the machine tool: Since on-the-fly drilling takes place while the part is in motion, the accuracy of the servo system is crucial to guaranteeing the correct locations of the holes. While conducting on-the-fly drilling trials, the servo accuracy was also found to be a major issue, especially at high acceleration and jerk levels. Compounded with the above two issues, it was observed that the hole locations could be shifted by as much as 0.25-1.5 mm with skewed hole orientations of up to 15° between repeating passes. The problem of servo

errors can be tackled through dynamic modeling of the machine tool and control system and improving the feedforward and feedback control settings, or at least determining new actuator level velocity, acceleration, and jerk limits which guarantee a minimum level of beam positioning dynamic accuracy.

Currently, industrial development and academic research are being conducted to tackle the above mentioned three issues. In the interim, there is still a noticeable trend in industry to apply percussion drilling. As the number of laser pulses per hole increases, and newer laser systems with higher pulsing frequency become available, percussion drilling will continue to be a more productive option, if not as advantageous in terms of material qualities, compared to on-the-fly drilling. This is due to the duration spent on re-positioning the axes becoming a smaller fraction of the total manufacturing cycle time, as the number of pulses per hole increases.

In the interest of exploring further process improvement in the 5-axis percussion laser drilling process, this chapter targets the development of a new sequencing algorithm to suit this operation. The novelty of the proposed approach is that the sequencing is integrated with the kinematic (i.e., velocity, acceleration, and jerk) capabilities of the individual actuators. Hence, rather than minimizing the shortest travel path in work or machine coordinates, an attempt is made to solve the Traveling Salesman Problem (TSP) that minimizes the total travel time, by considering all possible time-optimal point-to-point motions between all hole pairs. This approach allows the true kinematic configuration and limits of the laser drilling machine to be considered, and yields a more accurate estimate of the positioning (and drilling) cycle time than simply considering the hole distances in workpiece or machine coordinates.

As pointed out in Chapter 2, the problem of finding the optimum sequence for manipulator waypoints can be considered as an extension of the TSP [51]. The proposed sequencing algorithm has some parallels to [21], [46], [52], [63], [85], which are algorithms that have been proposed for semiconductor and circuit board manufacturing and assembly problems. Such methods use TSP solutions that minimize the distance traveled, which can also sometimes translate into reducing the travel time; e.g. when only Cartesian axes with identical actuator limits are used. In the case of more complex kinematic configurations; for example, when combined Cartesian and rotary axes are used, one to one correspondence between distance and time is not guaranteed. Hence, in this thesis, the solution of TSP is investigated while

considering the *actual* motion durations derived from the 5-axis machine configuration and actuator kinematic limits.

The proposed sequencing algorithm has been developed by modifying the method proposed in Chapter 3 to suit the percussion drilling operation. The design of this algorithm is explained in Section 5.2. Following its presentation, its application to gas turbine component manufacturing is demonstrated in Section 5.3 with simulation and experimental results. The principal advantages gained, and some of the difficulties encountered in the experimental implementation, are also discussed.

In the context of benchmarking the proposed sequencing algorithm with established and highly advanced TSP solutions, the ideal comparison would be to implement positioning duration based sequencing which is integrated with solvers like the Concorde Cutting-Plane method and the Lin-Kernighan Heuristic algorithm [81], [18]. However, such thorough comparison was unfortunately not possible within the scope and duration of this thesis. A way of modifying the algorithms in a straightforward manner, to work directly with other cost functions (like actual positioning duration) could not be worked out, and is recommended for future research. Nevertheless, the sequencing algorithm in Section 5.2 has been benchmarked with these two well-known and state-of-the-art solvers in the context of sequencing 2-dimensional geometric distances. This initial step can help gauge how much further improvement could be expected in cycle time, from the extension of these methods to 5-axis percussion laser drilling in future research; by considering the actual machine kinematics, and actuator velocity, acceleration, and jerk limits. The results of this benchmark are presented in Section 5.5. The conclusions for the chapter are in Section 5.6.

5.2 Proposed Sequencing Algorithm

An overview of the sequencing algorithm for percussion laser drilling is provided in Figure 5.1. The inputs to the sequencing algorithm are:

- Hole locations $\boldsymbol{q}_k\left(k=1\ldots M\right)$ defined in joint (actuator) coordinates $\boldsymbol{q}_k=\left[x_k \;\; y_k \;\; z_k \;\; a_k \;\; c_k\right]^T$;
- Feed drives' velocity, acceleration, and jerk limits ($\boldsymbol{v}_{\max}$, $\boldsymbol{a}_{\max}$, $\boldsymbol{j}_{\max}$, per Eq. (1.1)), hole elongation limit is not needed;

- In the situation where the positioning trajectories have to be integer multiples of a given sampling period (e.g., T_s =1/(160 Hz), which is the case when 'inverse-time feed programming' is used to replay pre-generated recorded trajectories by the CNC), the corresponding sampling period, T_s .

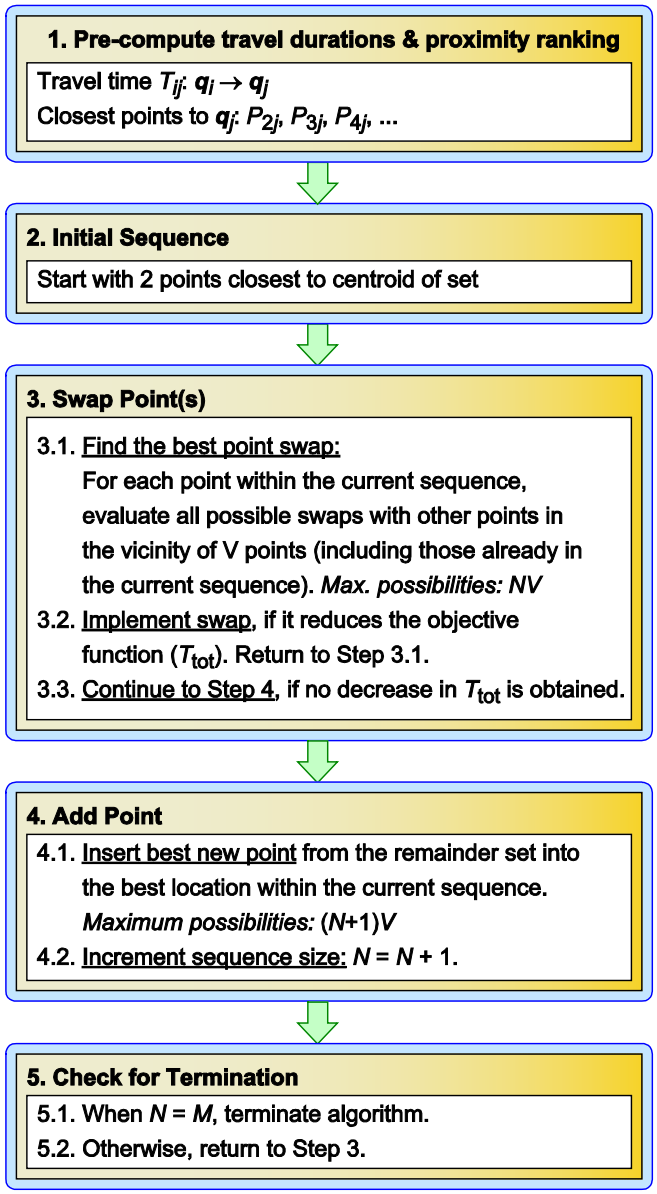

Figure 5.1: Percussion drilling sequencing algorithm.

Since in percussion drilling, the laser pulses are delivered while the part is (ideally) stationary, a constraint on the hole elongation, like the one used for on-the-fly drilling in Chapter 3, is not required. The steps of the algorithm are detailed in the following:

Step 1 – Determine Positioning Durations and Proximity Rankings for Hole Pairs

In this step, the time-optimal point-to-point motion duration is solved for traveling between every hole pair $\boldsymbol{q}_i$ and $\boldsymbol{q}_j$ using the jerk limited method explained in Appendix F. The resulting durations are stored in an array $\boldsymbol{T}_{M\times M}$, the elements ($T_{ij}$) which represent the positioning time from $\boldsymbol{q}_i$ to $\boldsymbol{q}_j$. Since the motion profile is generated only subject to actuator level velocity, acceleration, and jerk limits, and has a symmetrical shape with respect to time (as seen in Figure F.1), $T_{ij} = T_{ji}$ holds. Also, the diagonal elements of $\boldsymbol{T}$ are zero.

Using the travel duration data in $\boldsymbol{T}$, an array of proximity rankings is constructed for each hole. This is represented by a matrix $\boldsymbol{P}_{M\times M}$, where the *j*th column provides a ranked list of the closest waypoints to $\boldsymbol{q}_j$, with increasing travel durations downwards along the column. The following example helps visualize the relationship between $\boldsymbol{T}$ and $\boldsymbol{P}$:

$$\boldsymbol{T} = \begin{matrix} \textit{1} & \textit{2} & \textit{3} & \textit{4} \end{matrix} \begin{bmatrix} 0 & 40 & 30 & 20 \\ 40 & 0 & 50 & 10 \\ 30 & 50 & 0 & 60 \\ 20 & 10 & 60 & 0 \end{bmatrix}, \quad \boldsymbol{P} = \begin{bmatrix} 1 & 2 & 3 & 4 \\ 4 & 4 & 1 & 2 \\ 3 & 1 & 2 & 1 \\ 2 & 3 & 4 & 3 \end{bmatrix} \downarrow \textit{Increasing travel duration} \tag{5.1}$$

Step 2 – Initial Sequence

Since percussion drilling does not require the positioning trajectory to repeat itself, an open sequence can be used, which does not return to the initial point after reaching the last one. As an arbitrary choice for starting the algorithm, the two points closest to the centroid of the given set of M points are selected.

Defining the hole locations in normalized coordinates ($\boldsymbol{q}_k^n$), obtained by considering the actuator velocity limits ($\boldsymbol{v}_{\max} = \begin{bmatrix}\dot{x}_{\max} & \dot{y}_{\max} & \dot{z}_{\max} & \dot{a}_{\max} & \dot{c}_{\max}\end{bmatrix}^T$),

$$\boldsymbol{q}_k^n = \frac{1}{\boldsymbol{v}_{\max}}\boldsymbol{q}_k = \begin{bmatrix} \frac{x_k}{\dot{x}_{\max}} & \frac{y_k}{\dot{y}_{\max}} & \frac{z_k}{\dot{z}_{\max}} & \frac{a_k}{\dot{a}_{\max}} & \frac{c_k}{\dot{c}_{\max}} \end{bmatrix}^T \tag{5.2}$$

the centroid in normalized coordinates ($\bar{\boldsymbol{q}}^n$), and the normalized Euclidean distance of each point to the centroid ($\boldsymbol{d}_k$) is calculated as:

$$\bar{\boldsymbol{q}}^n = \frac{1}{M}\sum_{k=1}^{M}\boldsymbol{q}_k^n \qquad , \qquad d_k = \left\| \bar{\boldsymbol{q}}^n - \boldsymbol{q}_k^n \right\|_2 \tag{5.3}$$

As one of the points in the initial sequence, the hole location with the smallest value for d_k is chosen. Designating the first point index with $\bar{k}$, as the second point in the initial sequence, the hole location is chosen which has the closest proximity, in terms of travel time to $\boldsymbol{q}_{\bar{k}}$. Using the $\boldsymbol{P}$ matrix described in Eq. (5.1), the choice of the second point would be $P_{2,\bar{k}}$.

Sequence Data Structure and Objective Function Evaluation:

Similar to the method presented in Chapter 3, the sequence data structure contains the order of the waypoints inside an array $\boldsymbol{S}_{N\times 1} = \begin{bmatrix} l_1 & l_2 & \dots & l_N \end{bmatrix}$, where $l_1 \dots l_N$ are distinct (unrepeated) integers between 1 … M. The size of the array N represents the current size of the sequence. Since during the initialization in Step 1, the time-optimal travel durations between all points are pre-calculated inside the array $\boldsymbol{T}$, timings between the waypoints do not have to be recalculated for each candidate sequence. Given a candidate sequence, the objective function to be minimized is the total travel time:

$$\textbf{Objective function:} \quad T_{\textbf{tot}} = T_{l_1 l_2} + T_{l_2 l_3} + \ldots + T_{l_{N-1} l_N} \tag{5.4}$$

Step 3 - Swap Point(s)

For each point in the sequence, swaps with the neighborhood of closest V points (within or outside the sequence) are evaluated. In the implementation of percussion drilling sequencing, V was chosen as 20. If any of the tested swaps reduce T_{tot} in Eq. (5.4), then the swap that yields the

lowest value for T_{tot} is implemented. Testing of another round of swaps continues on until no further improvement(s) can be obtained. At each iteration, the current sequence $\boldsymbol{S}$ is updated by implementing the most successful swap operation.

Step 4 - Add Point

The 'best point' out of those not already in the sequence is inserted into the 'best location' in the sequence. For each edge connecting adjacent points $\boldsymbol{S}(k)$ and $\boldsymbol{S}(k+1)$, insertion of the nearest external V (=20) points is evaluated. The point insertion that yields the lowest T_{tot} for the new sequence size (N +1) is implemented.

Step 5 - Check for Termination

After Step 4, when $N = M$, this means that all waypoints have been sequenced. While a global optimum is very difficult to guarantee, the search procedure progresses from one local optimum to a next one.

Practical Implementation Considerations:

As done with the on-the-fly drilling sequencing algorithm in Chapter 3, logic was incorporated into Steps 3 and 4 to ensure that identical candidate sequences would not be re-evaluated, in order to save computational time. Upon finalization of the sequence, the connection trajectories are generated using the jerk-limited method explained in Appendix F at a sampling frequency of 160 Hz. The positioning trajectories are then programmed into the NC code in a manner that they can be executed in 'inverse-time' feed programming mode, as explained in Chapter 3 and shown in Figure 5.5.

5.3 Simulation Results

The proposed sequencing algorithm for percussion laser drilling complements, to a certain degree, the on-the-fly drilling trajectory generation method that was developed in Chapter 3. Of course, since on-the-fly and percussion laser drilling are two different approaches with distinct advantages over one another, as elaborated in Section 5.1, rather than comparing the results of

the two methods with each other, it makes sense to benchmark the algorithm in Section 5.2 with other sequencing and trajectory planning methods that are already being used in industry for 5-axis percussion laser drilling.

Naturally, the closest benchmark is the modified Nearest Neighbor (NN) sequencing method, currently in use at P&WC (which was explained in Chapter 3). This method chooses the closest next point, based on proximity in machine (actuator) coordinates, and initiates a new cluster (set/group of holes) each time the separation exceeds a given threshold. The proposed sequencing method in this chapter has two advantages over the NN method currently in use:

i) Actual positioning duration is considered rather than some form of 'distance' norm. This enables more realistic reduction of the total duration spent on beam positioning.

ii) The swap-add type sequencing algorithm is able to back-track over earlier steps and make incremental improvements, which typically leads to 'more optimal' sequences than the greedy 'Nearest-Neighbor' method.

The sequencing algorithm has been benchmarked in simulations to the modified NN method currently in use for percussion laser drilling. The benchmark was based on the three gas turbine combustion chamber panels shown earlier in Figure 3.5. The feed drive velocity, acceleration, and jerk limits are different than those that were used in the simulations in Chapter 3. The limits considered in the following simulations are very close to those used in the experimental results in this chapter. **While these limits are different than those used in the actual production, and the measured cycle times do <u>not</u> directly correspond to P&WC's actual production times, in order to avoid disclosing the full capabilities of the company's machine tool, the velocity acceleration, and jerk profiles shown here are only in normalized form with respect to arbitrarily adjusted kinematic limits.**

It is assumed that both drilling sequences, generated with the modified NN approach and the proposed algorithm in Section 5.2., would be executed by applying the jerk-limited minimum-time point-to-point positioning algorithm explained in Appendix F. While the actual positioning times of the laser drilling machine tool are not precisely known (and cannot be disclosed due to company disclosure restrictions), the proposed comparison is still a fair one since the modified NN-sequencing method relies on a measure of distance (in joint coordinates) rather than the actual duration in selecting the more favorable next waypoint.

The simulation results are presented in Figures 5.2, 5.3 and 5.4. The simulations consider only the total duration required to travel to each hole location once. Hence, the predicted durations represent the total time spent on beam positioning. These analyses are decoupled from the frequency and number of pulses of the laser drilling operation, which can be programmed and modified after-the-fact the sequence is determined. Total positioning times obtained with the two sequencing methods are compared in Table 5.1. As can be seen, the proposed sequencing method demonstrates between 9-22% reduction in the beam positioning time. The computational time taken to solve the percussion drilling sequence (following the proposed approach) was as follows: Sample Part #1: 52.46 [min], Sample Part #2: 66.33 [min], Sample Part #3: 28.35 [min].

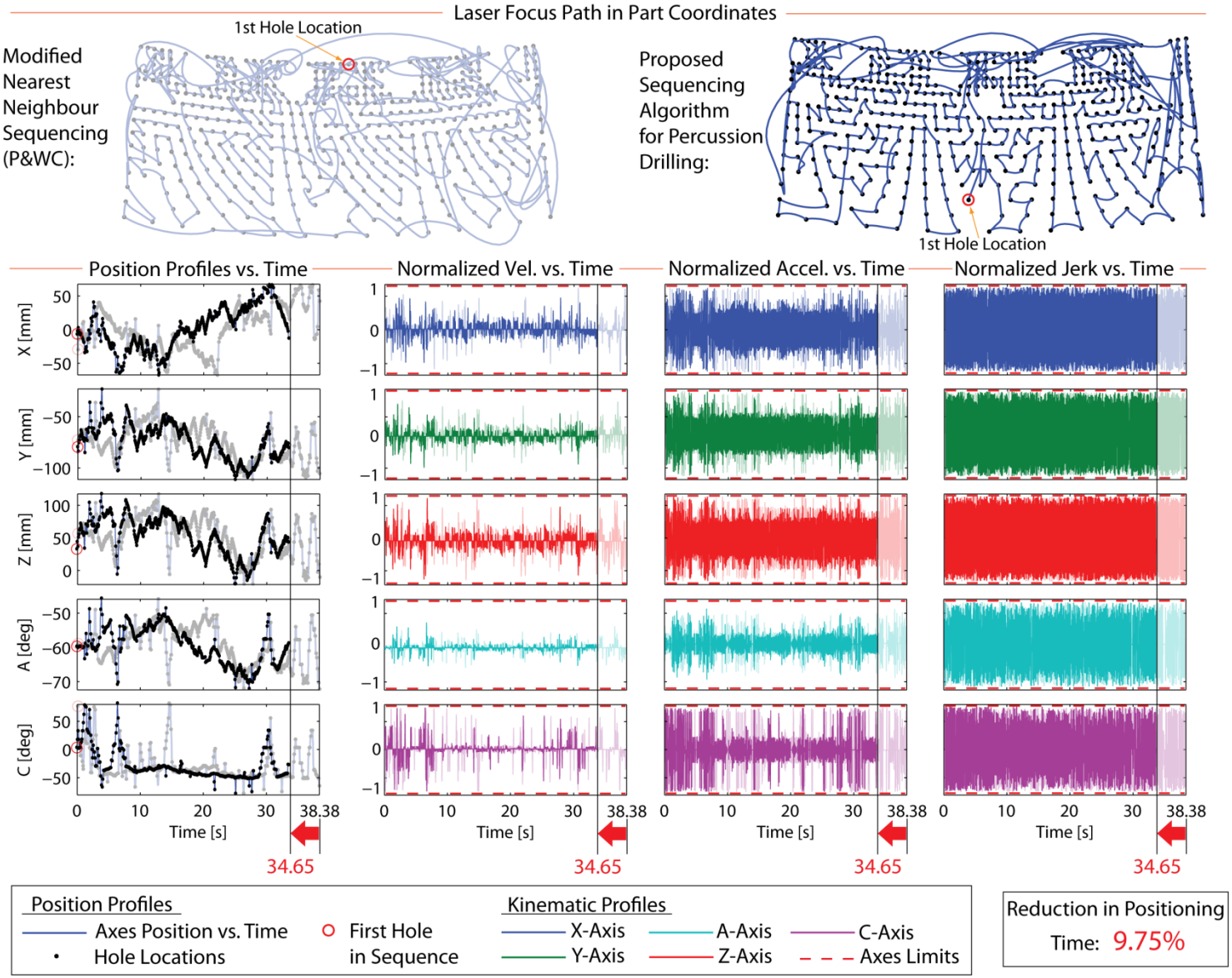

Figure 5.2: Comparison of sequencing results for Sample Part #1.

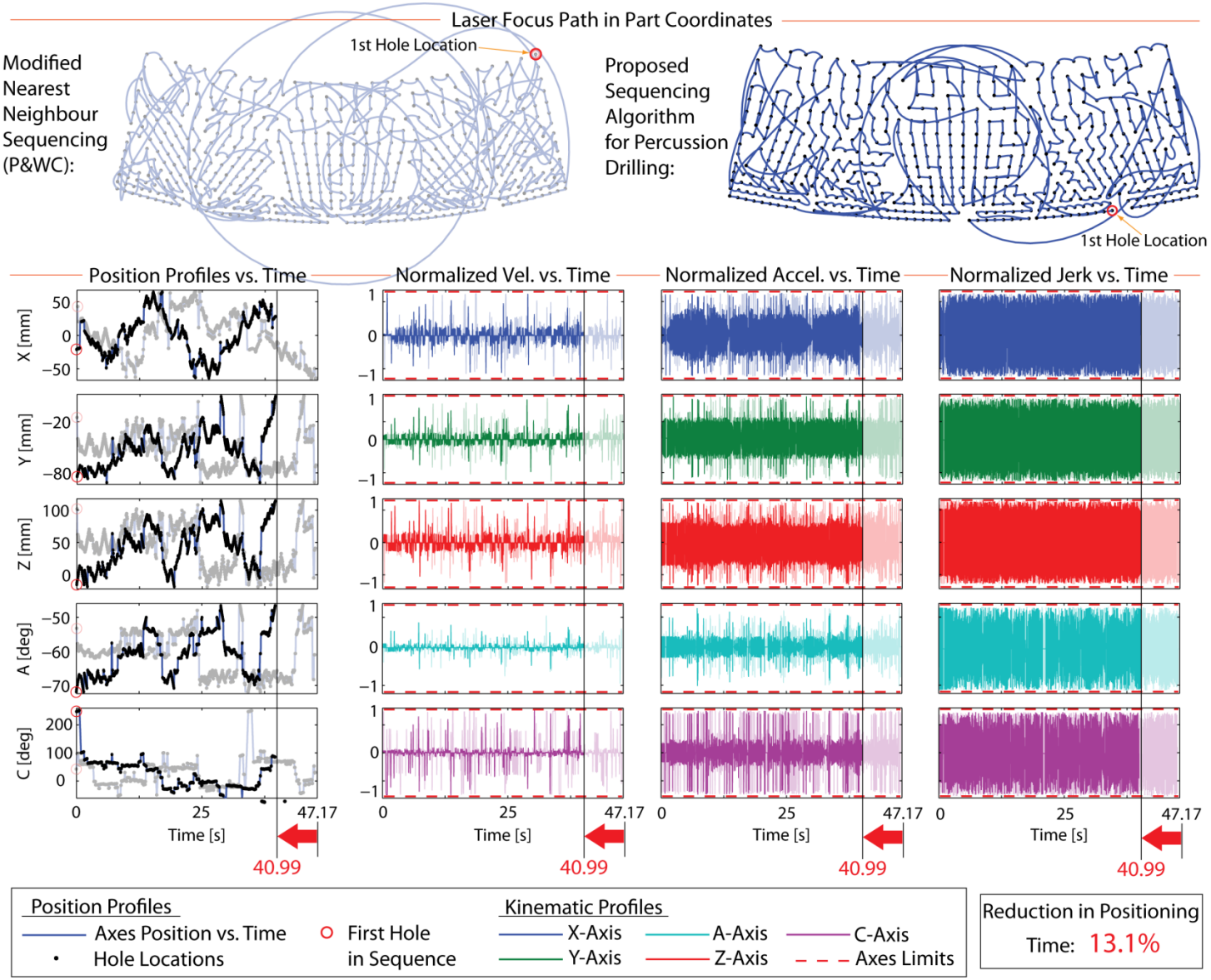

Figure 5.3: Comparison of sequencing results for Sample Part #2.

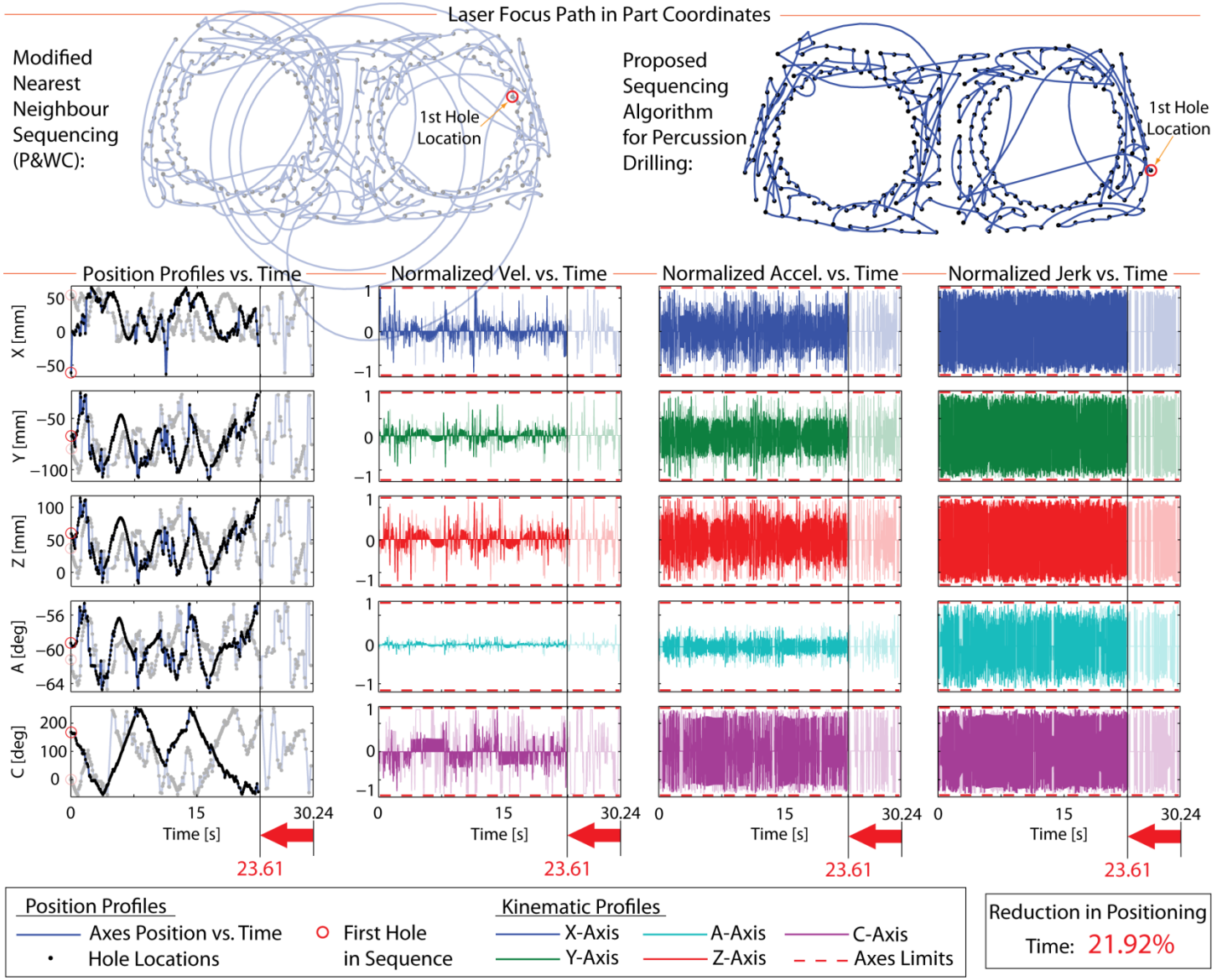

Figure 5.4: Comparison of sequencing results for Sample Part #3.

Table 5.1: Simulation results comparison table.

Sample part	# of holes	Beam positioning time with modified NN sequencing method [s]	Beam positioning time with proposed sequencing method [s]	Reduction in positioning time [%]
#1 (Figure 5.2)	474	38.38	34.65	9.75
#2 (Figure 5.3)	567	47.17	40.99	13.1
#3 (Figure 5.4)	284	30.24	23.61	21.92

5.4 Experimental Results

Sample Part #2 in Figure 5.3 (Sample Part #1 in Figures 3.5) was chosen for conducting percussion laser drilling experiments, which took place at P&WC. The tests were conducted using three different types of trajectory planning (i.e., sequencing and positioning) methods:

Type 1: Modified Nearest Neighbor sequencing with positioning using the G01 (linear interpolation) command, already built-in to the Fanuc 30i controller. The positioning duration between consecutive hole locations was set to a given time, e.g., 0.1 [s], by applying 'inverse-time' feed programming. These sequencing and interpolation methods combined reflect one of the standard practices applied at P&WC.

Type 2: Proposed (thesis) sequencing method, and applying G01 for actual positioning. Since the implementation details and function of the G01 command within the Fanuc controller is not well documented, and the outcome of this command is also difficult to predict exactly, the sequencing was carried out based on motion durations predicted with the time-optimal jerk-limited trajectory explained in Appendix F. In this case, the positioning durations between the consecutive hole locations obtained from these optimal trajectories were programmed into the NC code using inverse-time feed programming mode.

Type 3: Proposed (thesis) sequencing for percussion drilling, with the actual beam positioning taking place using the time-optimal jerk-limited method explained in Appendix F. In this case, the positioning trajectories were generated at 160 Hz, and programmed and executed on the Fanuc CNC using 'inverse-time' feed mode.

For each trajectory type, three different cases were considered in terms of the number of laser shots per hole (n). These were n = 1, 8, and 18. The laser drilling tests for each case were conducted three times; in order to validate the repeatability of the operation and measured production / cycle times. If inconsistency was spotted, the same test was conducted a fourth time (depending on machine availability). In total, 29 tests were performed.

The execution of each test was captured on video at 30 frames per second (FPS). This information helped resolve the durations spent on process initialization, actual part positioning (actuator motion), laser burst drilling, and various latencies (due to operational checks, communication delays, and compensation / correction features in the laser control system); by analyzing these videos frame by frame.

Excerpts from NC code used in the implementation of Types 1, 2, and 3 trajectory planning are shown in Figure 5.5. The left-hand side of Figure 5.5 shows the code structure for Types 1 and 2. The inverse-time feedrate value was set to 'F600 1/min' for Type 1, and other values which reflect the nominal travel duration of each positioning command in the case of Type 2. Specifically, 'F600 1/min' means that the positioning duration to the next hole will be T_{ij} = {60 [s/min]} / {F600 [1/min]} = 0.1 [s]. On the other hand, when the positioning time is calculated from the optimal motion generation for Type 2, for example to be 0.05 [s] (for positioning between two consecutive holes), the inverse feed value would have to be set to '{60 [s/min]} / {0.05 [s]} = F1200 [1/min]'. This value, in general, can change for each positioning step. For Type 3 trajectory planning, considering the right hand side of Figure 5.5(b), it can be seen that since the smooth trajectory is generated with a sampling period of T_s =1/160 = 0.00625 [s], the inverse-time feed value between pre-calculated waypoints is determined to be {60 [s/min]} / {0.00625 [s]} = F9600 [1/min]. According to the Fanuc CNC manual, the highest allowable value for the inverse-time feed (F) parameter is F9999; hence 160 Hz is a suitable upper bound for sampling and playing back custom generated trajectories using this method.

Cycle Time Summary: Table 5.2 show the total production cycle times for each test recorded from the CNC system's built-in cycle time measurement function. In these measurements, the duration spent on initialization type operations has been removed. These operations consist of setting up of the laser recipe, turning the vacuum system on, bringing the axes to home position, and bringing the laser optics to operating temperature. Looking at

Table 5.2, at first glance, it appears that improving the sequencing and trajectory generation does not seem to have a significant impact on the overall productivity of the process. However, by carefully examining the representative videos captured from each test configuration frame by frame, a more detailed timing analysis has been produced, as shown in Table 5.3 and Figure 5.6. This table shows that positioning cycle time reduction has indeed been achieved.

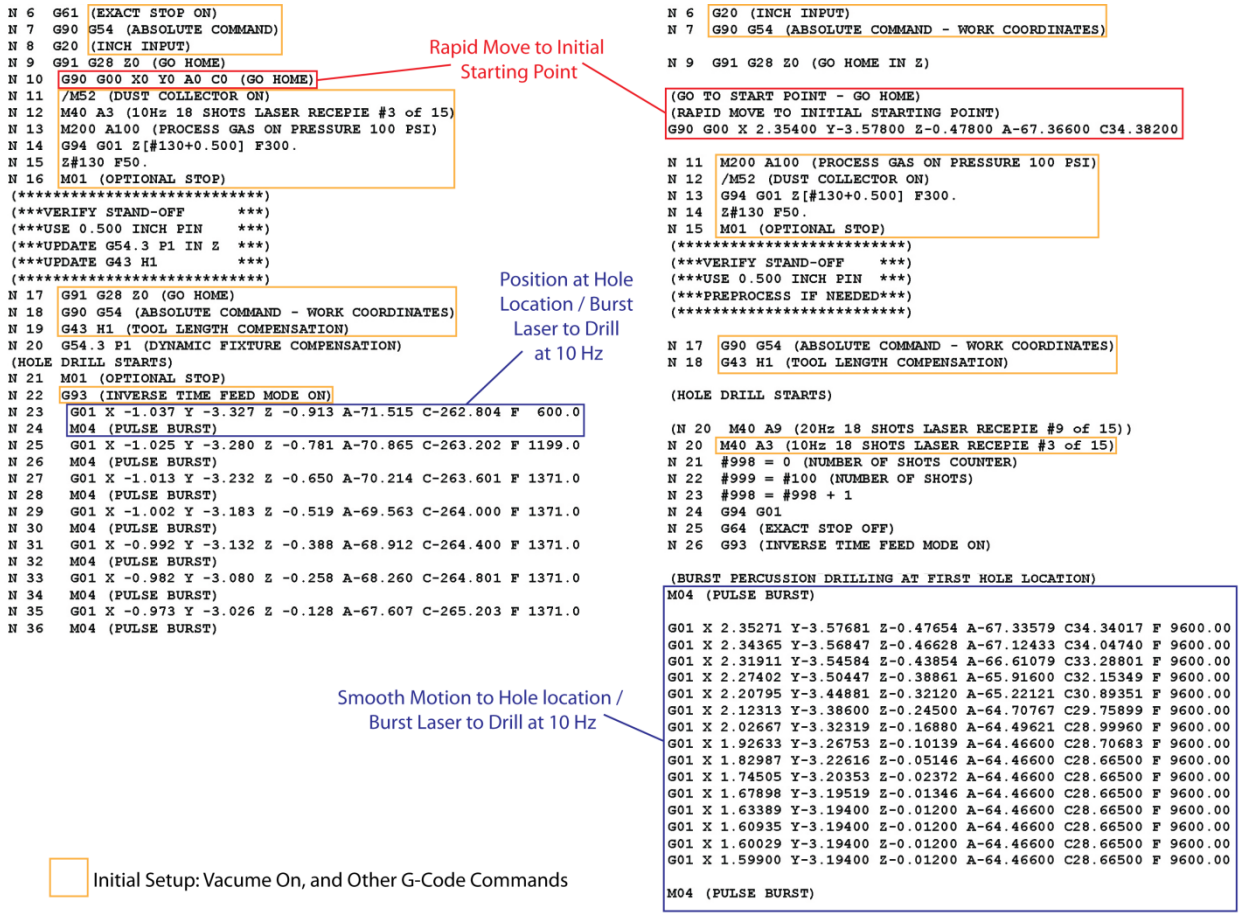

Figure 5.5: NC code structures used in tests of Types 1 and 2 (left) and Type 3 (right).

Table 5.2: Cycle time for tests on Sample Part #2. Time was registered from the CNC, process initialization time has been removed.

	Type 1: NN sequencing + G01 positioning	**Type 2:** Thesis sequencing + G01 positioning	**Type 3:** Thesis sequencing + smooth time-optimal positioning
1 shot per hole	**Test #1-4:** 172 s	**Test #5-8:** 169 s	**Test #9-11:** 166 s
8-shots per hole	**Test #12-14:** 564 s	**Test #15-17:** 566 s	**Test #18-20:** 564 s
18-shots per hole	**Test #21:** 1139 s **Test #22-23:** 1138 s	**Test #24-26:** 1133 s	**Test #27-29:** 1131 s

Table 5.3: Timing breakdowns for Sample Part #2 based on video frame analysis (30 FPS).

	Type 1: NN sequencing + G01 positioning	**Type 2:** Thesis sequencing + G01 positioning	**Type 3:** Thesis sequencing + smooth time-optimal positioning
1-shot per hole	(*Test 2*) Delays 45.87 Positioning **68.70** Laser burst 56.70 Total 171.27	(*Test 6*) Delays 67.93 Positioning **46.80** Laser burst 56.70 Total 171.43	(*Test 9*) Delays 72.67 Positioning **43.57** Laser burst 56.70 Total 172.93
8-shots per hole	(*Test 2*) Delays 41.67 Positioning **68.43** Laser burst 453.60 Total 563.70	(*Test 6*) Delays 63.87 Positioning **47.07** Laser burst 453.60 Total 564.53	(*Test 9*) Delays 66.10 Positioning **44.27** Laser burst 453.60 Total 563.97
18-shots per hole	(*Test 2*) Delays 50.40 Positioning **68.77** Laser burst 1020.60 Total 1139.77	(*Test 6*) Delays 63.23 Positioning **46.87** Laser burst 1020.60 Total 1130.70	(*Test 9*) Delays 68.23 Positioning **44.30** Laser burst 1020.60 Total 1133.13

In this table and figure, the durations spent for laser bursts, axis motion (i.e., beam positioning), and delays / stopping have been decoupled. The laser burst durations are reasonably deterministic, and can be calculated as $T_{laser\_burst} = MnT_{\text{laser}}$, where M (=567) is

the total number of holes, n (=1, 8, 18) is the number of shots per hole, and T_{laser} (=0.1 s) is the laser pulsing period.

It is interesting to note that as the sequencing is improved from the modified NN to the proposed method, the positioning time consistently decreases from an average value of 68.6 s to 46.91 s, which corresponds to a 32% reduction. As point-to-point trajectory generation is also improved from the CNC's built-in inverse-time mode linear interpolation (G01) to the developed time-optimal trajectory planning, the overall positioning time is further reduced to an average value of 44.05 s, achieving an overall 36% reduction in the positioning time.

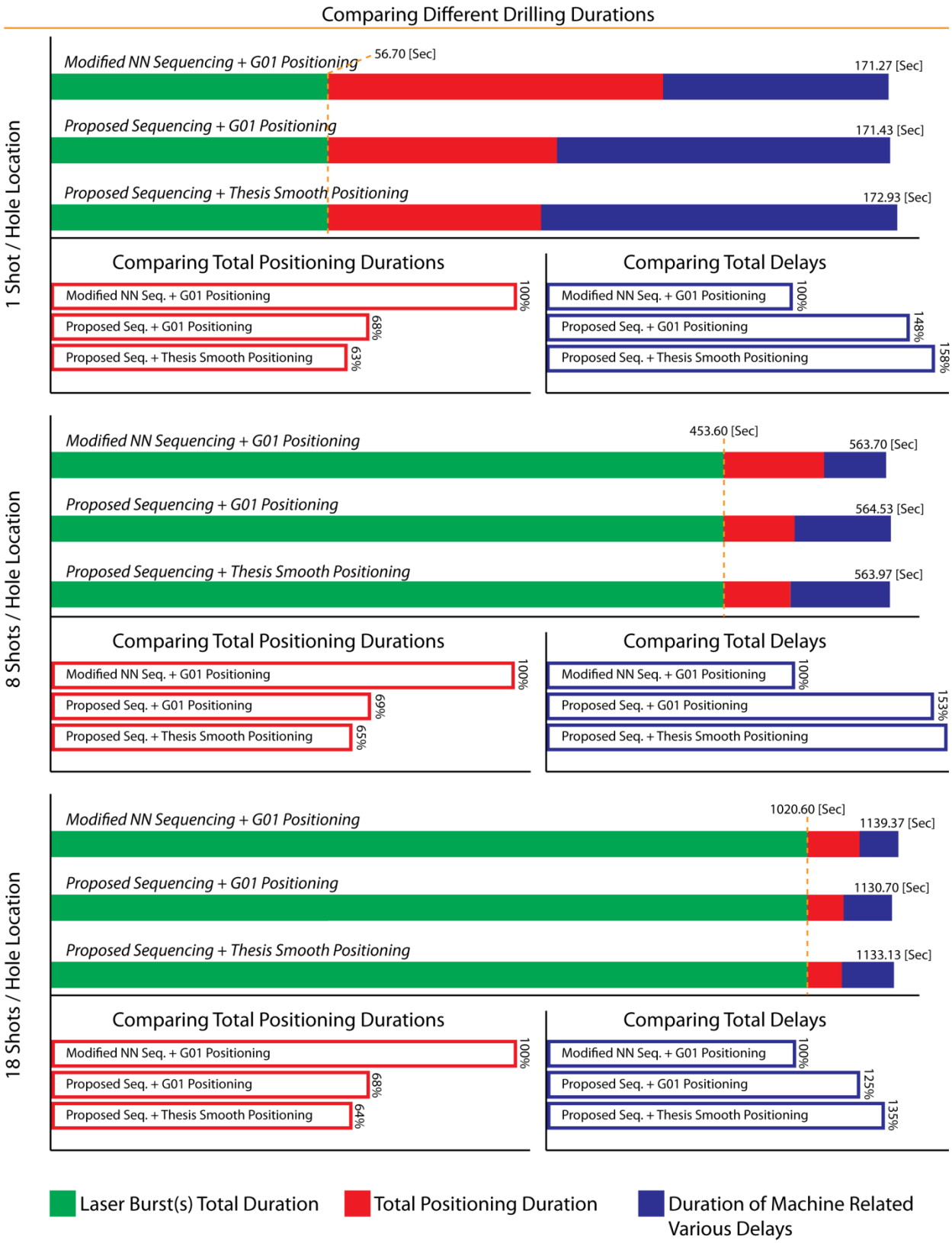

Figure 5.6: Timing breakdowns for Sample Part #2 (shown graphically).

Unfortunately, while the reduction in the motion duration is significant, the apparent time spent on CNC delays and keeping the axes at rest seems to have increased. The reduction in travel time is consistent across the 1-, 8-, and 18-shot cases, and so is nearly the increase in delay and stopping times. The increase in delays is believed to originate from the following reasons:

1) Utilizing inverse-time feed mode with non-uniform timing spacing in between the position commands (from Type 1 to Type 2). As the destination travel durations are still large enough, in the order of 100 milliseconds, this enables the CNC to perform intermediate trajectory planning, rather than directing the position commands straight to the drives. The CNC seems to require more complex calculations and perform additional checks in this case, than for the uniformly spaced inverse-time feed commands, as used in Type 1.
2) In Type 3 tests, a complex and smooth motion profile consisting of a large number of destination points, set apart by 6.25 ms, is sent between pulse bursts. This may be further increasing the complexity of processing the trajectory in between the programmed motion profiles.

Hence, while the research objective of demonstrating motion cycle time decrease has been achieved, a better CNC system is required which is capable of accurately executing the programmed motion commands, without inducing additional unwanted delays while the axes are at rest. This is needed in order to be able to take advantage of the gained cycle time reduction in practical manufacturing applications.

Vibrations Summary: Vibration data was calculated from the laser optics using a tri-axial accelerometer, as was done for on-the-fly drilling test in Chapter 3. The collected history in the x-, y-, and z-axes during the execution of the 8-shot drilling scenario is shown in Figure 5.7. A summary of peak to peak (PTP) and root mean square (RMS) amplitudes of the resultant vibration is presented in Figure 5.8.

The highest peak to peak magnitude of vibration is registered with the modified NN + G01 (Type 1) method. While the modified NN method seems to favor short travel distances, keeping the travel duration fixed for all motion commands (= 0.1 s) seems to induce significantly higher acceleration commands during the execution of some of the NC blocks.

This increases the residual vibrations induced on the machine tool structure and the laser optics.

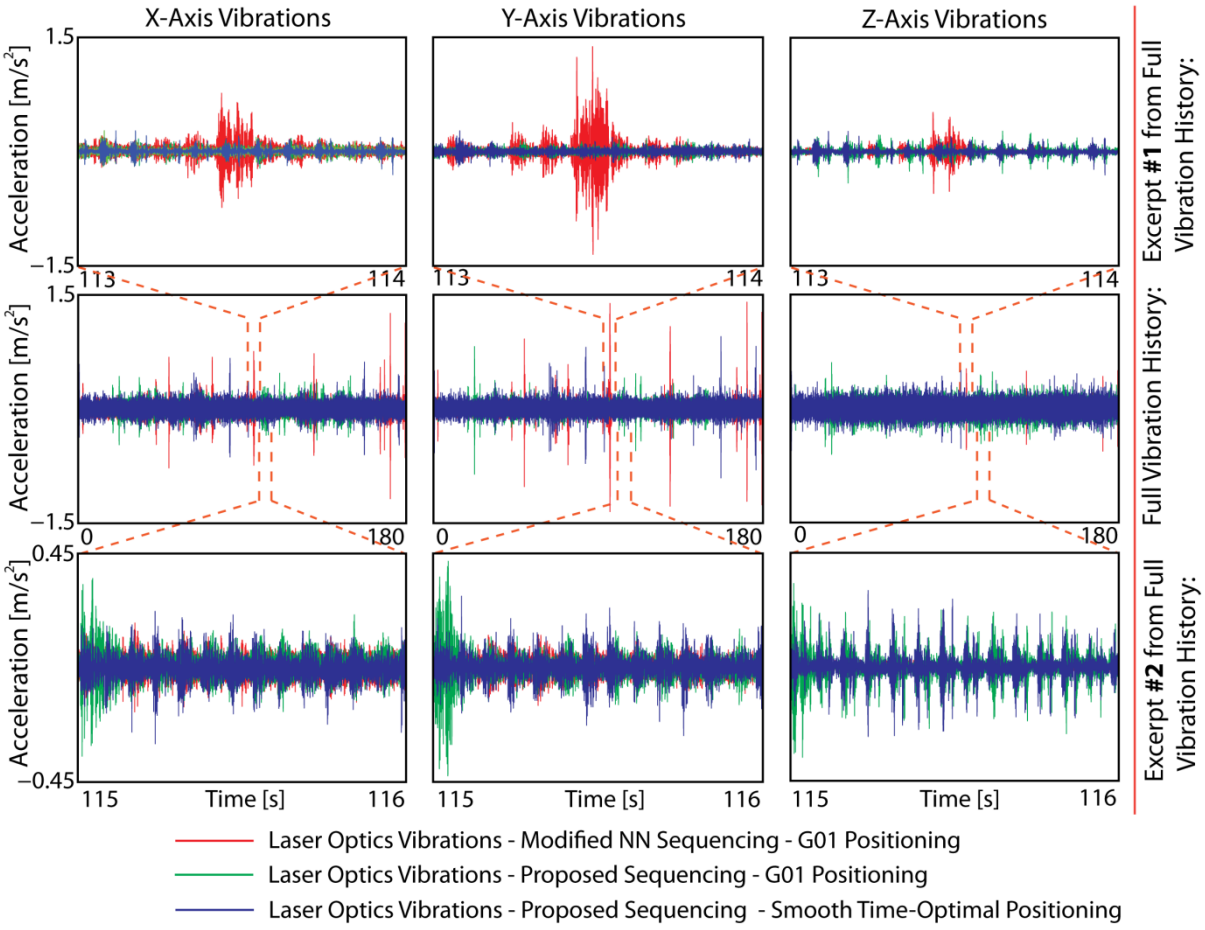

Figure 5.7: Optics vibrations captured for 8-shot percussion drilling of Sample Part #2.

The averaged resultant PTP vibration across 1-, 8-, and 18-shot cases is 1.99 m/s^2. With improved sequencing, and the coordination of the commanded motion durations to match the maximum velocity, acceleration and jerk capabilities of the drives, the induced accelerations also reduce significantly. As a result, with the proposed sequencing + G01 method (Type 2), the averaged PTP value of the resultant acceleration for 1-, 8-, and 18-shot cases reduces to 1.09 m/s^2. Replacing G01 with the time optimal positioning in Appendix F yields an averaged PTP value for resultant acceleration of 1.2 m/s^2 (10% larger than the Type 2 case). Overall, there is 45% and 39% reduction in peak vibrations, by switching from the NN method to the proposed sequencing and trajectory planning approaches. This is important,

because while 32-36% motion time reduction is achieved, quality and smoothness of the trajectory is not compromised, but rather improved (as measured from the laser optics), which implies longer term manufacturing productivity without requiring optics re-alignment. As a second remark, it is worth pointing out that even when the positioning method is kept identical switching over from the modified NN method to the proposed sequencing algorithm already provides a significant reduction in the motion time, as demonstrated in Section 5.3.

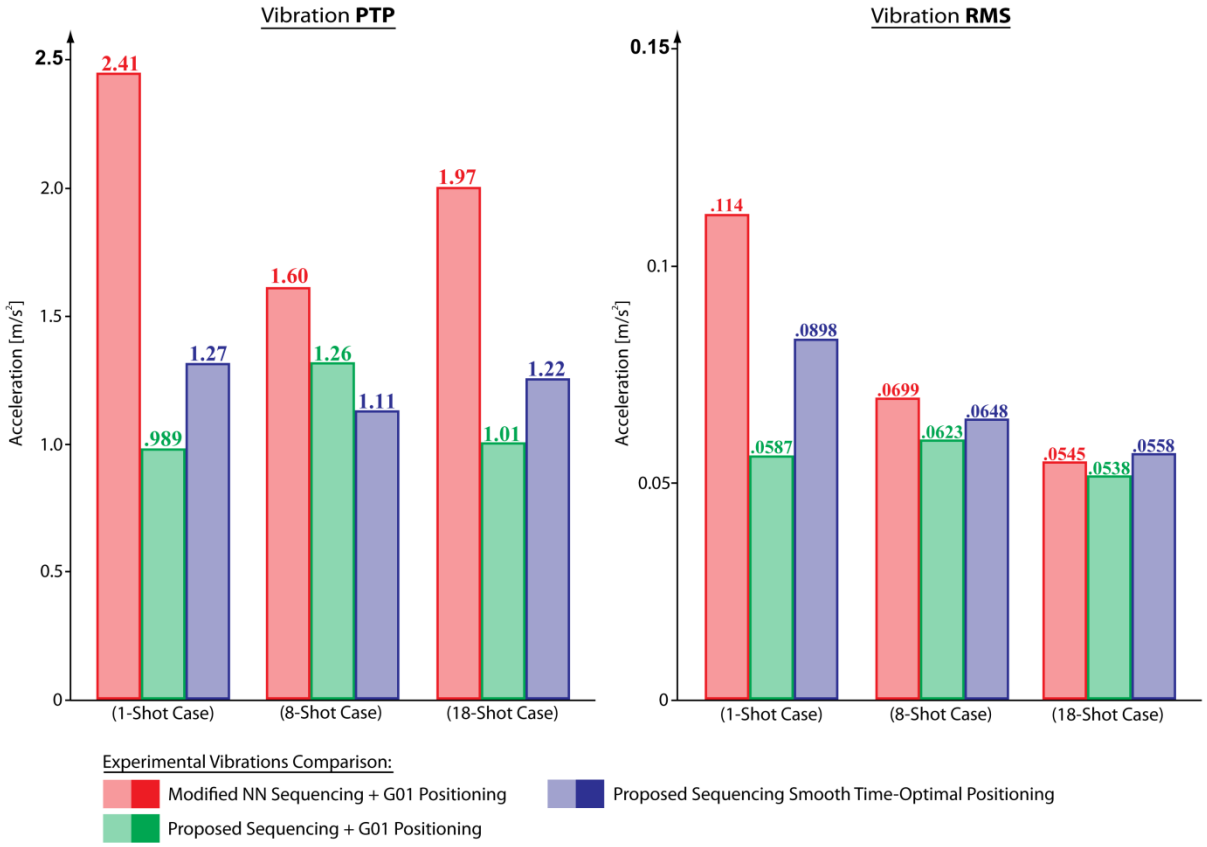

Figure 5.8: Peak to peak (PTP) and root mean square (RMS) values of resultant vibration.

Considering the plots for RMS values of resultant vibration in Figure 5.8, it is seen that as the number of shots increases (i.e., as the axes are allowed more time to settle to rest), the residual vibrations have more time to die out. Thus, there is a general decreasing trend in the RMS values of vibration from the 1-shot case to the 8-shot and 18-shot cases. In the 1-shot case, the strong vibration reduction facilitated by switching to Type 2 and Type 3 trajectory planning is evident. In 8- and 18-shot cases, longer portions of the stationary motion are

averaged into the RMS calculation, and the difference is less distinguishable. However, overall, it can be concluded that while the motion cycle time is reduced through improved waypoint sequencing, there is not a significant increase in the RMS value of vibration induced onto the laser optics. It is also worth mentioning that the RMS values of vibration are typically an order of magnitude lower than their PTP counterparts.

5.5 2-Axis Comparison to State-of-the-Art TSP Solvers

The proposed sequencing method has been compared to the Concorde cutting plane TSP solving method, and also the Lin-Kernighan TSP heuristic, which has been embedded within the Concorde package [18]. These two algorithms can be regarded as being among the gold standard of most powerful solutions that have been developed to solve the TSP.

At the time of writing this thesis (prior to defense), a method of embedding the proposed 5-axis optimized trajectory planning directly into the Concorde solver could not be contrived. Hence, as an alternative, Concorde solver's user interface was used to compare x-y type sequencing (based on Euclidian distance only) with proposed algorithm in this thesis. In future work, it is planned that Concorde algorithms (which also include the Lin-Kernighan heuristic) will be integrated with on-the-fly and percussion drilling scenarios. The proceeding benchmarks provide an estimate for the expected cycle time reduction that may be achieved beyond what is already realized with the current proposed algorithm.

The output of each method is the total travel distance between a random set of points (kept the same when benchmarking each algorithm). Figure 5.9 shows the difference between the proposed algorithm and the Concord TSP solver outputs. Figure 5.10 shows the Concorde TSP solver's graphical user interface. Table 5.4 gives the travel distance summary for random sets from 50 to 500 points. While the developed sequencing algorithm produces somewhat comparable results (in 2-dimensions), it is seen that a further cycle time improvement of up to 12% may be achievable by integrating algorithms from the Concorde TSP library together with 5-axis point-to-point time-optimal trajectory planning; in order to realize further gains in the percussion laser drilling process.

Table 5.4: Thesis sequencing method vs. Concorde and Lin-Kernighan TSP solvers.

# of Random Points	Concord TSP Solver	Lin-Kernighan (L-K) TSP Solver	Thesis Sequencing Method	Percent Difference from Concord Solver	Percent Difference from L-K Solver
50	589	589	589	0.0%	0.0%
100	748	748	781	4.3%	4.3%
200	1086	1086	1165	7.0%	7.0%
300	1295	1295	1461	12.0%	12.0%
400	1472	1475	1597	8.1%	7.9%
500	1657	1660	1833	10.1%	9.9%
Average Percent Difference				**6.9%**	

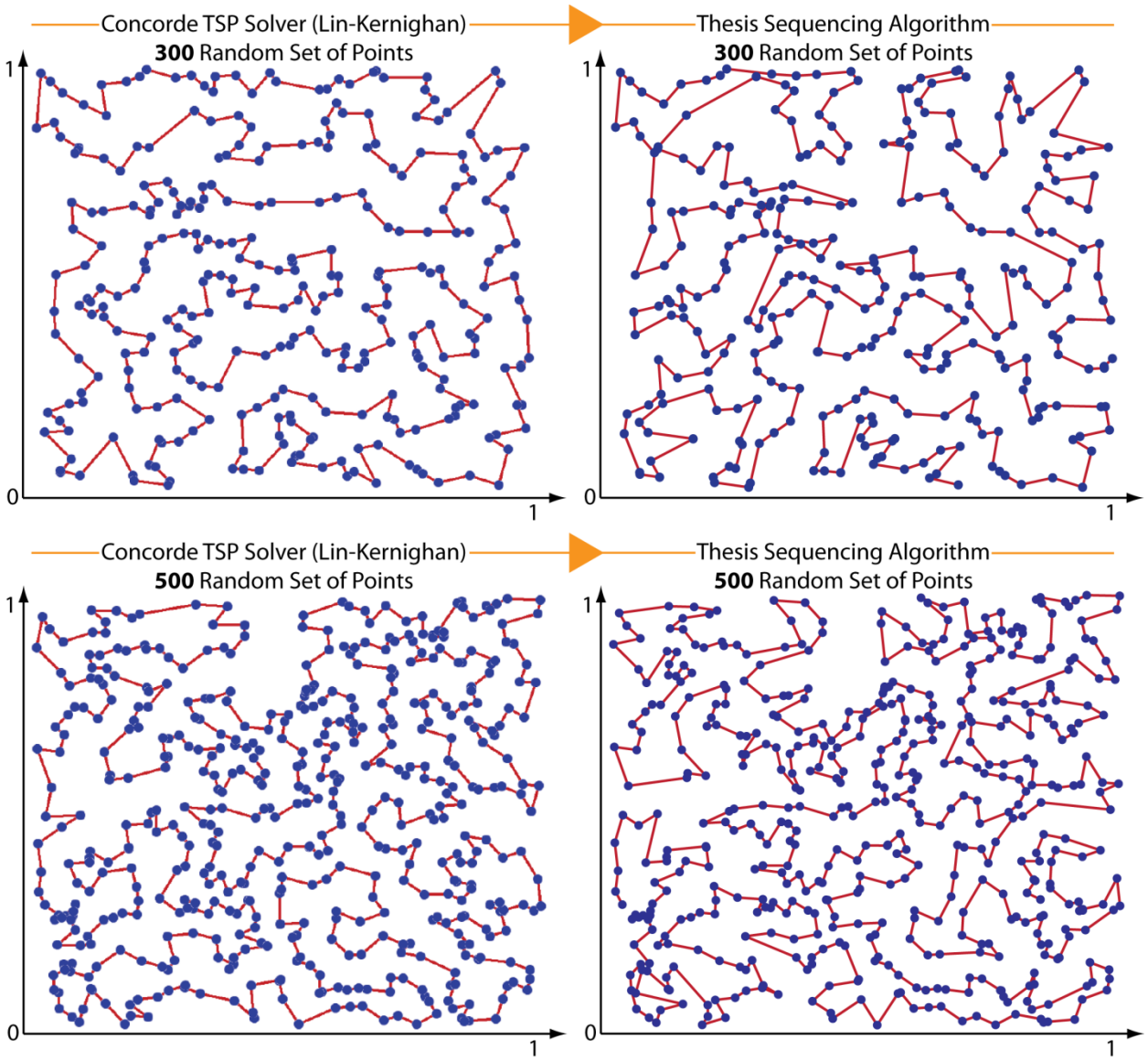

Figure 5.9: Thesis sequencing method comparison with Concorde TSP solver [2-Axis].

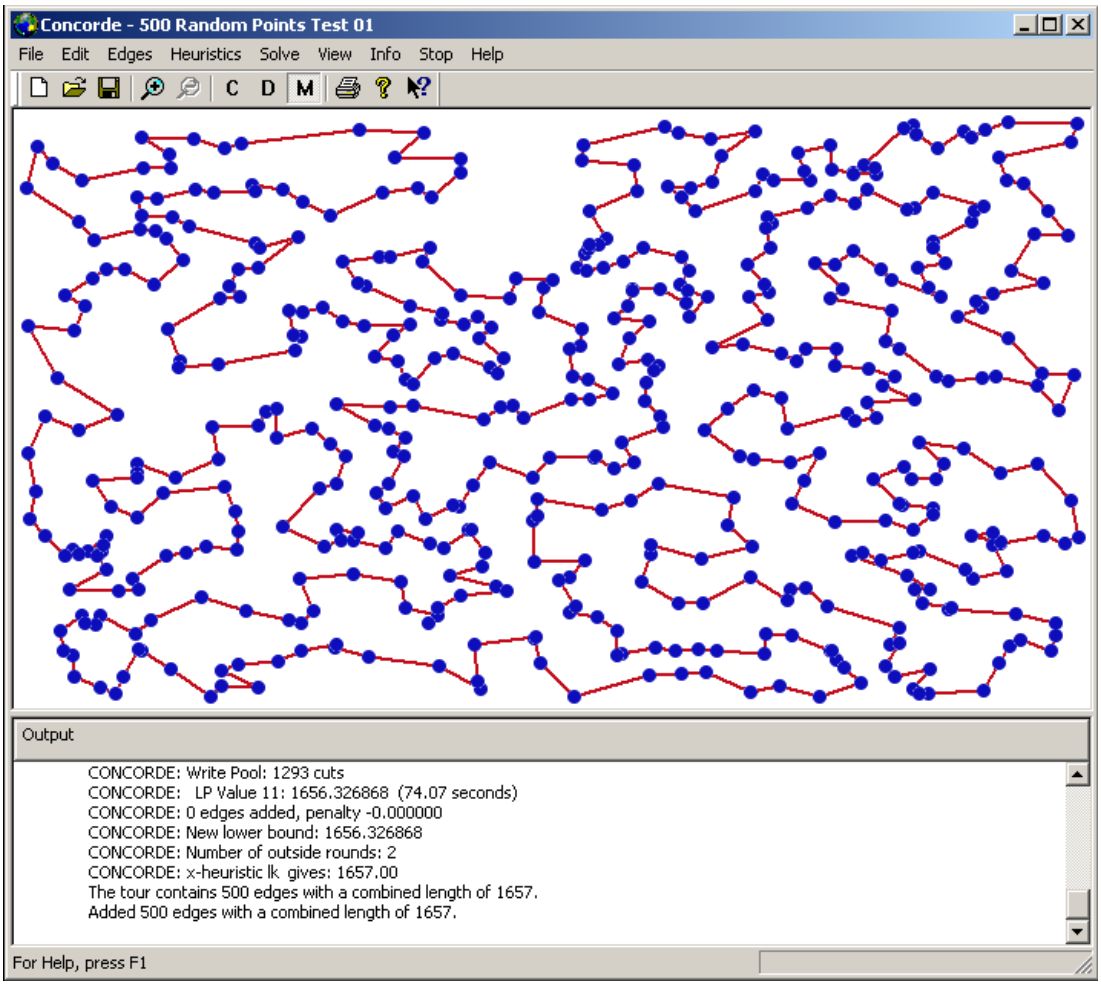

Figure 5.10: Concorde TSP solver graphical user interface.

5.6 5-Axis Comparison to State-of-the-Art TSP Solvers

Following the defense of this thesis, the proposed sequencing method was further compared with the Concorde and LKH TSP solvers, this time directly in the context of minimizing total travel time in 5-axis point-to-point positioning. This was achieved with instruction from Prof. S. Smith (UW-ECE), who kindly provided a short tutorial on the use of Concorde and LKH libraries, and MASc student Mr. Kyongjae (Jay) Woo, who provided assistance in running the additional benchmarks.

The pre-computed time-optimal point-to-point motion duration matrix $\boldsymbol{T}$ (Eq. (5.1)) was directly fed into the Concorde and LKH solvers as the objective weighting matrix. The algorithms were run with their (typical) default parameter settings. All three solutions directly targeted minimization of the total travel duration. One small comparison difference to note is that the proposed algorithm in the thesis solves an open path, whereas Concorde and LKH algorithms solve closed tours. Nevertheless, this comparison gives a concrete indication of the sub-optimality of the proposed solution in the context of optimizing laser percussion drilling paths for the three sample gas turbine engine components.

Figure 5.11 shows the difference between the proposed algorithm and Concorde and LKH solver outputs. Table 5.5 gives the travel durations summary. The developed algorithm seems to produce comparable results with the other two methods, with the sub-optimality ranging around 2%. However, these results are limited only to the three sample geometries, and are not as exhaustive in terms of measuring the overall improvement that can be gained by upgrading the sequencing algorithm to the Concorde and LKH methods. In the author's view, the results in Section 5.5 provide a more realistic and exhaustive benchmark serving this purpose.

Table 5.5: Thesis sequencing method vs. Concorde and LKH TSP solvers.

	Concorde TSP Solver	LKH TSP Solver	Proposed Thesis Algorithm	Percent Difference from Concorde & LKH
Sample Part #1	26.75 [sec]	26.76 [sec]	27.32 [sec]	2.11%
Sample Part #2	31.71 [sec]	31.71 [sec]	32.14 [sec]	1.35%
Sample Part #3	18.49 [sec]	18.49 [sec]	18.91 [sec]	2.24%
Average Percent Difference				**1.9%**

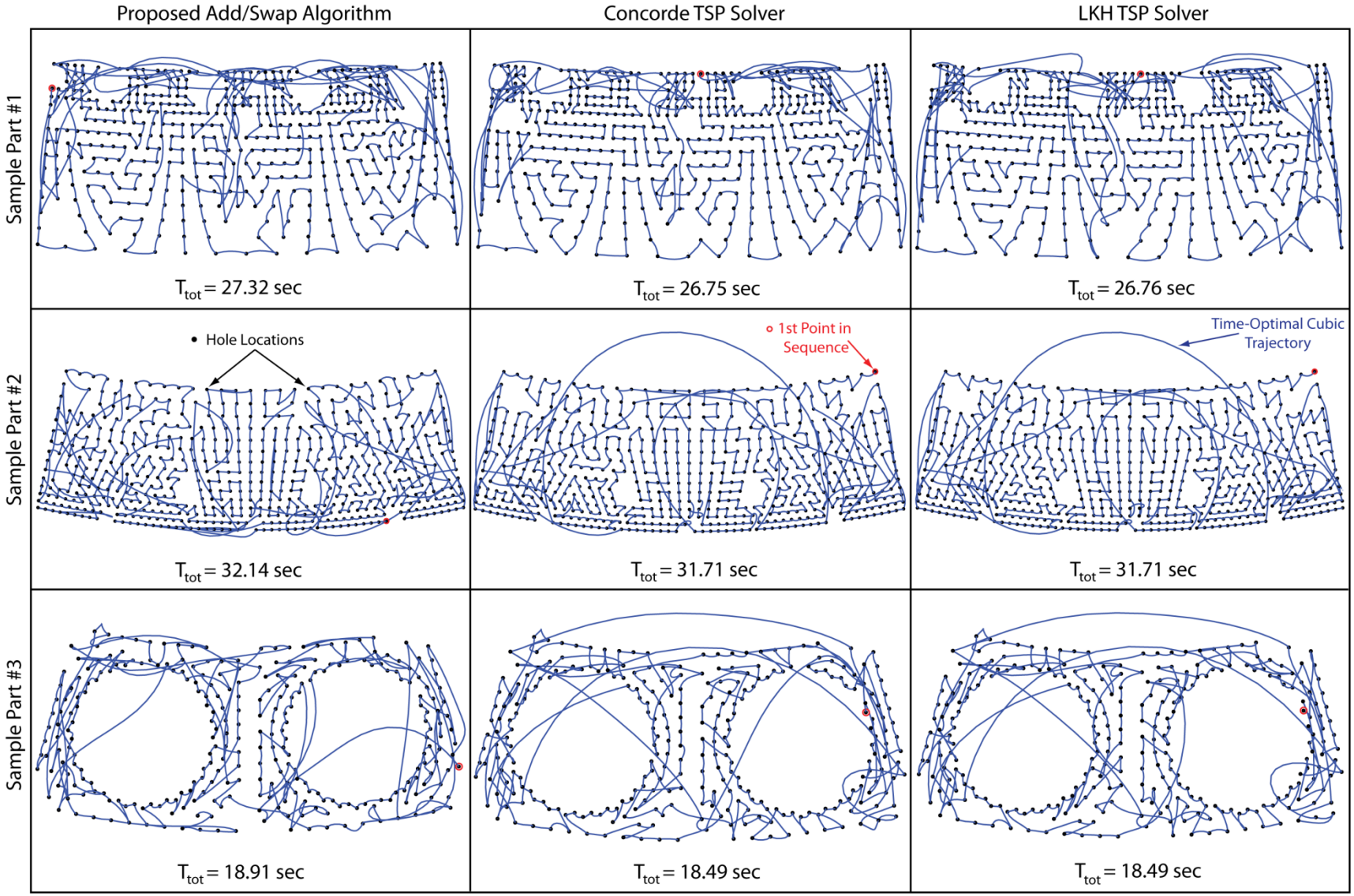

Figure 5.11: Thesis sequencing method comparison with Concorde TSP solver [5-Axis].

5.7 Conclusion

This chapter has presented a new waypoint sequencing algorithm for 5-axis percussion laser drilling. The algorithm is integrated with time optimal positioning subject to velocity, acceleration, and jerk limits in three translational and two rotary degrees of freedom. The principal advantage of the proposed sequencing method over the modified NN method has been benchmarked with three waypoint patterns; which have demonstrated 9-22% improvement in positioning time in the obtained simulation results.

In the experimental studies, benchmarks with the industrial practice of applying modified NN sequencing in conjunction with G01 (linear interpolation) based positioning were conducted. These benchmarks demonstrated 32-36% reduction in the time spent on positioning the laser focal point with respect to the beam. The peak vibration amplitude induced on the laser optics was also reduced by 39-45%. To be able to take advantage of the motion time reduction, achieved by the proposed sequencing and minimum-time trajectory generation method, improvements to the CNC system and laser electronics are still required, so that unnecessary delays while the actuators are at rest, can be avoided.

Currently, these algorithms are being tested further in production trials at Pratt & Whitney Canada, and plans are in place to evaluate them on laser drilling machines with different configurations.

Chapter 6

Conclusions and Future Work

6.1 Thesis Contributions

This thesis has presented novel trajectory planning algorithms for 5-axis on-the-fly and percussion laser drilling operations. For each process, a custom sequencing algorithm has been developed, which is integrated with adequate smooth trajectory generation capabilities that bounds the velocity, acceleration, and jerk profiles commanded to the laser drilling machine tool's actuators.

In the case of on-the-fly drilling, the beam positioning motion consists of a cyclical (closed-curve) cubic spline trajectory which is optimized by way of sequencing the drilling locations (i.e., waypoints) and by adjusting the timings in between the holes in order to yield kinematic profiles that achieve the shortest motion time, thus highest productivity. The sequencing algorithm consists of a combination of point swap, timing modification, and point add operations. Since the drilling takes place while the part is in transit, an extra kinematic constraint, limiting hole elongation, is also included.

The conducted simulation benchmarks reveal 55-76% motion time reduction compared to the candidate's earlier work, which was based on optimizing the trajectory shape (i.e., spline derivative boundary conditions) for pre-sequenced waypoints according to a 'greedy' Nearest Neighbor based algorithm. In experimental benchmarks, compared to two different trajectory planning methods currently used in industry for on-the-fly drilling and percussion drilling, the proposed sequencing and trajectory planning methods yield 17-25% reduction in the motion time, and also 17% mitigation in the RMS value of the resultant vibrations induced onto the laser optics. Time-optimal connections into and out of the cyclical trajectory, from and to zero (rest) boundary conditions have also been solved and implemented in the experimental evaluations.

In the case of percussion laser drilling, time-optimal point-to-point motions between all possible waypoint pairs are efficiently pre-computed a priori. Then, a sequencing algorithm based on point swap and point add operations seeks the best possible open sequence that minimizes the total travel time. Unlike traditional Traveling Salesman Problem (TSP)

solvers, the research in this thesis considers direct minimization of the motion time for 5-axis kinematics, rather than minimizing the Euclidean distance in two axes. The experimental results indicate 32-36% motion time reduction compared to the current industrial practice for 5-axis percussion laser drilling trajectory planning, in a sample application of gas turbine combustion chamber panel manufacturing. The developed algorithm, when benchmarked with some of the most advanced TSP solvers from literature (based on minimizing the total travel distance in 2-cartesian axes or minimizing total travel time in 5-axes) displays 2-12% sub-optimality, indicating room for further improvement. Nevertheless, the developed percussion laser drilling trajectory planning presents a first-of-its-kind for this application, based on the integration of TSP with time-optimized trajectory planning in a 5-axis kinematic configuration.

6.2 Future Research

A. Resolving Practical Issues

The developed algorithms have achieved promising results that are applicable to 5-axis on-the-fly and percussion laser drilling. However, during experimental implementation on a prototype machine tool, custom built for P&WC, several practical issues were encountered. The most significant was the lack of accurate synchronization between the CNC system and the laser power and optics control electronics. Another was the excessive servo errors, originating from the control system not having been tuned optimally.

For on-the-fly drilling, while the commanded trajectories were calculated and played back accurately, the jitter (timing fluctuation) in the laser electronics and the communication latencies between the CNC and quick shutter (which is supposed to divert unused laser pulses away from the workpiece) resulted in inaccuracy when performing the repeated drilling passes. Furthermore, the servo control system of the machine tool displayed significant dynamic positioning errors (0.25-1.5 mm). While the servo errors are repeatable, and mainly a function of the commanded trajectory, they still result in the holes being drilled at the incorrect locations and with the wrong orientations. They can be corrected by shifting the position commands (as required), or using recursive means like Iterative Learning Control (ILC).

During the percussion drilling experiments, it was observed that between playing back the custom generated point-to-point trajectories and turning the laser bursts on and off, there were unanticipated delays in the CNC system. These delays were so significant that they nearly nullified the positioning time savings achieved through the developed sequencing and trajectory planning algorithms.

The above described issues related to timing can be resolved through better integration of the CNC and laser control electronics. This effort is already underway at the sponsoring company, P&WC. Plans are in place to upgrade the laser drilling machinery with more accurately controlled laser sources, and with CNC systems that have advanced timing features supporting laser drilling operations.

B. Further Research in Trajectory Planning and Accuracy Improvement

It is proposed that the sequencing algorithms be developed further, by integrating the 5-axis closed cubic spline and high-speed point-to-point trajectory planning capabilities, developed in this thesis with more powerful TSP solvers, like the Concorde Cutting Plane and the Lin-Kernighan Heuristic methods. The combination of these approaches is expected to achieve even further reduction in the motion cycle time for industrial applications, and also contribute new trajectory planning methods to the motion controls literature.

Developing a virtual model of the machine tool dynamics, through multi-body modeling, vibration modal analysis, and analyzing the feedback and feedforward control loops, would also enable the prediction of the servo errors for different drilling and positioning trajectories, without having to conduct time consuming experiments on the actual machine tool. In this case, one easy correction would be to offset the position commands using means like Iterative Learning Control in a virtual production environment, so that the actual beam positioning would be achieved on the actual part with the given tolerances. Such a model would also enable the prediction and containment of residual vibrations, especially in the orthogonal plane to the laser beam axis, which would further improve the part quality.

References

[1] Aarts E., Lenstra J. K., 2003, “Local Search in Combinatorial Optimization”, Princeton University Press, ISBN: 978-0-691-11522-1.

[2] Abdel-Melek L., Li Z., “The application of inverse kinematics in the optimum sequencing of robot tasks”, Int. J. Prod. Res. 1990; 28(1), pp. 75-90.

[3] Altintas, Y., Erkorkmaz, K., 2003. "Feedrate Optimization for Spline Interpolation in High Speed Machine Tools”, Annals of CIRP, Vol. 49, No. 1, pp. 265-270.

[4] Alzaydi A., 2011. M.A.Sc. Thesis, “Time Optimal Trajectory Generation for 5-Axis On-the-Fly Drilling”, University of Waterloo, Waterloo, Ontario.

[5] Alzaydi A., Erkorkmaz K., Elfizy A., Engin S., 2010, “Time-Optimal Trajectory Generation for Laser Drilling”, Proc. 25th ASPE Annual Mtg., Atlanta, GA, Oct 31-Nov 5.

[6] Applegate D. L., Bixby R. E., Chvata V., Cook W. J., 2006, “The Travelling Salesman Problem: A Computational Study”, Princeton University Press, NJ.

[7] Bang-Jensen J., Gutin G., Yeo A., 2004, “When the greedy Algorithm Fails. Discrete Optimization 1”, pp. 121-127.

[8] Bellman, R. E., and S. E. Dreyfus, 1962, “Applied Dynamic Programming”, Princeton, N.J., Princeton University Press.

[9] Bendall G., Margot F., 2006, “Greedy Type Resistance of Combinatorial Problems, Discrete Optimization 3”, pp. 288-298.

[10] Bobrow, J. E., Dubowsky, S., Gibson, J. S., 1985, "Time-optimal Control of Robotic Manipulators Along Specified Paths”, International Journal of Robotics Research, Vol. 4, No. 3, pp. 3-17.

[11] Bohez E. L. J., 2002, “Five-Axis Milling Machine Tool Kinematic Chain Design and Analysis”, International Journal of Machine Tools and Manufacture, Vol. 42, No. 4, pp. 505-520.

[12] Busetti F., 2003, “Simulated Annealing Overview”.

[13] Butler J., Haack B., Tomizuka M., 1988, “Reference Generation for High Speed Coordinated Motion of a Two Axis System”, Symposium on Robotics, ASME Winter Annual Meeting, Chicago, Il, USA, DSC Vol. 11, pp. 457-470.

[14] Chakraborty N., Akella S., Wen J., 2007, “Coverage of a Planar Point Set with Multiple Constrained Robots”, Prof. 3rd Annual IEEE Conf. Autom. Sci., Eng., Scottsdale, AZ, USA, Sept 22-25.

[15] Chakraborty N., Akella S., Wen J. T., 2010, “Coverage of a Planar Point Set With Multiple Robots Subject to Geometric Constraints”, IEEE Transactions on Automation Science and Engineering, Vol. 7, No. 1, pp. 111-122.

[16] Chen Y.-C., Tlusty J., 1995, "Effect of Low-Friction Guideways and Lead-Screw Flexibility on Dynamics of High-Speed Machines", Annals of CIRP, Vol. 44/1/1995, pp. 353-356.

[17] Constantinescu D., Croft E. A., 2000, "Smooth and Time-Optimal Trajectory Planning for Industrial Manipulators Along Specified Paths", Journal of Robotic Systems, Vol. 17, No. 5, pp. 233-249.

[18] Cook W., 2012, “In Pursuit of the Travelling Salesman – Mathematics at the Limits of Computation”, Princeton University Press, ISBN 978-0-691-15270-7.

[19] Dantzig G. B., Ramser J. H., 1959, “The Truck Dispatching Problem”, Management Science. Vol. 6, pp. 80-91.

[20] Dinauer W.R., Weigman T.V., 2008, “Controller for a Laser Using Predictive Models for Materials Processing”, U.S. Patent 7,324,867 B2.

[21] Dini G., Santochi M., 1992, “Automated Sequencing and Subassembly Detection in Assembly Planning”, Institute of Mechanical Technology, University of Pisa, Italy.

[22] Dissanayake M., Gal J., 1994, “Workstation planning for redundant manipulators”, Int. J. Prod. Res. 1994; 32(5), pp. 1105-18.

[23] Dong, J., Ferreira, P.M., Stori, J.A., 2007, “Feed-rate optimization with jerk constraints for generating minimum time trajectories”, International Journal of Machine Tools and Manufacture, 47, pp. 1941-1955.

[24] Dubowski S., Blubaugh T., 1989, “Planning time-optimal robotic manipulator motions and work places for point-to-point tasks”, IEEE Trans Robotic Autom 1989; 5(3), pp. 377-81.

[25] Durbin R., Willshaw D., 1987, “An Analogue Approach to the Travelling Salesman Problem Using an Elastic Net Method”, Nature Publishing Group, Vol. 326, pp. 689-691.

[26] Edan Y., Flash T., Peiper U., Shmulevich I., Sarig Y., 1991, “Near-minimum-time task planning for fruit-picking Robots”, IEEE Trans Robotic Autom 1991; 7(1).

[27] Elfizy A., 2009, “High Speed Laser Drilling Machine and Method”, US Patent No US7,538,296 B2, May 26, 2009.

[28] Elfizy A., 2013, “Method for Drilling Holes According to an Optimized Sequence”, US Patent 8,362,392 B2.

[29] Erkorkmaz K., Alzaydi A.A., Elfizy A., Engin S., 2011, “Time-Optimal Trajectory Generation for 5-Axis On-the-Fly Laser Drilling”, Annals of CIRP, Vol. 60, Issue 1, 2011, P. 411-414.

[30] Erkorkmaz K., Alzaydi A.A., Elfizy A., Engin S., 2014, “Time-Optimized Hole Sequence planning for 5-axis on-the-fly laser drilling”, Annals of CIRP, Vol. 63, Issue 1, 2014, P. 377-380.

[31] Erkorkmaz K., Yeung C.-H., Altintas Y., 2006, “Virtual CNC System - Part II: High Speed Contouring Application”, Int. J. Machine Tools & Manuf., 46/10:1124-1138.

[32] Erkorkmaz, K., Altintas, Y., 2001, "High Speed CNC System Design: Part I - Jerk Limited Trajectory Generation and Quintic Spline Interpolation", International Journal of Machine Tools and Manufacture, Vol. 41, No. 9, pp. 1323-1345.

[33] Erkorkmaz, K., 1999, M.A.Sc. Thesis, “High Speed Contouring Control for Machine Tool Drives”, the University of British Columbia, Vancouver.

[34] Erkorkmaz, K., 2004, Ph.D. Thesis: Optimal Trajectory Generation and Precision Tracking Control for Multi-Axis Machines. The University of British Columbia, Vancouver.

[35] Flash T., Hogan N., 1985, "The Coordination of Arm Movements: an Experimentally Confirmed Mathematical Model", Journal of Neuroscience, Vol. 5, pp. 1688-1703.

[36] Garey M. R., Graham R. L. and Johnson D. S., 1976, “Some NP-Complete Geometric Problems,” Proceedings of ACM Symposium on Theory of Computing, Hershey, Pennsylvania, United States, pp. 10–22.

[37] Gavish B., Srikanth K., 1986, “An Optimal Solution Method for Large Scale Multiple Travelling Salesman Problem”, Operation Research Society of America, Vol. 34, No.5, pp. 698-717.

[38] Gorbunov S., Kisel I., 2006, “Elastic Net for Standalone Rich Ring Finding”, Elsevier, Vol. 559. Issue 1, pp. 139-142.

[39] Gutin G., Yeo A., 2002, “Traveling Salesman Should Not be Greedy: Domination Analysis of Greedy Type Heuristics for the TSP”, Discrete Applied Mathematics 117, pp. 81-86.

[40] Held M., Karp R., 1969, “The Travelling Salesman Problem and Minimum Spanning Trees”, IBM Systems Research Institute, New York, New York.

[41] Huang T, Wang PF, Mei JP, Zhao XM, Chetwynd DG , 2007, “Time Minimum Trajectory Planning of a 2-DOF Translational Parallel Robot for Pick-and-Place Operations”, Annals of the CIRP 56(1), pp. 365-368.

[42] Hu W., Shin Y. C., King G. B., 2010, “Micromachining of Metals, Alloys, and Ceramics by Picoseconds Laser Ablation”, ASME Journal of Manufacturing Science and Engineering, Vol. 132/011009.

[43] Jeon J.-W., Park S.-H., Kim D.-I., Kim S., 1993, "An Efficient Trajectory Generation for Industrial Robots", Proceedings of the 28th Annual Meeting of the IEEE Industry Applications Conference, Vol. 3, pp. 2137-2143.

[44] Jerome L. N., Feron E., Frazzoli E., 2012, “On the Dubins traveling salesman problem”, Automatic Contro, IEEE Transactions, Vol. 57.1, pp. 265-270.

[45] Yi J., Bi W., Yang Z., Tang Z., 2008, “A Fast Elastic Net Method for Travelling Salesman Problem”, Eighth International Conference on Intelligent Systems Design and Applicatins, Vol. 1, pp. 462-467.

[46] Kaihara T., Kurose S., Fujii N., 2012, “A proposal on optimized scheduling methodology and its application to actual-scale semiconductor manufacturing problem”, CIRP Annals – Manufacturing Technology, Vol. 61, pp. 467-470.

[47] Kirk, Donald E., 1970, “Optimal Control Theory – An Introduction”, Prentice-Hall NJ. ISBN: 978-0-486-43484-1.

[48] Kyriakopoulos K. J., Saridis G. N., 1988, "Minimum Jerk Path Generation", Proceedings of the IEEE Intl. Conf. on Robotics and Automation, Philadelphia, PA, USA, pp. 364-369.

[49] Kyriakopoulos K. J., Saridis G. N., 1994, "Minimum Jerk for Trajectory Planning and Control", Robotica, Vol. 12, No. 2, pp. 109-113.

[50] Laporte G., 2009, “Fifty Years of Vehicle Routing”, Transportation Science, Vol. 43, No. 4, pp. 408-416.

[51] Lawer E., Lenstra J., Rinnooy Kan A., Shmoys D., 1985 “The travelling salesman problem”, Chickester, UK: Wiley.

[52] Lazoglu I., Manav C., Murtezaoglu Y., 2009, “Tool path optimization for free form surface machining”, CIRP Annals – Manufacturing Technology, Vol. 58, pp. 101-104.

[53] Lin, M.-T., Tsai, M.-S., Yau, H.-T., 2007, “Development of a dynamics-based NURBS interpolator with real-time look-ahead algorithm, International Journal of Machine Tool and Manufacture”, 47/15, pp. 2246-2262.

[54] Little J., 1963, “An Algorithm for the Travelling Salesman Problem”. Massachusetts Institute of Technology.

[55] Liu, X., Ahmad, F., Yamazaki, K., Mori, M., 2005, “Adaptive interpolation scheme for NURBS curves with the integration of machining dynamics”, International Journal of Machine Tools and Manufacture, 45/4-5, pp. 433-444.

[56] Macfarlane, S., Croft, E.A., 2001, “Design of Jerk Bounded Trajectories for On-Line Industrial Robot Applications”, Proceedings IEEE International Conference on Robotics and Automation, Vol. 1, pp. 979-984.

[57] Makino H., Ohde T., 1991, “Motion Control of the Direct Drive Actuator”, Annals of CIRP, Vol. 40/1/1991, pp.375-378.

[58] Mark W. Spong, M. Vidyasagar. 1989, “Robot Dynamics and Control”, Wiley 1st.

[59] M.K. Jouaneh, Z. Wang, D.A. Dornfeld, Tracking of sharp corners using a robot and a table manipulator, Proceedings of USA–Japan Symposium on Flexible Automation, 1988, pp. 271–278.

[60] M.K. Jouaneh, Z. Wang, D.A. Dornfeld, Trajectory planning for coordinated motion of a robot and a positioning table. Part 1. Path specification, IEEE Transactions on Robotics and Automation 6 (6) (1990) 735–745.

[61] M.K. Jouaneh, D.A. Dornfeld, M. Tomizuka, Trajectory planning for coordinated motion of a robot and a positioning table. Part 2. Optimal trajectory specification, IEEE Transactions on Robotics and Automation 6 (6) (1990) 746–759.

[62] Nocedal J, Wright SJ, 1999, “Numerical Optimization”, Springer, NY.

[63] Nonaka Y., Erdos G., Kis T., Nakano T., Vancza J., 2012, “Scheduling with alternative routings in CNC workshops”, CIRP Annals – Manufacturing Technology, Vol. 61, pp. 449-454.

[64] Ostendorft A., 2013, “An Introduction to Laser Assisted Micro Fabrication, Current Status and Future Scope of Application”, Department of Mechanical Engineering, Ruhr-University Bochum, Springer Series in Materials Science, Laser-Assisted Fabrication of Materials. ISBN 978-3-642-28359-8.

[65] Papadimitriou C. H., 1977, “Euclidean TSP is NP-complete,” TCS 4, pp. 237–244.

[66] Petiot J., Chedmail P., Hashoet J., “Contribution to the scheduling of trajectories in robotics”, Robotic Comput. Integr Manuf 1998; 14, pp. 237-51.

[67] Piazzi A., Visioli A., 1998, "Global Minimum-Time Trajectory Planning of Mechanical Manipulators Using Interval Analysis", International Journal of Control, Vol. 71, No. 4, pp. 631-652.

[68] Piazzi A., Visioli A., 2000, "Global Minimum-Jerk Trajectory Planning of Robot Manipulators", IEEE Transactions on Industrial Electronics, Vol. 47, No. 1, pp. 140-149.

[69] Pritschow, G., 1997, Course notes: “Steuerungtechnik der Werkzeugmaschinen und Industrieroboter (control techniques of machine tools and industrial robots)”, Institute of Control Technology for Machine Tools and Manufacturing Units, Stuttgart University, Germany.

[70] R. Haschke, E Weitnauer, H Ritter, 2008, “On-line planning of time-optimal, jerk-limited trajectories”, IEEE, Intelligent Robots 2008, ISBN: 978-1-4244-2057-5.

[71] Ruegg A., Gygax P., 1992, “Generalized Kinematics Model for Three to Five-Axis Milling Machines and their Implementation in a CNC”, Annals of CIRP, Vol. 41, No. 1, pp. 547-550.

[72] Sencer B, Altintas Y, Croft E, 2008, “Feed Optimization for Five-Axis CNC Machine Tools with Drive Constraints”. Intl. J. Machine Tools & Manufacture 48, pp. 733–745.

[73] Sencer, B., 2005, M.A.Sc. Thesis, “Five-Axis Trajectory Generation Methods” The University of British Columbia, Vancouver.

[74] Shen L., Kernighan, B. W., 1973, “An Effective Heuristic Algorithm for the Travelling-Salesman Problem”. Operations Research 21 (2), pp. 498-516.

[75] Shin K., Mckay N., “Selection of near minimum time geometric paths for robotic manipulators”, IEEE Trans Automat Control 1986; 31(6), pp. 501-11.

[76] Simon D., Isik C., 1991, "Optimal Trigonometric Robot Joint Trajectories", Robotica, Vol. 9, No. 4, pp. 379-386.

[77] Simon D., Isik C., 1993, "Suboptimal Robot Joint Interpolation within User-Specified Knot Tolerances", Journal of Robotic Systems, Vol. 10, No. 7, pp. 889-911.

[78] Tomita Y., Makino K., Sugimine M., Taniguchi N., 1996, "High-Response X-Y Stage System Driven by In-Parallel Linear Motors", Annals of CIRP, Vol. 45/1/1996, pp. 359-362.

[79] TWI Ltd, 2014, Granta Park, Great Abington, Cambridge, CB21 6AL, United Kingdom.

[80] Van Willigenburg L. G., 1993, "Computation and Implementation of Digital Time-Optimal Feedback Controllers for and Industrial X-Y Robot Subjected to Path, Torque, and Velocity Constraints", International Journal of Robotics Research, Vol. 12, No. 5, pp. 420-433.

[81] Visioli, A., 2000, "Trajectory Planning of Robot Manipulators By Using Algebraic and Trigonometric Splines", Robotica, Vol. 18, No. 6, pp. 611-631.

[82] Van Willigenburg L. G. , 1993, "Computation and Implementation of Digital Time-Optimal Feedback Controllers for an Industrial X-Y Robot Subjected to Path, Torque,

and Velocity Constraints", International Journal of Robotics Research, Vol. 12, No. 5, pp. 420-433.

[83] Weck M., Meylahn A., Hardebusch C., 1999, "Innovative Algorithms for Spline-Based CNC Controller", Production Engineering Research and Development in Germany; Annals of the German Academic Society for Production Engineering, Vol. 6, No. 1, pp. 83-86.

[84] Workshop of Photonics (WOF), 2011, “Stainless Steel Foil Perforation – Application Note”, Vilnius, Lithuania.

[85] Wong H., Leu M. C., 1993, “Adaptive Genetic Algorithm for Optimal Printed Circuit Board Assembly planning”, New Jersey Institute of Technology, Newark, USA.

[86] Xidias E.K., Zacharia P.T., Aspragathos N.A., 2010, “Time-Optimal Task Scheduling for Articulated Manipulators”, Robotica, Vol. 28, pp. 427–440.

[87] Xu, R.Z., Xie, L., Li, C.X., Du., D.S., 2008, “Adaptive parametric interpolation scheme with limited acceleration and jerk values for NC machining”, International Journal of Advanced Manufacturing Technology, 36/3-4, pp. 343-354.

[88] Y. Kanayama, N. Miyake, Trajectory generation for mobile Robots, Third International Symposium on Robotics Research, Cambridge, MA, 1986, pp. 333–340.

[89] Yeo C. Y., Tam S. C., Jana S., Lau M. W. S., 1994, “A Technical Review of the Laser Drilling of Aerospace Materials”, Journal of Materials Processing Technology, Vol. 42, pp. 15-49.

[90] Yoshikawa T., 1990, “Foundations of Robotics”, MIT Press, MA, USA.

[91] Zacharia P., Asparagathos N., 2005, “Optimal Robot Task Scheduling Based on genetic Algorithms”, Robotics and Computer-Integrated Manufacturing, Vol. 21, pp. 67-79.

Appendix A:

Fitting Cyclic (i.e., Closed Curve) Cubic Splines

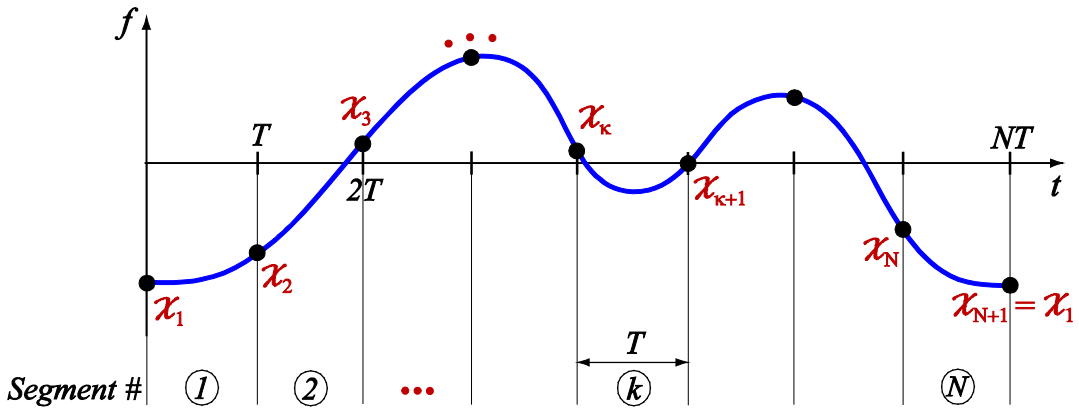

Figure A.1: Example cubic spline fit through given hole locations

The position, velocity, acceleration and jerk profiles for the *k*th segment in the x-axis can be expressed as in Eq. (A.1).

$$\begin{aligned} x_k(t) &= A_{x,k}t^3 + B_{x,k}t^2 + C_{x,k}t + D_{x,k} \\ \dot{x}_k(t) &= 3A_{x,k}t^2 + 2B_{x,k}t + C_{x,k} \\ \ddot{x}_k(t) &= 6A_{x,k}t + 2B_{x,k} \qquad , \quad 0 \le t \le T_k \\ \dddot{x}_k(t) &= 6A_{x,k} \end{aligned} \tag{A.1}$$

The closed cubic spline has to pass through N points, (X_k) represents the x-axis coordinate of the k^{th} point. N positions and N velocities define N cubic segments. The connection point velocities need to be solved to guarantee acceleration continuity.

$$\left[\ddot{x}(T)\right]_k = \left[\ddot{x}(0)\right]_{k+1}, \qquad k = 1,\ldots,N-1 \qquad k: \textit{Segment number} \tag{A.2}$$

and

$$\underbrace{\left[\ddot{x}(T)\right]_N}_{\substack{End\ of \\ segment\ N}} = \underbrace{\left[\ddot{x}(0)\right]_1}_{\substack{Start\ of \\ segment\ 1}} \tag{A.3}$$

The coefficients of a cubic profile segment $\left(A_{x,k}, B_{x,k}, C_{x,k}, D_{x,k}\right)$ can be solved with knowledge of the time parameter range $\left(T_k\right)$ and position and velocity boundary conditions at the start and end of that segment (i.e., X_k, $V_{x,k}$ and X_{k+1}, $V_{x,k+1}$, respectively).

For segment k**:**

$$A_{x,k} = \frac{V_{x,k}+V_{x,k+1}}{T_k^2} - \frac{2\left(X_{k+1}-X_k\right)}{T_k^3}, \quad B_{x,k} = \frac{3\left(X_{k+1}-X_k\right)}{T_k^2} - \frac{2V_{x,k}+V_{x,k+1}}{T_k},$$
$$C_{x,k} = V_{x,k}, \; D_{x,k} = X_k \tag{A.4}$$

Eq. (A.4) was obtained using the given boundary conditions and applying Gauss elimination to Eq. (A.1).

Combining Eq. (A.2) and (A.1):

$$6A_{x,k}T_k + 2B_{x,k} = 2B_{x,k+1}$$

$$6\left(\frac{V_{x,k}+V_{x,k+1}}{T_k^2} - \frac{2\left(X_{k+1}-X_k\right)}{T_k^3}\right)T_k + 2\left(\frac{3\left(X_{k+1}-X_k\right)}{T_k^2} - \frac{2V_{x,k}+V_{x,k+1}}{T_k}\right)$$
$$= 2\left(\frac{3\left(X_{k+2}-X_{k+1}\right)}{T_{k+1}^2} - \frac{2V_{x,k+1}+V_{x,k+2}}{T_{k+1}}\right)$$

$$V_{x,k}\underbrace{\left(\frac{6}{T_k}-\frac{4}{T_k}\right)}_{2/T_k} + V_{x,k+1}\underbrace{\left(\frac{6}{T_k}-\frac{2}{T_k}+\frac{4}{T_{k+1}}\right)}_{4/T_k} + V_{x,k+2}\left(\frac{2}{T_{k+1}}\right)$$
$$= \underbrace{\left(X_{k+1}-X_k\right)}_{\Delta X_k}\underbrace{\left(\frac{12}{T_k^2}-\frac{6}{T_k^2}\right)}_{6/T_k^2} + \underbrace{\left(X_{k+2}-X_{k+1}\right)}_{\Delta X_{k+1}}\left(\frac{6}{T_{k+1}^2}\right)$$

$$\left(\frac{2}{T_k}\right)V_{x,k} + \left(\frac{4}{T_k}+\frac{4}{T_{k+1}}\right)V_{x,k+1} + \left(\frac{2}{T_{k+1}}\right)V_{x,k+2} = \left(\frac{6}{T_k^2}\right)\Delta X_k + \left(\frac{6}{T_{k+1}^2}\right)\Delta X_{k+1}$$

The above expression holds for $k = 1, 2, ..., N$, note that $V_{x,N+1}$ would be substituted with $V_{x,1}$, $V_{x,N+2}$ would be replaced by $V_{x,2}$, as follows:

$$V_{x,N+1} \to V_{x,1} \qquad \Delta X_N = X_1 - X_N$$

$$V_{x,N+2} \to V_{x,2} \qquad \Delta X_{N+1} = \Delta X_1 = X_2 - X_1$$

$$T_{N+1} \to T_1$$

The set of N equations can be solved using the following matrix formulation:

$$\begin{bmatrix} \frac{2}{T_1} & \frac{4}{T_1}+\frac{4}{T_2} & \frac{2}{T_2} & 0 & \cdots & 0 & 0 & 0 \\ 0 & \frac{2}{T_2} & \frac{4}{T_2}+\frac{4}{T_3} & \frac{2}{T_3} & \cdots & 0 & 0 & 0 \\ 0 & 0 & \frac{2}{T_3} & \frac{4}{T_3}+\frac{4}{T_4} & \cdots & 0 & 0 & 0 \\ \vdots & \vdots & \vdots & \vdots & \ddots & \vdots & \vdots & \vdots \\ 0 & 0 & 0 & 0 & \cdots & \frac{2}{T_{N-2}} & \frac{4}{T_{N-2}}+\frac{4}{T_{N-1}} & \frac{2}{T_{N-1}} \\ \frac{2}{T_N} & 0 & 0 & 0 & \cdots & 0 & \frac{2}{T_{N-1}} & \frac{4}{T_{N-1}}+\frac{4}{T_N} \\ \frac{4}{T_N}+\frac{4}{T_1} & \frac{2}{T_1} & 0 & 0 & \cdots & 0 & 0 & \frac{2}{T_N} \end{bmatrix} \begin{bmatrix} V_{x,1} \\ V_{x,2} \\ V_{x,3} \\ \vdots \\ V_{x,N-2} \\ V_{x,N-1} \\ V_{x,N} \end{bmatrix}$$

$$= \begin{bmatrix} \frac{6}{T_1^2}\Delta X_1 + \frac{6}{T_2^2}\Delta X_2 \\ \frac{6}{T_2^2}\Delta X_2 + \frac{6}{T_3^2}\Delta X_3 \\ \frac{6}{T_3^2}\Delta X_3 + \frac{6}{T_4^2}\Delta X_4 \\ \vdots \\ \frac{6}{T_{N-2}^2}\Delta X_{N-2} + \frac{6}{T_{N-1}^2}\Delta X_{N-1} \\ \frac{6}{T_{N-1}^2}\Delta X_{N-1} + \frac{6}{T_N^2}\Delta X_N \\ \frac{6}{T_N^2}\Delta X_N + \frac{6}{T_1^2}\Delta X_1 \end{bmatrix}$$

Appendix B:
Evaluation of Kinematic Constraints from Spline Coefficients

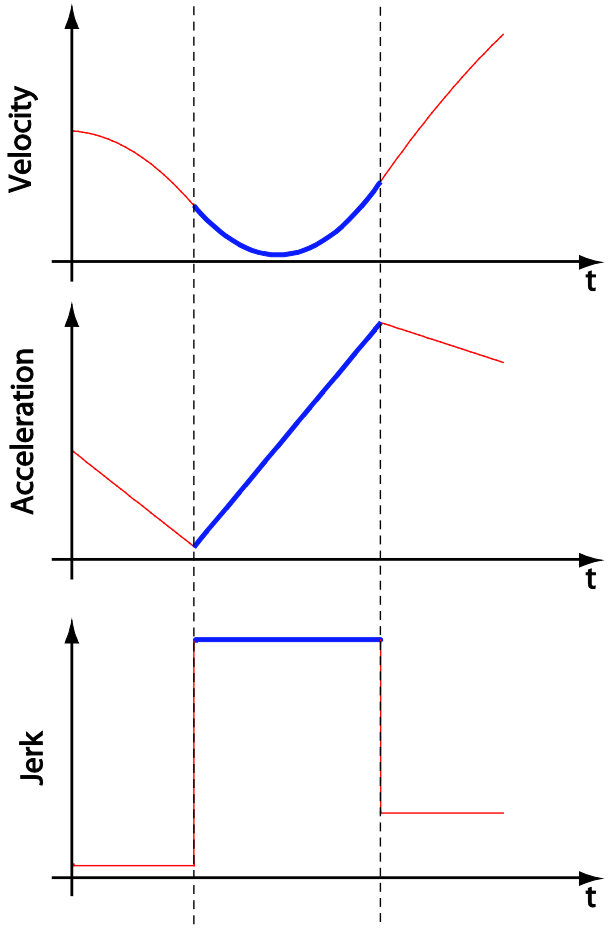

Figure B.1: Example of piecewise constant jerk, linear acceleration and parabolic velocity.

The cubic closed curve derived in Appendix A has piecewise constant jerk, linear acceleration, and parabolic velocity in each segment (as shown in Figure B.1), thus allowing peak jerk, acceleration, and velocity values to be evaluated analytically without requiring interpolation. The velocity component v_{xy} at the drilling location, which influences hole elongation, is also calculated from the spline coefficients and by considering the machine tool kinematics (Appendix C).

The evaluation (or inspection) of the kinematic constraints from spline coefficients and adjustment of the time scaling factor (α, Appendix D), to ensure that all of the constraints are respected, is achieved through the following set of equations:

- Piece-wise constant jerk in each segment:

$$j_{x,k} = 6A_{x,k},\ j_{y,k} = 6A_{y,k}, \cdots,\ j_{c,k} = 6A_{c,k}$$

Maximum jerk magnitude in x-axis (normalized with respect to axis jerk limit $j_{x\max}$):

$$\frac{6}{j_{x\max}} \max\left(\left|A_x\right|\right)$$

Time scaling to apply (Appendix D) to ensure that all actuator jerk commands are within their given limits:

$$\alpha_j = \left\{ 6\max\left(\left[\frac{\max\left(\left|A_x\right|\right)}{j_{x\,\max}}, \frac{\max\left(\left|A_y\right|\right)}{j_{y\,\max}}, \cdots, \frac{\max\left(\left|A_c\right|\right)}{j_{c\,\max}} \right] \right) \right\}^{1/3} \tag{B.1}$$

- Since acceleration varies linearly within each trajectory segment, it is sufficient to check the acceleration values only at the connection points:

$$a_x = 2B_x, \cdots,\ a_c = 2B_c$$

Maximum acceleration magnitude in x-axis (normalized w.r.t. the axis acceleration limit):

$$\frac{2}{a_{x\,\max}} \max\left(\left|B_x\right|\right)$$

Required time scaling to hold acceleration constraints:

$$\alpha_a = \left\{ 2\max\left(\left[\frac{\max\left(\left|B_x\right|\right)}{a_{x\,\max}}, \frac{\max\left(\left|B_y\right|\right)}{a_{y\,\max}}, \cdots, \frac{\max\left(\left|B_c\right|\right)}{a_{c\,\max}} \right] \right) \right\}^{1/2} \tag{B.2}$$

- Since the velocity profile is parabolic, both the extreme value, and the values at the connection points need to be checked.

Checking the extreme value:

$\dot{x} = \underbrace{3A_x}_{a} t^2 + \underbrace{2B_x}_{b} t + \underbrace{C_x}_{c}$, solving root values for t as a quadratic equation.

$0 = at^2 + bt + c$, taking the time derivative $\rightarrow 2at + b = 0$, gives

$$t^* = \frac{-b}{2a} \rightarrow t^* = \frac{-2B_x}{2\times 3A_x} = \frac{-B_x}{3A_x}.$$

$$\dot{x}^* = \begin{cases} if \quad 0 \le t^* \le T_k \rightarrow \dot{x}^*_{\max} = C_x - \dfrac{B_x^2}{3A_x} \\ Else \qquad\qquad \rightarrow \dot{x}^*_{\max} = 0 \end{cases}$$

Verification:

$$\dot{x}^* = \dot{x}\left(t = t^*\right)$$

$$= 3A_x\left(\frac{-B_x}{3A_x}\right)^2 + 2Bx\left(\frac{-B_x}{3A_x}\right) + C_x = C_x - \frac{B_x^2}{3A_x}$$

Thus, the time scaling required to ensure that all velocity constraints hold:

$$\alpha_v = \max\left[\beta\right]$$

$$For \quad \beta = \frac{\max\left(\dfrac{\left|\dot{x}^*\right|}{\left|C_x\right|}\right)}{v_{x,\max}}, \frac{\max\left(\dfrac{\left|\dot{y}^*\right|}{\left|C_y\right|}\right)}{v_{y,\max}}, \cdots, \frac{\max\left(\dfrac{\left|\dot{c}^*\right|}{\left|C_c\right|}\right)}{v_{c,\max}}, \frac{\max\left(\left|v_{xy}\right|\right)}{v_{xy,\max}} \tag{B.3}$$

v_{xy} is calculated using the kinematic model in Appendix C.

Appendix C:

5-Axis Laser Drilling Machine Kinematic Analysis

C.1 Kinematic Transformation

A diagram of the 5-axis kinematics is shown in Figure C.1.

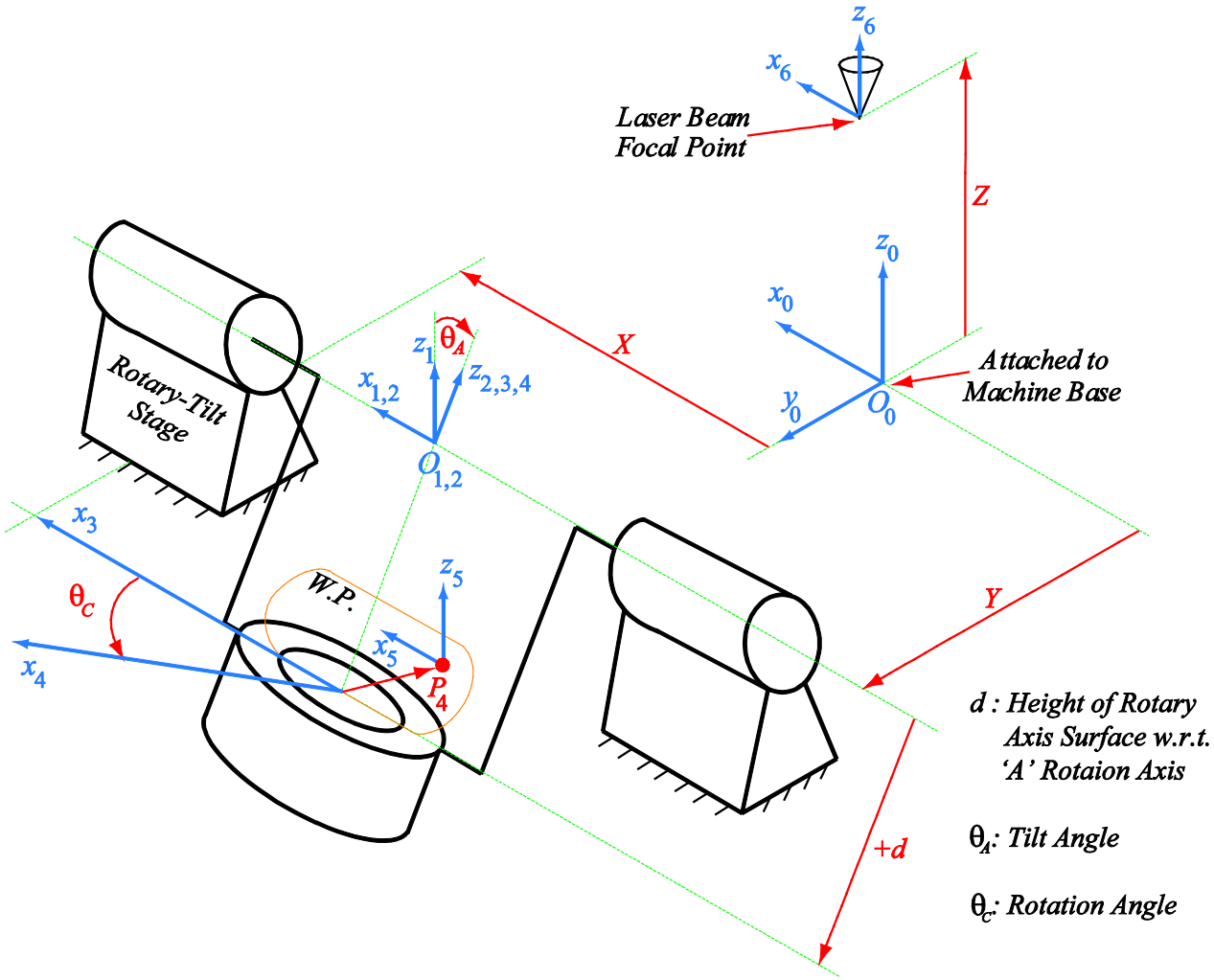

Figure C.1: 5-axis machine coordinate frames.

The following coordinate systems (C.S's) are considered:

C.S.0 ($O_0\, x_0\, y_0\, z_0$): This frame is fixed to the machine base; its axes are parallel to the translating joints of the machine.

C.S.1 ($O_1\, x_1\, y_1\, z_1$): Attached to the moving X-Y stage, x_1 and y_1 are parallel to the x_0

and y_0 axes. The center of frame (O_1) is located at mid-point of the tilt axis.

C.S.2 ($O_2 x_2 y_2 z_2$): O_2 and z_2 are identical to O_1 and z_1. C.S.2 is obtained by rotating C.S.1 around its x-axis (x_1) by θ_A .

C.S.3 ($O_3\ x_3 y_3 z_3$): x_3 , y_3 and z_3 are identical to x_2 , y_2 , and z_2 . This frame is obtained by translating C.S.2 by "d" along its z-axis (z_2). The value for "d" can be negative or positive depending on the workpiece fixture being used.

C.S.4 ($O_4\ x_4 y_4 z_4$): O_4 and z_4 are identical to O_3 and z_3. This frame is obtained by rotating C.S.3 around its z-axis (z_3) by θ_C .

C.S.5 ($O_5\ x_5\ y_5 z_5$): This frame is parallel to C.S.4. Its origin (O_5) is translated to coincide with the hole being drilled on the workpiece.

C.S.6 ($O_6\ x_6\ y_6 z_6$): This frame is parallel to C.S.0 ($O_0 x_0 y_0 z_0$) and is fixed at the laser focal point.

Vector P_4: Position vector of current hole location on the workpiece defined in reference to C.S.4.

The transformation from C.S.1 to C.S.4 is as follows:

$$H_{14} = H_{12}H_{23}H_{34} = Rot_{x,\theta_A}\ Trans_{z,d}\ Rot_{z,\theta_C} \tag{C.1}$$

$$Rot: Rotational\ Matrix$$

$$Trans: Translational\ Matrix$$

Calculating each transformation matrix from O_0 to O_5 yields:

$$H_{05} = \underbrace{Trans_{x,y}}_{H_{01}}\ \underbrace{Rot_{x,\theta_A}}_{H_{12}}\ \underbrace{Trans_{z,d}}_{H_{23}}\ \underbrace{Rot_{z,\theta_C}}_{H_{34}}\ \underbrace{Trans_{P_4}}_{H_{45}} \tag{C.2}$$

In order to solve for the transformation matrix H_{05}, the in-between transformations H_{01}, H_{12} , H_{23} , H_{34} and H_{45} need to be calculated. In the following calculations $\{X, Y, Z\}$ represent X, Y and Z values read from the NC file. Also, $S_4 = \sin\theta_A$, $C_4 = \cos\theta_A$,

$S_5 = \sin\theta_C$, $C_5 = \cos\theta_C$ and $\{x_h, y_h, z_h\}$ represent hole coordinates (P_4) in C.S.4. Therefore,

$$H_{01} = \left[\begin{array}{ccc|c} & I_3 & & \begin{matrix}X\\Y\\0\end{matrix} \\ \hline 0 & 0 & 0 & 1 \end{array}\right] \quad H_{12} = \left[\begin{array}{ccc|c} 1 & 0 & 0 & 0 \\ 0 & C_4 & -S_4 & 0 \\ 0 & S_4 & C_4 & 0 \\ \hline 0 & 0 & 0 & 1 \end{array}\right] \quad H_{23} = \left[\begin{array}{ccc|c} & I_3 & & \begin{matrix}0\\0\\d\end{matrix} \\ \hline 0 & 0 & 0 & 1 \end{array}\right]$$

$$H_{34} = \left[\begin{array}{ccc|c} C_5 & -S_5 & 0 & 0 \\ S_5 & C_5 & 0 & 0 \\ 0 & 0 & 1 & 0 \\ \hline 0 & 0 & 0 & 1 \end{array}\right] \quad H_{45} = \left[\begin{array}{ccc|c} & I_3 & & \begin{matrix}x_h\\y_h\\z_h\end{matrix} \\ \hline 0 & 0 & 0 & 1 \end{array}\right]$$

Hence, H_{05} can be composed as:

$$H_{02} = H_{01}H_{12} = \left[\begin{array}{ccc|c} & I_3 & & \begin{matrix}X\\Y\\0\end{matrix} \\ \hline 0 & 0 & 0 & 1 \end{array}\right]\left[\begin{array}{ccc|c} 1 & 0 & 0 & 0 \\ 0 & C_4 & -S_4 & 0 \\ 0 & S_4 & C_4 & 0 \\ \hline 0 & 0 & 0 & 1 \end{array}\right] = \left[\begin{array}{ccc|c} 1 & 0 & 0 & X \\ 0 & C_4 & -S_4 & Y \\ 0 & S_4 & C_4 & 0 \\ \hline 0 & 0 & 0 & 1 \end{array}\right]$$

$$H_{03} = H_{02}H_{23} = \left[\begin{array}{ccc|c} 1 & 0 & 0 & X \\ 0 & C_4 & -S_4 & Y \\ 0 & S_4 & C_4 & 0 \\ \hline 0 & 0 & 0 & 1 \end{array}\right]\left[\begin{array}{ccc|c} 1 & 0 & 0 & 0 \\ 0 & 1 & 0 & 0 \\ 0 & 0 & 1 & d \\ \hline 0 & 0 & 0 & 1 \end{array}\right] = \left[\begin{array}{ccc|c} 1 & 0 & 0 & X \\ 0 & C_4 & -S_4 & Y - d\,S_4 \\ 0 & S_4 & C_4 & d\,C_4 \\ \hline 0 & 0 & 0 & 1 \end{array}\right]$$

$$H_{04} = H_{03}H_{34} = \left[\begin{array}{ccc|c} 1 & 0 & 0 & X \\ 0 & C_4 & -S_4 & Y - d\,S_4 \\ 0 & S_4 & C_4 & d\,C_4 \\ \hline 0 & 0 & 0 & 1 \end{array}\right]\left[\begin{array}{ccc|c} C_5 & -S_5 & 0 & 0 \\ S_5 & C_5 & 0 & 0 \\ 0 & 0 & 1 & 0 \\ \hline 0 & 0 & 0 & 1 \end{array}\right] = \left[\begin{array}{ccc|c} C_5 & -S_5 & 0 & X \\ C_4S_5 & C_4C_5 & -S_4 & Y - d\,S_4 \\ S_4S_5 & S_4C_5 & C_4 & d\,C_4 \\ \hline 0 & 0 & 0 & 1 \end{array}\right]$$

$$\therefore H_{05} = H_{04}H_{45} = \left[\begin{array}{ccc|c} C_5 & -S_5 & 0 & X \\ C_4S_5 & C_4C_5 & -S_4 & Y - d\,S_4 \\ S_4S_5 & S_4C_5 & C_4 & d\,C_4 \\ \hline 0 & 0 & 0 & 1 \end{array}\right]\left[\begin{array}{ccc|c} 1 & 0 & 0 & x_h \\ 0 & 1 & 0 & y_h \\ 0 & 0 & 1 & z_h \\ \hline 0 & 0 & 0 & 1 \end{array}\right] = \left[\begin{array}{ccc|c} C_5 & -S_5 & 0 & X_{05} \\ C_4S_5 & C_4C_5 & -S_4 & Y_{05} \\ S_4S_5 & S_4C_5 & C_4 & Z_{05} \\ \hline 0 & 0 & 0 & 1 \end{array}\right]$$

The position of the hole location (O_5) on the workpiece (X_{05}, Y_{05}, Z_{05}) with respect to the machine reference frame ($O_0\,x_0\,y_0\,z_0$) can be calculated with the following equations:

$$X_{05} = X + x_h C_5 - y_h S_5$$

$$Y_{05} = Y - d\,S_4 + x_h C_4 S_5 + y_h C_4 C_5 - z_h S_4$$

$$Y_{05} = Y + C_4(x_h S_5 + y_h C_5) - S_4(d + z_h)$$

$$Z_{05} = x_h S_4 S_5 + y_h S_4 C_5 + z_h C_4 + d\,C_4$$

$$= S_4(x_h S_5 + y_h C_5) + C_4(z_h + d)$$

Remembering that $C_4 = \cos\theta_A$, $S_4 = \sin\theta_A$, $C_5 = \cos\theta_C$, $S_5 = \sin\theta_C$,

$$X_{05} = X + x_h \cos\theta_C - y_h \sin\theta_C$$

$$Y_{05} = Y + \cos\theta_A(x_h \sin\theta_C + y_h \cos\theta_C) - \sin\theta_A(d + z_h) \qquad \text{(C.3)}$$

$$Z_{05} = \sin\theta_A(x_h \sin\theta_C + y_h \cos\theta_C) + \cos\theta_A(z_h + d)$$

The z-axis motion with respect to machine base can be expressed as:

$$H_{06} = Trans_z = \left[\begin{array}{ccc|c} & I_3 & & \begin{matrix}0\\0\\Z\end{matrix} \\ \hline 0 & 0 & 0 & 1 \end{array}\right]$$

Hence, the hole motion with respect to laser head focal point can be obtained as:

$$H_{65} = H_{60}H_{05} = (H_{06})^{-1}H_{05}$$

$$H_{65} = \left[\begin{array}{ccc|c} 1 & 0 & 0 & 0 \\ 0 & 1 & 0 & 0 \\ 0 & 0 & 1 & -Z \\ \hline 0 & 0 & 0 & 1 \end{array}\right]\left[\begin{array}{ccc|c} C_5 & -S_5 & 0 & X_{05} \\ C_4S_5 & C_4C_5 & -S_4 & Y_{05} \\ S_4S_5 & S_4C_5 & C_4 & Z_{05} \\ \hline 0 & 0 & 0 & 1 \end{array}\right] = \left[\begin{array}{ccc|c} C_5 & -S_5 & 0 & X_{05} \\ C_4S_5 & C_4C_5 & -S_4 & Y_{05} \\ S_4S_5 & S_4C_5 & C_4 & Z_{05} - Z \\ \hline 0 & 0 & 0 & 1 \end{array}\right]$$

$$\therefore \quad \begin{aligned} X_{65} &= X_{05} \\ Y_{65} &= Y_{05} \\ Z_{65} &= Z_{05} - Z \end{aligned} \qquad \text{(C.4)}$$

C.2 Reconstruction of Hole Position Data from NC Code

With the knowledge that every hole is to be drilled at the laser focus point ($X_{65}=0$, $Y_{65}=0$, $Z_{65}=0$), it is possible to re-construct the position of each hole $P_4=(x_h, y_h, z_h)$ in the workpiece coordinate system, using the drilling actuator coordinates contained in the NC (Numerical Control) file:

$$\begin{aligned} X_{65} &= X + x_h\cos\theta_C - y_h\sin\theta_C = 0 \\ Y_{65} &= Y + \cos\theta_A(x_h\sin\theta_C + y_h\cos\theta_C) - \sin\theta_A(d+z_h) = 0 \\ Z_{65} &= \sin\theta_A(x_h\sin\theta_C + y_h\cos\theta_C) + \cos\theta_A(z_h+d) - Z = 0 \end{aligned} \tag{C.5}$$

Isolating the unknown variables $(x_h,\ y_h,\ z_h+d)$:

$$\begin{bmatrix} \cos\theta_C & -\sin\theta_C & 0 \\ \cos\theta_A\sin\theta_C & \cos\theta_A\cos\theta_C & -\sin\theta_A \\ \sin\theta_A\sin\theta_C & \sin\theta_A\cos\theta_C & \cos\theta_A \end{bmatrix} \bullet \begin{bmatrix} x_h \\ y_h \\ d+z_h \end{bmatrix} = \begin{bmatrix} -X \\ -Y \\ Z \end{bmatrix}$$

$$\underbrace{\begin{bmatrix} C_5 & -S_5 & 0 \\ C_4S_5 & C_4C_5 & -S_4 \\ S_4S_5 & S_4C_5 & C_4 \end{bmatrix}}_{R_{65}=R_{05}} \bullet \underbrace{\begin{bmatrix} x_h \\ y_h \\ d+z_h \end{bmatrix}}_{Unknown} = \underbrace{\begin{bmatrix} -X \\ -Y \\ Z \end{bmatrix}}_{Known} \tag{C.6}$$

Noting that $R_{05}^{-1}=R_{05}^{T}$ (property of rotation matrices), also noting that $R_{05}(\theta_A,\ \theta_C)$, the unknowns can be calculated as:

$$\therefore \begin{bmatrix} x_h \\ y_h \\ d+z_h \end{bmatrix} = R_{05}^{T} \begin{bmatrix} -X \\ -Y \\ l+Z \end{bmatrix} \tag{C.7}$$

A sample implementation of this solution is shown in Figure C.2 and Figure C.3. Figure C.2 shows the x-y-z actuator positions programmed in the NC code for the machine's movement and Figure C.3 show the re-constructed hole locations on the workpiece, by applying the transformation in Eq. (C.7). This transformation has also been used for visualizing the path of the laser focal point on the workpiece coordinates (C.S.4).

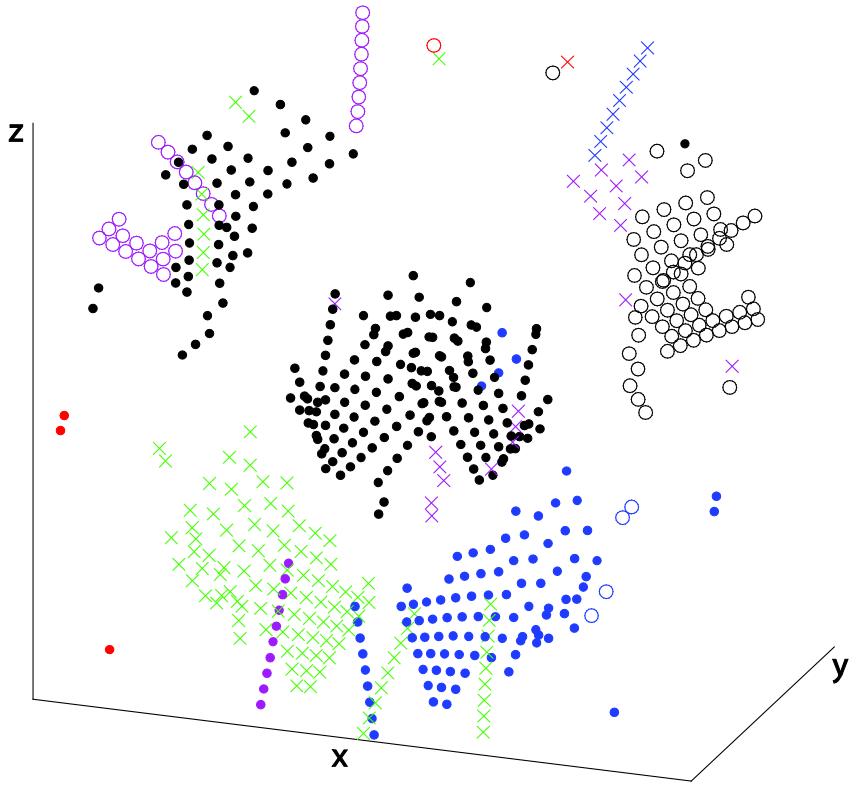

Figure C.2: NC data denoting X, Y, Z actuator movement locations.

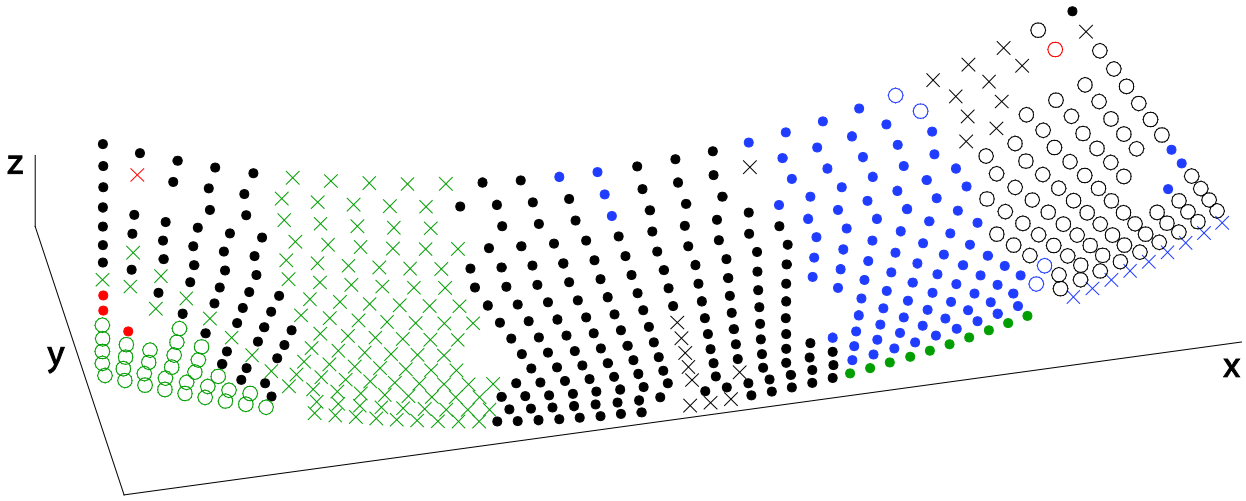

Figure C.3: Workpiece hole locations re-constructed in C.S.4.

C.3 Part Velocity Component at Hole Location Orthogonal to the Laser Beam

After successfully calculating the hole locations x_h, y_h and $z_h + d$ with respect to C.S.4, it is possible to calculate the part velocity with respect to the laser focal point at the holes as well:

By differentiating Eq. (C.5) with respect to time, we obtain:

$$\dot{x}_{65} = \dot{X} - x_h \sin\theta_C \bullet \dot{\theta}_C - y_h \cos\theta_C \bullet \dot{\theta}_C$$

$$\dot{x}_{65} = \underbrace{1}_{*}\,\dot{X} - \underbrace{\left(x_h \sin\theta_C + y_h \cos\theta_C\right)}_{**} \bullet \dot{\theta}_C \tag{C.8}$$

Note that $*$ and $**$, in Eq. (C.8) represent terms in the 5-axis machine Jacobian matrix.

Similarly for the y-axis:

$$\begin{aligned}\dot{y}_{65} = \dot{Y} &+ \cos\theta_A \bullet \dot{\theta}_C \bullet \left(x_h \cos\theta_C - y_h \sin\theta_C\right) \\ &- \sin\theta_A \bullet \dot{\theta}_A \bullet \left(x_h \sin\theta_C + y_h \cos\theta_C\right) \\ &- \cos\theta_A \bullet \dot{\theta}_A \bullet \left(d + z_h\right)\end{aligned}$$

$$\begin{aligned}\dot{y}_{65} = \dot{Y} &+ \cos\theta_A \bullet \dot{\theta}_C \bullet \left(x_h \cos\theta_C - y_h \sin\theta_C\right) \\ &- \dot{\theta}_A \bullet \left[\sin\theta_A \left(x_h \sin\theta_C + y_h \cos\theta_C\right) + \cos\theta_A \left(d + z_h\right)\right]\end{aligned} \tag{C.9}$$

and for z-axis:

$$\begin{aligned}\dot{z}_{65} = -\dot{Z} &+ \sin\theta_A \bullet \dot{\theta}_C \bullet \left(x_h \cos\theta_C - y_h \sin\theta_C\right) \\ &+ \dot{\theta}_A \bullet \left[\cos\theta_A \left(x_h \sin\theta_C + y_h \cos\theta_C\right) - \sin\theta_A \left(d + z_h\right)\right]\end{aligned} \tag{C.10}$$

The X-Y plane velocity governing hole elongation during drilling the operation can be obtained as:

$$V_{xy} = \sqrt{\dot{x}_{65}^{\,2} + \dot{y}_{65}^{\,2}} \tag{C.11}$$

Appendix D:

Effect of Uniform Time Scaling on the Derivative Profile

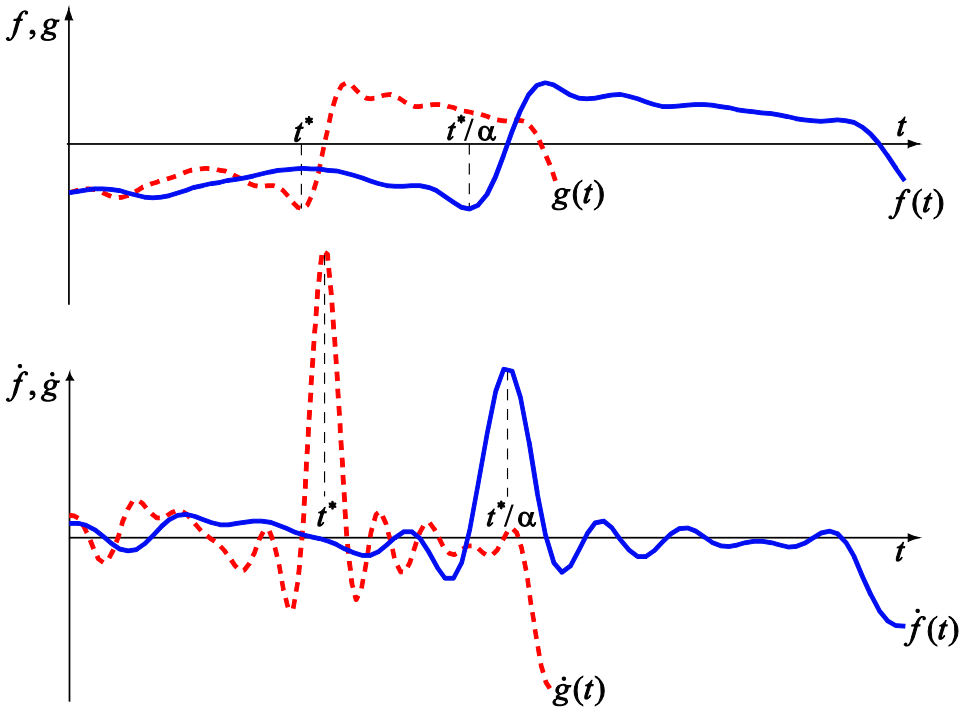

Figure D.1: Effect of time scaling a function on its derivative profile.

Considering that the position profile can be expressed as a function of time (i.e., $x = f(t)$), scaling the time variable by α will modify the position profile to become $g(t) = f(t/\alpha)$. In the following, it is analytically verified that this will also scale the velocity, acceleration, and jerk profiles by $1/\alpha$, $1/\alpha^2$, and $1/\alpha^3$:

$$\dot{g}(t) = \frac{1}{\alpha}\dot{f}(t/\alpha),\ \ddot{g}(t) = \frac{1}{\alpha^2}\ddot{f}(t/\alpha),\ \dddot{g}(t) = \frac{1}{\alpha^3}\dddot{f}(t/\alpha) \tag{D.1}$$

Given a function $f(t)$, as shown in Figure D.1, define an input (time) scaled function:

$$g(t) = f(t/\alpha) \tag{D.2}$$

for the scaling factor $\alpha > 0$. At a particular value of time: $t = t^*$, it can be shown that: $g(t^*) = f(t^*/\alpha)$. The objective is to find:

$$\left.\frac{dg(t)}{dt}\right|_{t=t^*} = \dot{g}(t^*) \tag{D.3}$$

Defining $\tau = \frac{t}{\alpha}$, then $\frac{d\tau}{dt} = \frac{1}{\alpha}$ and for $t = t^* \Rightarrow \tau = \tau^* = \frac{t^*}{\alpha}$. Therefore, the effect of time scaling on the velocity profile can be obtained as:

$$\left.\frac{dg}{dt}\right|_{t=t^*} = \left.\frac{df\left(\frac{t}{\alpha}\right)}{dt}\right|_{t=t^*} = \left.\underbrace{\frac{df(\tau)}{d\tau}}_{=\left.\frac{df(t)}{dt}\right|_{t=\tau}} \cdot \underbrace{\frac{d\tau}{dt}}_{\frac{1}{\alpha}}\right|_{\tau=\tau^*=t^*/\alpha} = \frac{1}{\alpha}\left.\frac{df}{dt}\right|_{t=t^*/\alpha} = \frac{1}{\alpha}\dot{f}(t^*/\alpha)$$

Hence, for a particular value of time $t = t^*$,

$$\dot{g}(t^*) = \frac{1}{\alpha}\dot{f}(t^*/\alpha) \tag{D.4}$$

For any value of time ($t^* = t$), verifying the velocity scaling identity in Eq. (D.1), we have:

$$\boxed{\dot{g}(t) = \frac{1}{\alpha}\dot{f}(t/\alpha)} \quad \leftarrow \text{Velocity scaling by } \frac{1}{\alpha} \tag{D.5}$$

Similarly, $\ddot{g}(t)$ and $\dddot{g}(t)$ can be investigated as follows:

$$\left.\frac{d\dot{g}}{dt}\right|_{t=t^*} = \frac{d}{dt}\left[\frac{1}{\alpha}\dot{f}\left(\frac{t}{\alpha}\right)\right]_{t=t^*} = \frac{1}{\alpha}\cdot\left.\frac{d\dot{f}\left(\frac{t}{\alpha}\right)}{\underbrace{d\left(\frac{t}{\alpha}\right)}_{\tau}}\cdot\underbrace{\frac{d\left(\frac{t}{\alpha}\right)}{dt}}_{\frac{1}{\alpha}}\right|_{\tau=\tau^*=\frac{t^*}{\alpha}}$$

$$= \frac{1}{\alpha}\underbrace{\frac{d\dot{f}(\tau)}{d\tau}}_{\left.\frac{d\dot{f}}{dt}\right|_{t=\tau}}\cdot\left.\frac{1}{\alpha}\right|_{\tau=\tau^*=\frac{t^*}{\alpha}} = \frac{1}{\alpha^2}\ddot{f}(t^*/\alpha)$$

Therefore,

$$\ddot{g}(t^*) = \frac{1}{\alpha^2}\ddot{f}(t^*/\alpha) \quad \Rightarrow \quad \boxed{\ddot{g}(t) = \frac{1}{\alpha^2}\ddot{f}(t/\alpha)} \quad \leftarrow \text{Acceleration scaling by } \frac{1}{\alpha^2} \tag{D.6}$$

And, for the jerk profile:

$$\left.\frac{d}{dt}\dddot{g}\right|_{t=t^*} = \frac{d}{dt}\left[\frac{1}{\alpha^2}\ddot{f}\left(\frac{t}{\alpha}\right)\right]\Bigg|_{t=t^*} = \frac{1}{\alpha^2}\cdot\underbrace{\frac{d\ddot{f}\left(\overbrace{\frac{t}{\alpha}}^{\tau}\right)}{d\left(\frac{t}{\alpha}\right)}}_{\left.\frac{d\ddot{f}(t)}{dt}\right|_{t=\tau}}\cdot\overbrace{\frac{d\tau}{dt}}^{\frac{1}{\alpha}}\Bigg|_{\tau=\tau^*=\frac{t^*}{\alpha}} \tag{D.7}$$

Therefore,

$$\dddot{g}(t^*) = \frac{1}{\alpha^3}\dddot{f}(t^*/\alpha) \quad \Rightarrow \quad \boxed{\dddot{g}(t) = \frac{1}{\alpha^3}\dddot{f}(t/\alpha)} \quad \leftarrow \text{Jerk scaling by } \frac{1}{\alpha^3} \tag{D.8}$$

Appendix E:
Timing Perturbations, Masks and Possibilities

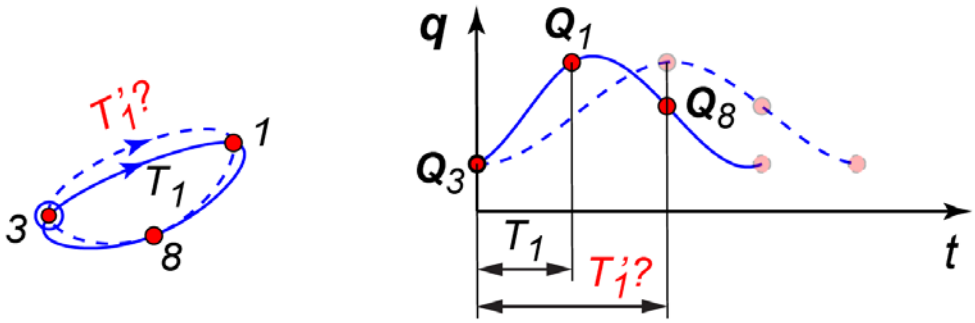

Figure E.1: Effect of modifying the travel duration (i.e. parameter range) of a given segment.

This appendix presents the details regarding the travel duration perturbation masks that were implemented in the sequencing algorithm in Chapter 3. The objective is to perturb the integer travel durations in $\boldsymbol{P}$ such that the 'shape' of the kinematic profiles are optimized to enable the shortest possible total travel time, T_{tot}.

Considering Figure E.1, it can be seen that the closed cubic trajectory profile is affected by the parameterization range chosen for each travel segment. Hence, modifying the duration of a given segment (e.g., segment #1) modifies both the temporal (i.e., time dependent) and geometric shape of the trajectory. Sometimes, this idea can be helpful for alleviating sharp transitions (i.e., sudden velocity and acceleration changes) in the kinematic profiles in the current and adjacent segments. As a result, the whole trajectory can be traveled with tighter (i.e., faster) time-scaling α (explained Appendix D), thus enabling an overall cycle time reduction.

1-Element Perturbation Mask

If a 1-element perturbation mask is considered with a magnitude of one laser pulse, then its possible variations would be {-1}, {0}, {+1}. However, since the {0} case is not worth testing, as it has no modification effect on the timing sequence, then only the {-1} and {+1} cases need to be considered. In an N -element closed sequence, the two modifying masks ({-1} and {+1}) can be applied at any of the N durations between the drilling waypoints within one round of testing, thus leading to $2N$ possibilities.

Hence, for r =1 element $Z_r = Z_1 = 3^1 - 1 = 2$ mask variations are possible; and $2N$ perturbation choices to apply to the sequence being optimized.

2-Element Perturbation Mask

All possible instances of the 2-element mask are listed in the following table:

Case	Mask		Case	Mask		Case	Mask	
1	-1	-1	4	0	-1	7	+1	-1
2	-1	0	5	0	0	8	+1	0
3	-1	+1	6	0	+1	9	+1	+1

New cases (variations) to test Covered by 1-element mask

Cases 2, 4, 5, 6, 8 in which the left-most or right-most element is zero (which are shown with shaded color) would already be tested while implementing perturbations with the 1-element mask. Hence, they do not need to be considered a second time. This brings the number of new masks introduced by stepping up the perturbation size from r =1 to 2 as Z_r = $9 - 5 = 4$.

Generalizing on this idea, if a given mask size is r -elements its total resulting number of variations will be 3^r (when its elements are allowed to assume values of {-1}, {0}, or {+1}). However, a third of these cases will have {0} as their left-most element. These do not need to be included into the testing, as their effect will already have been covered by smaller sized masks up to size $r-1$. Thus, there will be $\frac{2}{3} \times 3^r = 2 \times 3^{r-1}$ cases in which the left-most

element is non-zero. However, out of this set once again a third of the cases will have the right-most element as being zero. In total, two-thirds of this remainder set will contain the new possibilities achieved by stepping up the mask size from $r-1$ to r. Or, more precisely:

Number of *new* perturbation masks Z_r introduced by a mask of size r:

$$Z_r = \frac{2}{3}\times\frac{2}{3}\times 3^r = 4\times 3^{r-2} \quad , \quad \text{for}: \quad r = 2,3,...,N \tag{E.1}$$

When r=2, it can be verified that the above expression yields $Z_2 = 4\times 3^{2-2}$ = 4 variations, as already observed for the two element perturbation case.

3-Element Perturbation Mask

When r=3, as seen in the following table, only cases 1, 3, 4, 6, 7, 9, 19, 21, 22, 24, 25, 27 contribute new masks which are not captured by the 1- and 2-element masks; resulting in only 12 new perturbation shapes. This can be verified by the generalized formula in Eq. (E.1) (for r=3) as being equal to $Z_3 = 4\times 3^{3-2}$=12 variations.

Case	Mask			Case	Mask			Case	Mask		
1	-1	-1	-1	10	0	-1	-1	19	+1	-1	-1
2	-1	-1	0	11	0	-1	0	20	+1	-1	0
3	-1	-1	+1	12	0	-1	+1	21	+1	-1	+1
4	-1	0	-1	13	0	0	-1	22	+1	0	-1
5	-1	0	0	14	0	0	0	23	+1	0	0
6	-1	0	+1	15	0	0	+1	24	+1	0	+1
7	-1	+1	-1	16	0	+1	-1	25	+1	+1	-1
8	-1	+1	0	17	0	+1	0	26	+1	+1	0
9	-1	+1	+1	18	0	+1	+1	27	+1	+1	+1

New cases (variations) to test Already Covered by $r = 1,2$

Higher Order Perturbation Masks

Continuing on the same logic, perturbation masks for 4-, 5-, and 6- element cases were also constructed and implemented in the sequencing algorithm detailed in Chapter 3. Since the lists of these masks are lengthy, and they can be easily constructed with the above explanation, the higher order cases are not presented here. However, a brief analysis of the number of possibilities to be tested in Steps 3 and 5 of the sequencing algorithm in Chapter 3 is presented in the table below. As before, the perturbation mask size is denoted by r, and the current sequence size by N.

Mask size r	New number of possibilities to test with the introduction of the r-element mask	Total number of possibilities to be checked (including those from using the smaller sized masks):
rN	$Z_r N = (4 \times 3^{r-2}) \times N$	$(2 + \sum_{k=2}^{r} Z_r) \times N = (2 + \sum_{k=2}^{r} 4 \times 3^{k-2}) \times N$
1-Element	$2N$	$2N$
2-Element	$4N$	$6N$
3-Element	$12N$	$18N$
4-Element	$36N$	$54N$
5-Element	$108N$	$162N$
5-Element	$324N$	$486N$

Appendix F:
Jerk Limited Trajectory with Zero Initial and Final Velocity and Acceleration Conditions

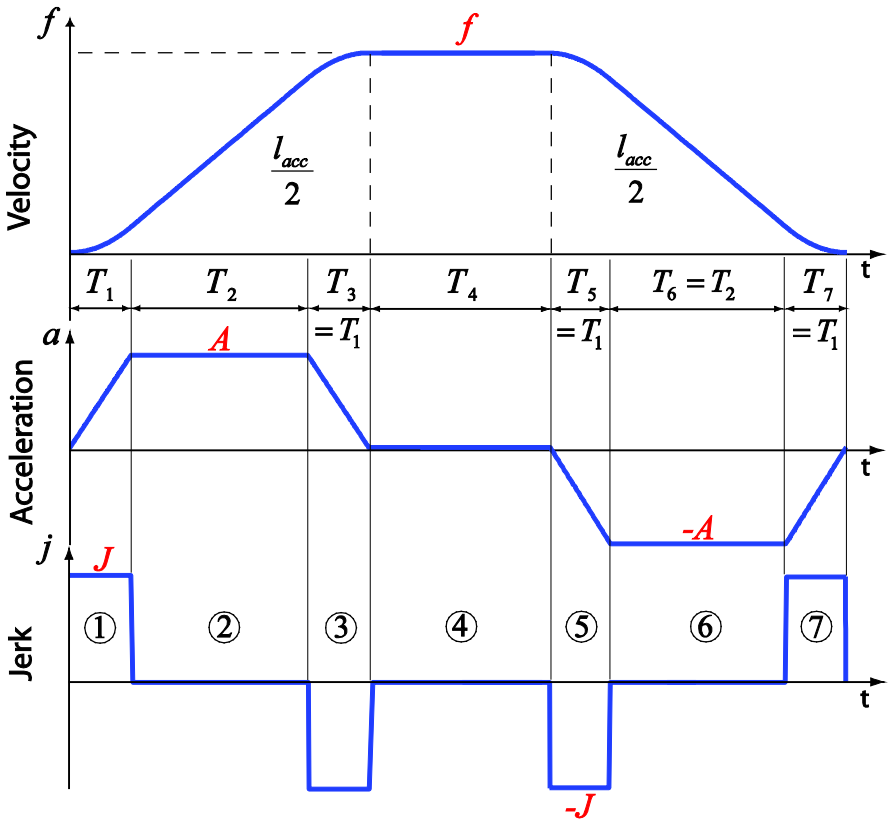

Figure F.1: Jerk limited trajectory profile with zero initial and final velocity and acceleration boundary conditions.

Figure F.1 displays the time-optimal motion profile [70] with zero initial and final velocity and acceleration boundary conditions (B.C.) for single-dimensional motion. This can either represent the motion executed by a single actuator, or a composite feedrate (i.e., tangential velocity) profile used in delivering coordinated multi-axis motion along a toolpath. For the case of rapid positioning between percussion laser drilled hole locations, the motion of a single actuator is considered.

The magnitude of jerk (i.e., rate of change of acceleration) is limited by $J > 0$. The magnitude of tangential acceleration is limited by $A > 0$. It is assumed that the planned

motion is in the positive direction of displacement, covering a specified travel distance of $L > 0$. Hence the maximum velocity (or feedrate), designated by f, is also positive. This feedrate is to be capped by a given velocity limit $F > 0$. In the case of laser drilling, J, A, and F correspond to the jerk, acceleration, and velocity magnitude limits for a given moving axis.

In the following, some basic properties of the motion curve (shown in Figure F.1) are reviewed in Section F.1. Afterwards, the methodology for generating the time-optimal positioning trajectory, subject to the travel length specification, is explained in Section F.2. Validation of the method is presented in Section F.3, and its application to 5-axis point-to-point beam positioning is explained in Section F.4.

F.1 Kinematic Properties of the Jerk Limited Motion Profile with Zero B.C.

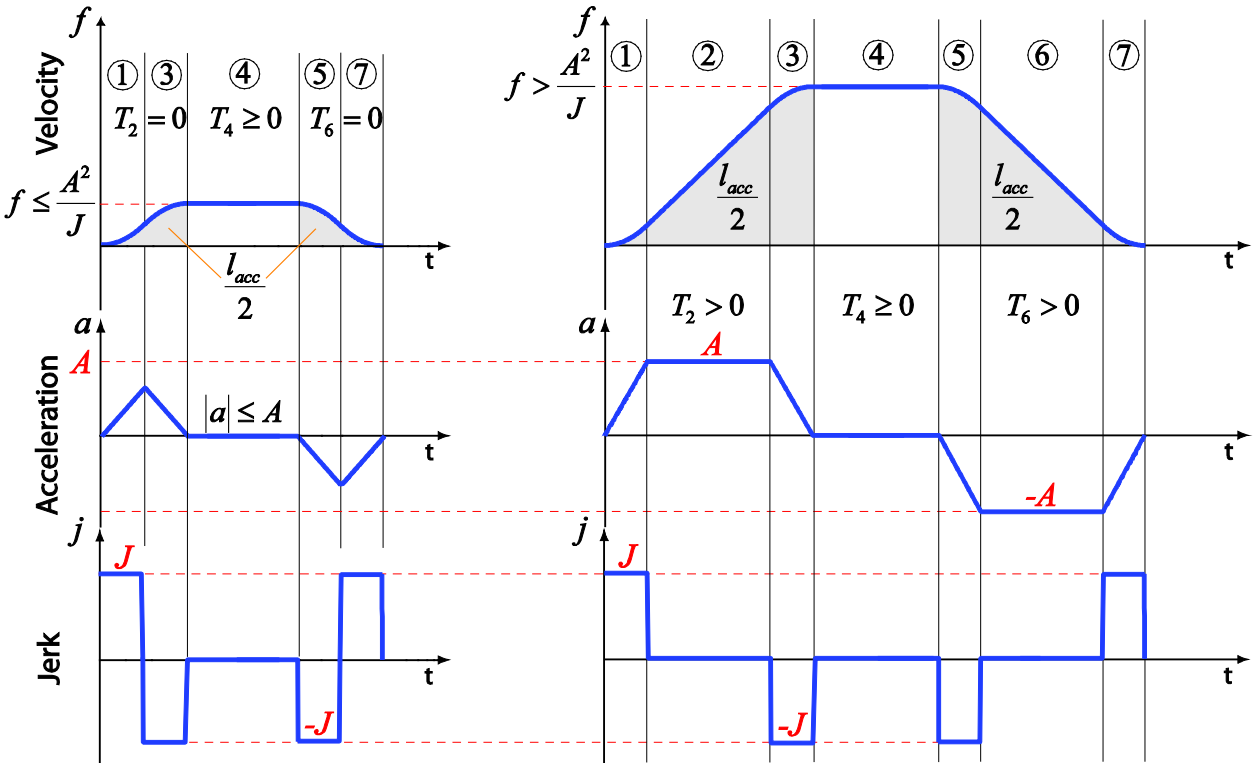

Figure F.2: Jerk limited trajectory profile with different feedrate values.

Considering Figure F.1, from the symmetry of the acceleration and velocity profiles, enabled through the requirement of zero initial and final boundary values in these curves, it

can be concluded through inspection that the following durations will be equal to each other: $T_1 = T_3 = T_5 = T_7$, and $T_2 = T_6$; when the magnitude of jerk used in Phases ①, ③, ⑤, and ⑦, is equal ($= J$), and the acceleration magnitude reached in Phases ② and ⑥ is also the same ($= A$).

Depending on the value of the achieved velocity f in relation to A^2 / J, the following two possibilities emerge as illustrated in Figure F.2 and explained in detail in Chapter 4.

i) If $f \le A^2 / J$,

- The acceleration profiles are triangular, as shown in Figure F.2a. (i.e., $T_2 = T_6 = 0$)
- The achieved maximum acceleration magnitude is capped by its given limit: $|a| \le A$.
- The total distance traveled during the acceleration / deceleration phases can be calculated to be:

$$l_{\text{acc}} = 2\sqrt{f^3 / J} \tag{F.1}$$

(obtained by considering that: $T_1 = \sqrt{f / J}$, $T_2 = 0$, $\frac{l_{\text{acc}}}{2} = \frac{1}{2} f (2T_1 + T_2)$)

- If the total travel distance available for acceleration / deceleration (i.e., Phases ①-②-③ and ⑤-⑥-⑦) is known, the achievable feedrate, based on the triangular acceleration shape, can be solved from Eq. (F.1) as:

$$f = \left(\frac{l_{\text{acc}} \sqrt{J}}{2} \right)^{2/3} \tag{F.2}$$

- In the limit case when $f = A^2 / J$, the total travel distance required for acceleration and deceleration becomes (from Eq. (F.1))

$$l_{\text{acc}}^0 = 2\sqrt{\frac{(A^2 / J)^3}{J}} = \frac{2A^3}{J^2} \tag{F.3}$$

ii) If $f > A^2 / J$,

- The acceleration profiles are trapezoidal, as shown in Figure F.2b. (i.e., $T_2 = T_6 > 0$)
- The achieved maximum acceleration magnitude is equal to its given limit: $|a| = A$.
- The total distance traveled during the acceleration / deceleration phases can be calculated to be:

$$l_{\text{acc}} = \frac{f^2}{A} + \frac{Af}{J} \tag{F.4}$$

l_{acc} is determined by considering that: $T_1 = A/J$ and $T_2 = f/A - A/J$. Thus,

$$\frac{l_{\text{acc}}}{2} = \frac{1}{2} f(2T_1 + T_2) \Rightarrow l_{\text{acc}} = f\left(2\frac{A}{J} + \frac{f}{A} - \frac{A}{J}\right) = \frac{Af}{J} + \frac{f^2}{A}$$

(T_2 is obtained by considering that $f = A(T_1 + T_2) = A^2/J + AT_2$)

- If the total travel distance available for acceleration / deceleration (i.e., Phases ①-②-③ and ⑤-⑥-⑦) is known, the achievable feedrate with the use of the trapezoidal acceleration profile can be obtained as:

$$f = \frac{1}{2}\left(\frac{-A^2}{J} + \sqrt{\frac{A^4}{J^2} + 4Al_{\text{acc}}}\right) \tag{F.5}$$

Eq. (F.5) is obtained by solving the upper root of f from Eq. (F.4). The lower root with a negative sign before the square root term cannot be used, as it would result in a solution for feed that is negative.

Regardless of whether the acceleration profile is triangular or trapezoidal, in either case, the duration of the constant feedrate phase ④, if it exists, can be found by dividing the difference between the total and the acceleration / deceleration travel distances by the achieved feedrate:

$$T_4 = \frac{L - l_{\text{acc}}}{f} \tag{F.6}$$

Since $L > 0$ and $f > 0$, this implies that Eq. (F.6) will always have a defined solution. In planning the motion profile, ensuring $l_{\text{acc}} \le L$ guarantees that $T_4 \ge 0$, as explained in Section F.2.

F.2 Generation of Jerk Limited Trajectory with Time Optimal Properties

The objective is to allow for the velocity to reach its maximum allowable value (F), while respecting the limits on the acceleration and jerk magnitudes. After planning the acceleration and deceleration, if there is still travel distance that remains unused, this remaining distance is to be traveled at the constant velocity of F.

First, the acceleration and deceleration distance, $l_{\text{acc}}^{\max}$, required to reach the maximum velocity and decelerate to a full stop, is computed:

$$l_{\text{acc}}^{\max} = \begin{cases} 2\sqrt{F^3/J} & \text{if} \quad F \le A^2/J \quad \text{(triangular acceleration)} \\ \dfrac{F^2}{A} + \dfrac{AF}{J} & \text{if} \quad F > A^2/J \quad \text{(trapezoidal acceleration)} \end{cases} \tag{F.7}$$

i) If the commanded travel distance L is larger than $l_{\text{acc}}^{\max}$ (i.e., $L \ge l_{\text{acc}}^{\max}$), then the maximum velocity can be reached. Hence, the actual velocity to be used is set to its maximum allowable value ($f = F$), and the phase durations T_1, T_2, and T_4 are calculated using the procedure outlined in Section F.1.

ii) If the commanded travel distance L is smaller than $l_{\text{acc}}^{\max}$ (i.e., $L < l_{\text{acc}}^{\max}$), then the maximum velocity cannot be reached, even if the complete available travel distance was employed only for acceleration and deceleration phases. In this case, the achievable velocity will be lower than the desired (limit) value ($f < F$). Hence, in order to maximize f, i.e., to achieve minimum-time motion, the travel distance is used solely to generate the acceleration and deceleration phases (i.e., $l_{\text{acc}} = L$), and there is no constant velocity phase ($T_4 = 0$). Depending on the value of L, two possibilities emerge:

ii. a) If the given travel distance L allows for the maximum acceleration magnitude to be reached (i.e., $L \geq l_{\text{acc}}^{0}$, see Eq. (F.3)), then the acceleration profile will be trapezoidal, indicating that $f \geq A^2 / J$. In this case, the highest possible velocity can be found by substituting $l_{\text{acc}} = L$ inside Eq. (F.5):

$$f = \frac{1}{2}\left(\frac{-A^2}{J} + \sqrt{\frac{A^4}{J^2} + 4AL} \right) \tag{F.8}$$

ii. b) If the given travel distance L does not allow for the maximum acceleration magnitude to be reached (i.e., $L < l_{\text{acc}}^{0}$, see Eq. (F.3)), then the acceleration profile will be triangular, indicating that $f < A^2 / J$. In this case, the highest possible velocity can be found by substituting $l_{\text{acc}} = L$ inside Eq. (F.2):

$$f = \sqrt[3]{\frac{JL^2}{4}} \tag{F.9}$$

Once the peak velocity value is determined from Eq. (F.8) or (F.9), the phase durations T_1, T_2, and T_4 can be calculated using the procedure outlined in Section F.1

Finally, integrating a jerk sequence of $j = [J \quad 0 \quad -J \quad 0 \quad -J \quad 0 \quad J]^T$ with the timings of $T = [T_1 \quad T_2 \quad T_1 \quad T_4 \quad T_1 \quad T_2 \quad T_1]^T$, starting with zero initial position, velocity, and acceleration boundary conditions will yield the jerk-, acceleration-, and velocity-bounded time-optimal positioning trajectory which achieves an exact travel distance of L.

F.3 Validation for Single-Axis Implementation

The trajectory planning method in Section F.2 has been validated for the limits J = 14,000 [mm/s^3], A = 1000 [mm/s^2], F =250 [mm/s], and a displacement array of L = [0.01, 8.3425, 10.204, 16.675, 25.008, 33.34, 41.672, 50.005, 58.337, 66.67, 75.002, 80.357, 83.335, 91.667, 100] [mm]. The displacement values of 10.204 [mm] and 80.357 [mm] correspond to the values of l_{acc}^{0} and $l_{\text{acc}}^{\max}$. The results are shown in Figure F.3. Figure F.3a shows the phase plane view for all displacement values tested, and Figure F.3b shows the sample results for only for L = 10.204, 41.672, 80.357, and 100 (to avoid cluttering the time-domain kinematic profiles' figure). These results validate the correctness of the formulation and implementation, and also illustrate the different cases explained in Section F.2.

F.4 Validation in 5-Axis Implementation for Beam Positioning in Percussion Laser Drilling

The trajectory planning method in Section F.2 has also been validated for the 5-axis case. Figure F.4 shows the displacement for each of the X, Y, Z, A, and C axes (presented in Figure 1.1), and their kinematic profiles. Some axes (such as the X-axis) arrive quicker than others to their destination hole location. In this case, the faster axes remain at rest waiting for the slower axes to arrive at the designated hole location. These results validate the correctness of the formulation when implemented in a practical 5-axis case. To simplify the figure, the velocity, acceleration, and jerk profiles have been shown in normalized form.

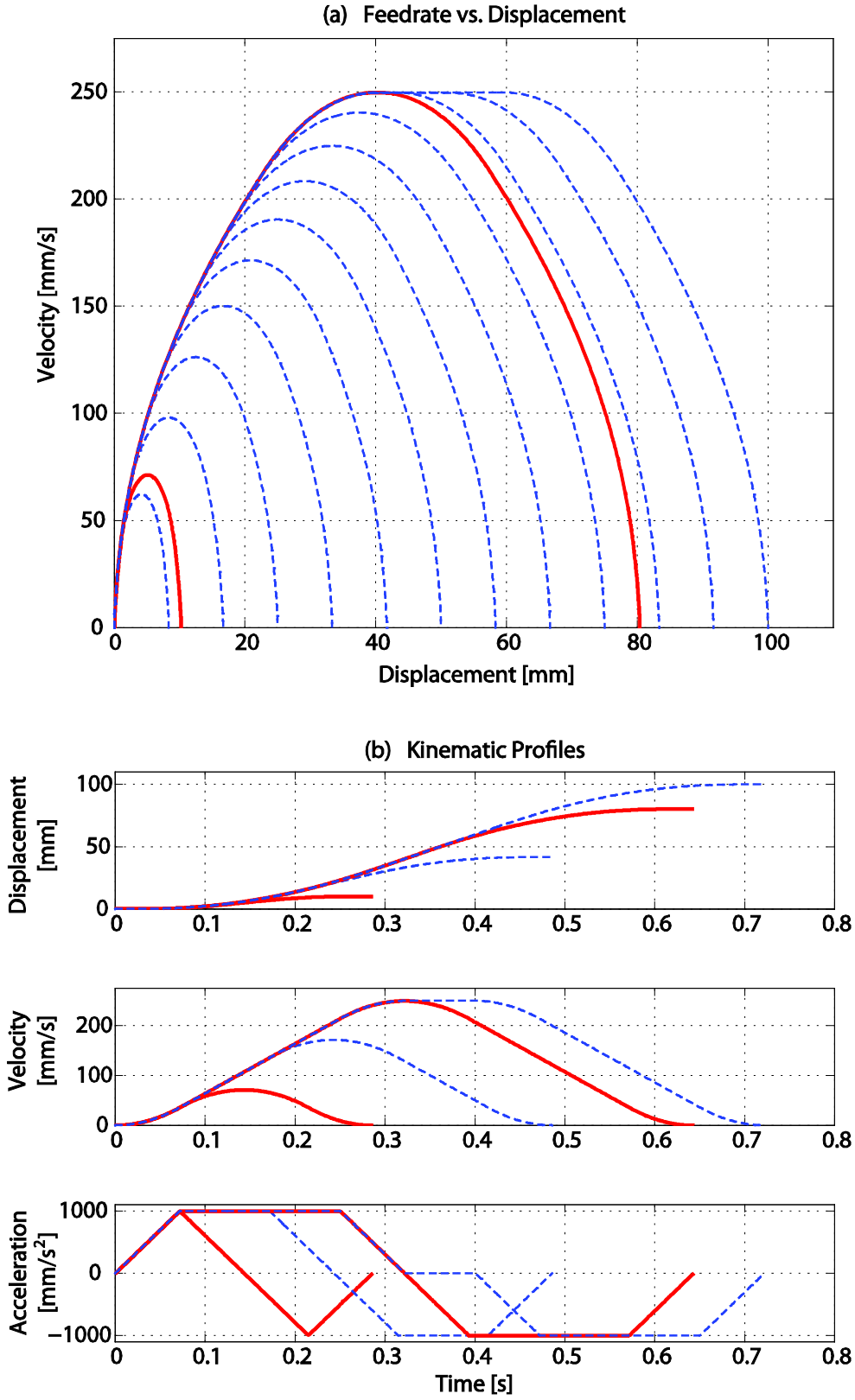

Figure F.3: Progression of time-optimal trajectories with increasing travel distance: (a) Phase-plane view (b) Kinematic profiles as a function of time.

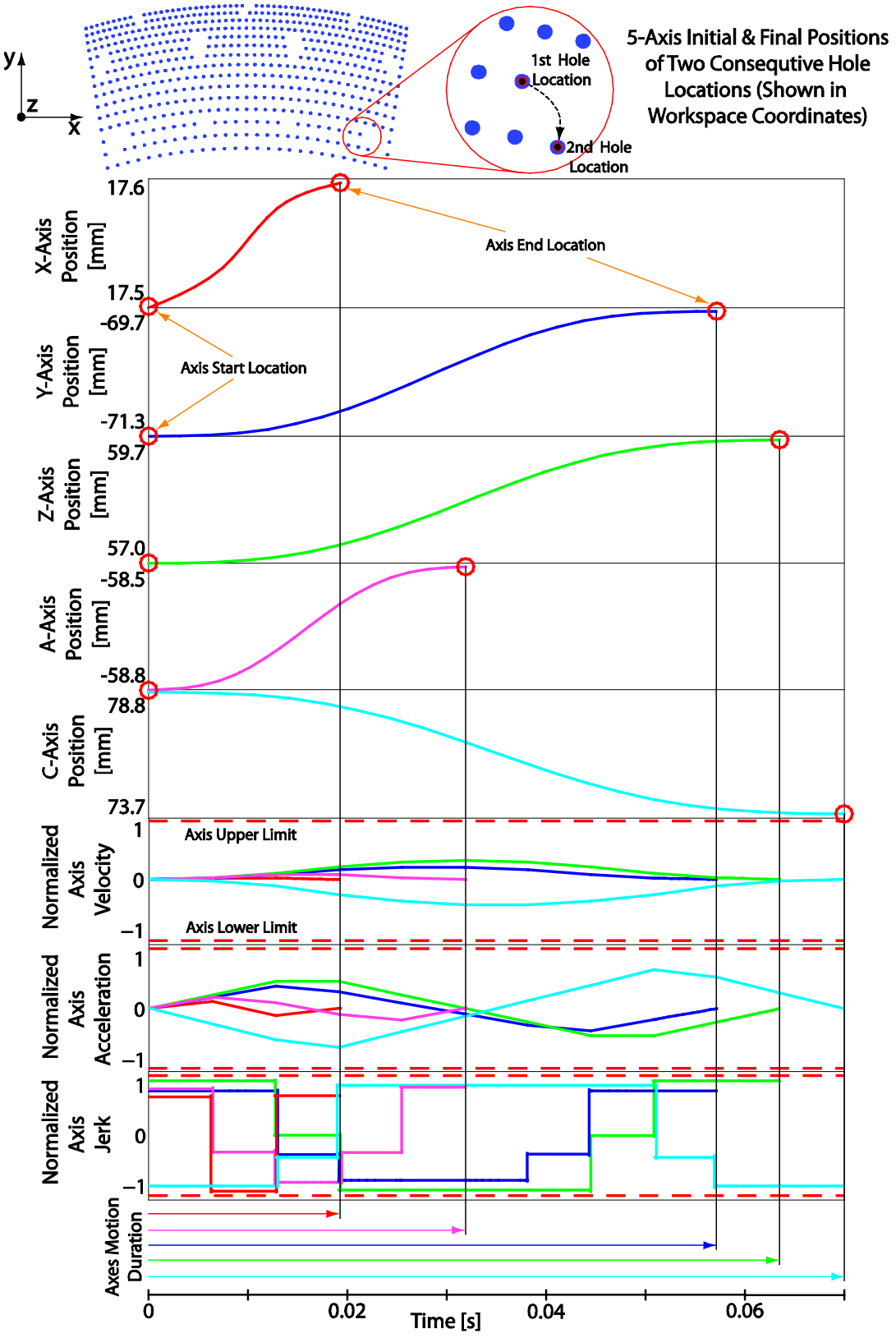

Figure F.4: Time-optimal trajectories for 5-axes and Kinematic profiles as a function of time.